Electrical Post-Compensation for Four-Wave Mixing Nonlinear Impairments Using Digital Coherent Detection in WDM Optical Communication Systems

Jing LIANG

A dissertation submitted to
Kochi University of Technology
in partial fulfillment of the requirements
for the degree of

Doctor of Philosophy

Special Course for International Students

Graduate School of Engineering

Kochi University of Technology

Kochi, Japan

August 2011

Abstract

Wavelength-division multiplexing (WDM) is a promising technology to accommodate the explosive growth of the Internet and telecommunication traffic in wide-area and local-area network. Under the current long-distance WDM transmission system, erbium-doped single mode fiber amplifier (EDFA) is more and more utilized indispensably. This makes the system performance more vulnerable to fiber nonlinear impairments. Therefore, the transmission capacity of dense WDM systems is determined mainly by the degree to which the fiber impairments are compensated. Among the numerous nonlinearities, Kerr effects, especially four-wave mixing (FWM) has been viewed as the most detrimental factor in dense WDM systems.

Several methods have been put forward to suppress the FWM impairments. However there are drawbacks. Post-compensation with backward propagation (BP) method using digital coherent detection is developed recently and can compensate fiber transmission degradation including fiber nonlinearity impairments. Moreover, this method offers great flexibility to transmission length, fiber characteristics. However, for complete compensation, the extra detectors for out of band information produced by FWM are required. Additionally, great computation power is required since many compensation steps are necessary in the segmenting of the transmitted fibers for processing.

We propose, therefore, a novel FWM impairments compensation method based on estimating FWM components and then substituting the estimated components for the generated ones in this dissertation. With estimation method, the number of detectors is reduced since only signal channels are detected and information of other FWM channels

is deduced based on these detected channels. Simulation is performed based on a five-channel DPSK modulated WDM system, in which compensation performance is compared between our estimation method and BP method. The compensation performance is evaluated by eye penalty of each signal. The compensation results indicate that the input optical power tolerance is improved by nearly 5.5dB.

The compensation performance is also verified experimentally. This method is preferable in terms of fewer employed detectors, less computation power, and fewer actual circuits involved. It is also discussed in multi-channel systems, in which the total efficiency of FWMs on center channel with respect to different channel spacing is calculated. For the case of 100GHz channel spacing, 30 channels are considered to be degraded and utilized for a rough FWM estimation.

We also propose to experimentally demonstrate the feasibility of electrical post compensation with BP before putting forward the estimation method. Various fiber propagation degradations may be digitally compensated, relieving the need for complex and expensive optical solutions. The difficulties of FWM electrical compensation are to convert optical signal information to electrical signal with remaining the phase relation of individual channels after coherent detection. We modulate a local oscillator (LO) light using a phase modulator to realize fixed phase relationship among LOs when coherent detected by individual detectors. The combined individual detected signals are compensated by observing the signal-to-FWM crosstalk ratio as well as the eye penalty for non-degenerate case as well as degenerate case. The compensation possibilities by reducing detectors and the required are demonstrated. Simulation for observing the number of required detectors is also performed on different number of signal channels as well as optical input power.

Table of Contents

Chapter 1

Introduction

1.1 Background & problem statement

The rapid expansion of the communication business has resulted in the explosive growth of Internet traffic. Internet traffic has been continuing to exhibit exponential traffic growth, and it will increase by a factor of one thousand in roughly 20 years [1], which becomes challenging for an ultrahigh-capacity long-distance transmission system to keep pace with the level of growth without requiring prohibitively large increases in network cost and power consumption. The amount of Internet traffic crisscrossing the world will quadruple by 2015 according to a report from Cisco [2].

It is desirable to exploit the bandwidth of fiber optics by wavelength-division multiplexing (WDM) to overcome the electronic limitations, thus to further increase the transmission capacity, due to the broad optical bandwidth in excess of 30 THz available in the low-loss transmission window of the optical fibers [3]. WDM is a promising technology to accommodate the explosive growth of the Internet and telecommunication traffic in wide-area and local-area network. In order to increase the transmission capacity of WDM optical system, both transmission data rate per wavelength as well as the number of wavelengths can be increased. However, there are different transmission issues to be dealt with for these two approaches. First, when the transmitting data rate becomes higher, the chromatic dispersion (CD) as well as polarization-mode dispersion (PMD) will have to be solved even before dealing with fiber nonlinearity induced

penalties [1]. Additionally, increasing number of wavelengths, i.e., decreasing channel spacing in WDM systems will result in that optical nonlinearity-induced impairments from four-wave mixing (FWM) and cross-phase modulation (XPM) are more liable to undermine system performance and come to play even more decisive role. Therefore, CD and fiber nonlinearities are considered as two major degradation factors in WDM transmission system. CD was typically regarded as more significant obstacle, while nonlinear effects were usually neglected prior to the 1990's before optical fiber amplifiers were developed. Data rates have increased constantly, and meanwhile, erbium-doped single mode fiber amplifier (EDFA) is more and more utilized indispensably under the current long-distance WDM transmission system. The problem of fiber CD has been mitigated to some extent because of the improvements in dispersion shifted fibers (DSF), dispersion compensation fibers (DCF), and other dispersion management technologies [4-6]. However, the high optical power levels available from EDFAs make system performance more vulnerable to fiber nonlinear effects [7-10]. This leads to interference, distortion, and excess attenuation of the transmitted signals and results in system degradations [8]. Therefore, fiber nonlinearities have appeared as the most significant limiting factor and become crucial to be settled.

The origin of the nonlinearities that are most detrimental is due to the refractive index of the optical fiber, which is varies with the intensity of the optical signal. It is also named Kerr effects. The component of intensity-dependent refractive index becomes significant when high powers are launched. Although the individual power in each channel may be below the level needed to produce nonlinearities, the total power summed over all channels will become significant. The combination of high total optical power and large number of channels at closely spaced wavelengths is a source

for many kinds of nonlinear interactions. Among the numerous nonlinearities, FWM has been viewed as the most detrimental factor in WDM systems [11-15]. Therefore, the transmission capacity of dense WDM systems is determined mainly by the degree to which the fiber impairments are compensated.

1.2 FWM suppression/ compensation schemes

There are several schemes to avoid FWM nonlinear impairments, which can be classified primarily into two categories: optical compensation and electrical compensation.

1.2.1 Optical compensation schemes

Optical compensation schemes are utilized commonly, such as dispersion management [16-18], unequal channel spacing [19-21], optical compensators [22-25], non-zero DSF (NZ-DSF) [26, 27] such as large effective area fiber [27], and so on. However, these methods have their intrinsic drawbacks. The dispersion management method can not only suppress FWM, but also keep the average CD of an entire transmission line close to zero. However, the available wavelength range is restricted to apply FWM compensation and complicated cable management is required in some cases. It is possible to employ the un-equal channel spacing in order that the FWM crosstalk is minimized directly for the WDM systems in which the transmitted channels are not many. However, this method is not applicable for large channel number, since the required bandwidth is too broad. What is more, the frequency allocation should be computed beforehand and stringent requirements on optical frequency stabilities for transmitters are required. The solutions of optical compensators (such as optical phase conjugation) also have drawbacks such as expensive cost, complex configuration, additional loss, bulky size and lack of adaptability. The advantage of NZ-DSF is that,

while the inter-channel FWM is suppressed due to the non-zero dispersion, the dispersive pulse broadening is much lower than in single-mode fiber (SMF). NZ-DSF can be utilized attractively for future WDM system. Especially, by using large effective area fiber, the optical power density is reduced due to the increased the effective area, and thus lower FWM impact is resulted in. However, it can not solve the problem in ready installed fiber. Table 1.1 summarizes the characteristics of conventional compensation methods as well as electrical compensation schemes mentioned in Section 1.2.2.

Table 1.1 Characteristics of conventional compensation methods

Compensation method	Advantage	Disadvantage
Dispersion management [16-18]	Suppress FWM, average dispersion approaches zero	Restricted available wavelength range, complicated cable management
Un-equal channel spacing [19-21]	Minimize FWM crosstalk directly for few-channel systems	Broader bandwidth, stringent requirements on optical frequency stabilities
Optical compensator (e.g.: Optical phase conjugation) [22-25]	Realize in-line compensation directly	High-cost, physical size, additional loss and nonlinearity, lack of adaptability
NZ-DSF [26,27]	Attractive for future	Problem in ready

	WDM system	installed fiber
Pre-compensation [28-32]	Relieve need of optical solutions	Need feedback for transmission characteristics analysis
Post-compensation [33-38]	Relieve need of optical solutions, flexible, no feedback	Great number of detectors, Computation power

1.2.2 Electrical compensation schemes

Electrical compensation for both CD and fiber nonlinearity has received significant attention in recent years. Several electrical pre-compensation schemes have been demonstrated to compensate for the fiber nonlinearities in WDM systems by simulation [28-32]. In these schemes, the transmitted signals are pre-distorted, which is calculated using optical phase conjugation or backward propagation (BP), i.e., the signal is distorted by virtual fiber while compensated through the real fiber transmission.

Electrical BP was first studied as a transmitter-side compensation method by Roberts et al. in 2006 [31]. We usually call it pre-compensation as above. In the absence of coherent detection, it is applicable at the modulator only. By coherent detection, however, the transmitted signals can be recovered electrically [33, 35], which enables the receiver-side BP also known as post-compensation. Electrical post-compensation methods using coherent detection with subsequent digital signal processing (DSP), since then, have been attracted much attention as the most promising technique for long-haul optical transmission [33-38]. Post-compensation is more adaptive since feedback is unnecessary, and the entire robust compensation and demodulation process is done at

the receiver side. DSP alleviates the requirement for optical phase locking of the local oscillator (LO). Moreover, this method offers great flexibility to transmission length, fiber characteristics and network configuration change. Various fiber propagation effects may be digitally compensated, relieving the need for complex optical solutions.

In this dissertation, the feasibility of receiver-side digital distributed compensation is demonstrated experimentally within a WDM system.

1.3 Motivation and overview of the thesis

From the above-mentioned reasons, this dissertation is aimed to get an insight into nonlinear effect caused specifically by FWM in WDM optical communication systems and present a study on electrical post-compensation for FWM nonlinearity impairments with digital coherent detection, in order that the original information can be retrieved at the receiver. Both the novel estimation method as well as BP method in experimental demonstration is proposed to compensate for FWM impairments.

The dissertation is organized as follows. Chapter 2 introduces the Signal propagation in WDM optical fiber systems. The nonlinear Schrödinger equation (NLSE) required for the rest of the thesis is explained. Linear and nonlinear fiber impairments that degrade transmission system performance are described in this part.

Chapter 3 introduces the FWM compensation using backward propagation (BP) method, including the general configuration of WDM systems for FWM compensation, in which optical coherent detection combined with electrical post compensation using digital signal processing is explained. The experimental demonstration of the feasibility based on the electrical post compensation with BP compensation method is proposed. The difficulties of FWM electrical compensation are to convert optical signal information to electrical signal with remaining the phase relation of individual channels. We modulate

a local oscillator (LO) light using a phase modulator to realize fixed phase relation among LOs when coherent detected by individual receivers. Split-step Fourier method is involved for compensation. Both simulation demonstration and experimental confirmation are performed on multi-channel WDM system. The compensation results are evaluated by eye penalty, the system performance is improved by BP compensation. Simulation is performed for observing the number of required detectors. The result indicates that great number of detectors must be employed when the optical input power is increased even in the systems with few number of signal channels.

FWM estimation compensation method is proposed in Chapter 4. First, the principle of this novel method is described. This FWM compensation method is based on estimating FWM components and then substituting the estimated components for the generated ones. The number of detectors is reduced in our estimation method since only signal channels are detected and information of other FWM channels are deduced based on these detected channels. The compensation performance is verified through simulation as well as experiment. In addition, the FWM estimation method is contrasted with BP method. This method is preferable in terms of fewer employed detectors, less computation power, and fewer actual circuits involved. Multi-channel system is also discussed in this part.

Finally, the thesis is summarized in Chapter 5.

Reference

[1] Adel A. M. Saleh, Jane M. Simmons, “Technology and architecture to enable the explosive growth of the Internet,” *IEEE communications magazine*, pp.126-132, Jan., 2011.

[2] http://www.techbeta.org/news/2011/06/cisco-internet-traffic-to-quadruple-by-2015-2/

[3] C. A. Brackett, “Dense wavelength division multiplexing networks: principles and applications,” *IEEE Journal on Selected Areas in Communications*, Vol.8, No.6, pp. 948-963, Aug., 1990.

[4] T. Yu, E. A. Golovchenko, A. N. Pilipetskii, and C. R. Menyuk, “Dispersion-managed soliton interactions in optical fibers,” *Optics letters*, Vol. 22, No.11, pp. 793-795, Jun., 1997.

[5] S. K. Turitsyn, M. P. Fedoruk, W. Forysiak, and N. J. Doran, “Dispersion-management in fiber communication lines using Raman amplification,” *Optics communications*, Vol. 170, Issues 1-3, pp. 23-27, Oct., 1999.

[6] M. Murakami, T. Matsuda, H. Maeda, and T. Imai, “Long-haul WDM transmission using higher order fiber dispersion management,” *J. Lightw. Technol.*, Vol. 18, No. 9, pp. 1197-1204, Sep., 2000.

[7] G. P. Agrawal, *Nonlinear Fiber Optics*, San Diego, CA: Academic Press, 2001.

[8] A. R. Chraplyvy, “Limitations on lightwave communications imposed by optical fiber nonlinearities,” *J. Lightw. Technol.*, Vol. 8, No.10, pp. 1548–1557, Oct., 1990.

[9] F. Forghieri, R. W. Tkach, and A. R. Chraplyvy, “Fiber nonlinearities and their impact on transmission systems,” in *Optical Fiber Telecommunications IIIA*, Academic Press, 1997.

[10] P. P. Mitra and J. B. Stark, “Nonlinear limits to the information capacity of optical fiber communications,” *Nature*, Vol. 411, pp. 1027–1030, Jun., 2001.

[11] Kyo Inoue, “Four-wave mixing in an optical fiber in the zero-dispersion wavelength region,” *J. Lightw. Technol.*, Vol. 10, No.11, pp. 1553-1561, Nov.,

1992.

[12] R.W. Tkach, A. R. Chraplyvy, F. Forghieri, A. H. Gnauck, and R. M. Derosier, "Four-photon mixing and high-speed WDM systems," *J. Lightw. Technol.*, Vol. 13, No. 5, pp. 841–849, May., 1995.

[13] M. Eiselt, "Limits on WDM systems due to four-wave mixing: a statistical approach," *J. Lightw. Technol.*, Vol. 17, No.11, pp. 2261–2267, Nov., 1999.

[14] A. V. Ramprasad, and M. Meenakshi, "Four Wave Mixing on Dense wavelength division Multiplexing Optical system- a study," *Academic Open Internet Journal*, Vol. 17, No.1, pp. 1-8, 2006.

[15] Paula B. Harboe, and Edilson da Silva, "Analysis of FWM penalties in DWDM systems based on G.652, G.653, and G.655 optical fibers," *World Academy of Science, Engineering and Technology*, Vol. 48, 2008.

[16] K. Nakajima, M. Ohashi, T. Horiguchi et al, "Design of dispersion managed fiber and its FWM suppression performance," *Optical Fiber Communication Conference*, OSA, Vol. 3, ThG3, pp.87-89, 1999.

[17] A. Mecozzi et al., "Dispersion management in phase modulated optical transmission systems," *ECOC2010*, Mo.2.C.2, 2010.

[18] T. Matsuda, M. Murakami, and T. Imai, "Dispersion management scheme for suppressing FWM in DWDM transmission," *Lasers and Electro-Optics Society Annual Meeting* (*LEOS'98*)*, IEEE* WBB2, 1998.

[19] M. N. Alam, S. P. Majumder et al., "Bit error rate performance comparison of equal channel spacing and repeated unequal spacing in reducing the four wave mixing effect in a WDM ring network", *Proc. ATNAC'07*, Christchurch, New Zealand, pp. 431-434, Dec., 2007.

[20] M. Faisal et al., “Performance of Wavelength Shift Keying and Repeated Unequal Channel Spacing Schemes in Reducing the Four-wave Mixing Effect in Optical WDM Systems,” *Journal of Optical Engineering*, Vol. 44, pp. 015002 (1-6), 2006.

[21] T. Numai, and O. Kubota, “Analysis of repeated unequally spaced channels for FDM lightwave system,” *J. Lightw. Technol.*, Vol. 18, No. 5, pp. 656-664, May., 2000.

[22] J. Y. Huh, S.B. Jun et al, “A novel four-wave mixing compensator,” *IEEE Photon. Technol. Lett.*, Vol.19, No.1, pp. 36-38, Jan., 2007.

[23] S. Suda, F. Koyama, N. Nishiyama et al, “Optical compensation of fiber nonlinearity using vertical micro-cavity saturable absorber,” *Semiconductor Laser Conference 2008*, Paper TuC1, Sep., 2008.

[24] S. Watanabe and M. Shirasaki, “Exact compensation for both chromatic dispersion and Kerr effect in a transmission fiber using optical phase conjugation,” *J. Lightw. Technol.*, Vol. 14, pp. 243–248, 1996.

[25] P. Minzioni, V. Pusino, I. Cristiani et al, “Optical phase conjugation in phase-modulated transmission systems: experimental comparison of different nonlinearity-compensation method,” *Optics Express*, Vol. 18, No. 17, pp. 18119-18124, Aug., 2010.

[26] R. I. Killey, S. Appathurai, V. Mikhailov, H. J. Thiele, P. Bayvel, “Nonlinear signal distortion in WDM transmission with 10- and 40- Gbit/s channel rates,” *London Communications Symposium (LCS 2000)*, London, Sep., 2000.

[27] T. Katagiri, T. Naito, A. Miura, K. Amemiya, “FWM crosstalk suppression using wavelength grouping in 25-GHz-Spaced 10-Gbps-Based WDM transmission over NZ-DSF in C-band,” *OFC 2003*, pp. 664-665, 2003, Paper FE6.

[28] E. Yamazaki, F. Inuzuka et al., "Digital compensation of inter-carrier nonlinear distortion with carrier phase locking," *J. Lightw. Technol.*, Vol.28, No.5, pp. 828-836, Mar., 2010.

[29] L. Du, and A. Lowery, "Fiber nonlinearity pre-compensation for long-haul links using direct-detection optical OFDM," *Opt. Express*, Vol. 16, No.9, pp. 6209-6215, Apr., 2008.

[30] R. I. Killey, P. M. Watts, M. Glick, and P. Bayvel, "Electronic pre-compensation techniques to combat dispersion and nonlinearity in optical transmission," in *Proc. of 31st European Conf. on Optical Communication*, Vol. 2, pp. 251–254, 2005.

[31] K. Roberts, C. Li, L. Strawczynski, M. O'Sullivan, and I. Hardcastle, "Electronic pre-compensation of optical nonlinearity," *IEEE Photon. Technol. Lett.*, Vol. 18, pp. 403–405, Jan., 2006.

[32] C. Weber, J. K. Fischer, C. A. Bunge, and K. Petermann, "Electronic pre-compensation of intra-channel nonlinearities at 40 Gb/s," *IEEE Photon. Technol. Lett.*, Vol. 18, pp. 1759–1761, Aug., 2006.

[33] X. Li, X. Chen, G. Goldfarb et al, "Electronic post-compensation of WDM transmission impairments using coherent detection and digital signal processing," *Opt. Express*, Vol.16, No.2, pp. 880-888, Jan., 2008.

[34] E. Ip and J. M. Kahn, "Compensation of dispersion and nonlinear impairments using digital back propagation," *J. Lightw. Technol.*, Vol.26, No.20, pp. 3416-3425, Oct., 2008.

[35] E. F. Mateo, L. Zhu, and G. Li, "Impact of XPM and FWM on the digital implementation of impairment compensation for WDM transmission using backward propagation," *Opt. Express*, Vol. 16, No. 20, pp. 16124–16137, Sep.,

2008.

[36] E. F. Mateo, and G. Li, “Compensation of inter-channel nonlinearities using enhanced coupled equations for digital backward propagation,” *Applied Optics*, Vol. 48, No. 25, pp. F6-F10, Sep., 2009.

[37] N. Ahmed, M. I. Hayee, and Q. Zhang, “Electronic post-compensation of fiber nonlinearity for 40 Gbit/s WDM systems,” *Journal of Optical Communications and Networking*, Vol. 2, No. 7, Jul., 2010.

[38] D. Yang, S. Kumar, M. Nakazawa, “Investigation and comparison of digital backward propagation schemes for OFDM and single-carrier fiber-optic transmission systems,” *Optical Fiber Technology*, Vol. 17, pp. 84-90, 2011.

Chapter 2

Signal propagation in WDM optical fiber systems

The optical signals suffer from not only linear degradation but also nonlinear degradation and they are degraded during the fiber propagation. Therefore, an objective of any optical communication systems focuses on the cancellation or compensation for the transmission-related degradations in order that the original information can be retrieved at the receiver, which is also the target of our study.

Figure 2.1 shows the WDM optical transmission system. In the transmitters, the data bits are modulated onto the optical carriers at wavelengths λ_1, λ_2, … , λ_N using a specific modulation format. The individual wavelength division multiplexing (WDM) signals are combined by the optical multiplexer into the same optical transmission fiber. During propagation the signal is affected by several linear and nonlinear fiber impairments such as attenuation, CD and fiber nonlinearities. After multi-repeater transmission, the WDM signals are split into the individual wavelength channels by the demultiplexer which acts as an optical band-pass filter. The propagated signals are demodulated to recover the transmitted information after they are detected by individual receivers.

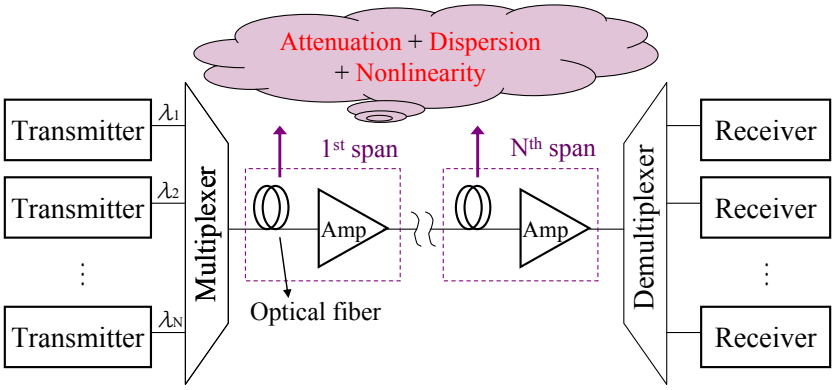

Fig 2.1 WDM optical transmission system

2.1 Basic propagation equation

In optical communication systems, the input signal to the fiber is usually a composite optical signal modulated with information bit streams. When all the input signal frequencies interact due to fiber nonlinearities, the output bit stream may behave in a complicated way giving detrimental effects on system performance. The output waveform can be obtained by solving the nonlinear Schrödinger equation (NLSE). It is impossible to solve the equation analytically in general. In this dissertation, the split-step Fourier method as one of pure numerical methods is utilized for analyzing fiber nonlinearities and their compensations, which will be introduced in Chapter 3.

The electrical field associated with the optical bit stream can be expressed as [1]:

$$\mathbf{E}(\mathbf{r},t) = \mathrm{Re}\left[\hat{\mathbf{e}}F(x,y)A(z,t)\exp\left(i\beta_0 z - i\omega t\right)\right] \tag{2.1}$$

where $\hat{\mathbf{e}}$ is the polarization unit vector, $F(x,y)$ is spatial distribution of the fundamental fiber mode, $A(z,t)$ is the complex amplitude of the field envelope at a distance z inside the fiber, and β_0 is the mode-propagation constant at the carrier frequency ω. By assuming that the birefringence effects can be ignored and treating $\hat{\mathbf{e}}$ as a constant, the only quantity that changes with propagation is the complex amplitude $A(z,t)$ associated with the optical signal since $F(x,y)$ does not depend on z.

The basic propagation equation that describes the propagation of optical pulses through optical fiber channels is represented as [1]:

$$\frac{\partial A}{\partial z} + \beta_1\frac{\partial A}{\partial t} + \frac{i\beta_2}{2}\frac{\partial^2 A}{\partial t^2} - \frac{\beta_3}{6}\frac{\partial^3 A}{\partial t^3} = i\beta_{NL}A - \frac{\alpha}{2}A \tag{2.2}$$

where α is the attenuation constant responsible for fiber loss. As given in Appendix C, β_1 is related inversely to the group velocity v_g, β_2 and β_3 are named as second- and

third-order dispersion parameters, respectively. β_2 is related to the CD parameter: $D_c = \frac{d}{d\lambda}\left(\frac{1}{v_g}\right) = -\frac{2\pi c}{\lambda^2}\beta_2$, where c is light velocity in vacuum, λ represents wavelength. For all the fibers, D_c varies with wavelength and becomes zero at a wavelength called the zero-dispersion wavelength (ZDW), which is denoted as λ_0. Near ZDW λ_0, D_c varies linearly as $D_c = S(\lambda - \lambda_0)$. Here, S represents the dispersion slope at λ_0, and there is a relationship between S and β_3 as $S = \left(2\pi c/\lambda^2\right)^2 \beta_3$. $\beta_{NL} = \delta n_{NL}(\omega_0/c)$ is the nonlinear part of the propagation constant. The nonlinear change in the refractive index is formed as: $\delta n_{NL} = n_2 I$, where n_2 is nonlinear-index coefficient whose value is around 2.6×10^{-20} m^2/W, and I represents the optical intensity. The intensity is related to optical power as $I(z,t) = P(z,t)/A_{eff}$ at any distance z, where A_{eff} is the effective core area of the fiber. $|A|^2$ represents optical power by normalizing the amplitude A in Eq. (2.2). Therefore, we obtain $\beta_{NL} = \gamma|A|^2$, where $\gamma = \frac{2\pi n_2}{\lambda A_{eff}}$ is known as nonlinear parameter.

Since the term of β_1 corresponds to a constant delay and this delay does not affect the signal quality in any way, Eq. (2.2) can be simplified by assuming $t' = t - \beta_1 z$ and $z' = z$, and rewritten as:

$$\frac{\partial A}{\partial z'} + \frac{i\beta_2}{2}\frac{\partial^2 A}{\partial t'^2} - \frac{\beta_3}{6}\frac{\partial^3 A}{\partial t'^3} = i\gamma|A|^2 A - \frac{\alpha}{2}A \tag{2.3}$$

The third-order dispersive effects are negligible in practice as long as β_2 is not too close to zero, or pulses are not shorter than 5 ps [1]. If so, Eq. (2.3) can be shorten as:

$$\frac{\partial A}{\partial z} + \frac{i\beta_2}{2}\frac{\partial^2 A}{\partial t^2} = i\gamma|A|^2 A - \frac{\alpha}{2}A \tag{2.4}$$

Here, we drop the apostrophe in Eq. (2.2) for simplicity. Eq. (2.4) is known as NLSE. The three parameters α, β_2, γ cover three distinct kinds of degradations occur when

optical signals propagate through optical fibers. This is the theoretical principle of Chapter 3.

2.2 Linear degradation

2.2.1 Fiber losses

The optical power decreases exponentially as $e^{-\alpha z}$ at a distance z because of fiber losses. Therefore, when we substitute $A(z,t) = B(z,t)\exp(-\alpha z/2)$ into Eq. (2.4) and rewrite it in terms of $B(z,t)$, we can obtain:

$$\frac{\partial B}{\partial z} + \frac{i\beta_2}{2}\frac{\partial^2 B}{\partial t^2} = i\gamma e^{-\alpha z}|B|^2 B \tag{2.5}$$

From this equation, it is obvious that the power decrease also weakens the nonlinear effects.

It is customary to express the fiber loss in unit of dB/km by the following relationship:

$$\alpha_{dB} = -\frac{10}{L}\log_{10}\left(\frac{P(L)}{P_0}\right) = 4.343\alpha \tag{2.6}$$

where $P(L)$ represents the output power and $P(L) = P_0\exp(-\alpha L)$ with a transmission length of L. The total attenuation of an optical fiber is shown in Fig 2.2 [2]. Optical fiber loss is caused by a number of factors that are indicated in the figure as well. The red curve plots the total loss. As shown in this figure, α_{dB} has the smallest value around 0.2 dB/km near 1550nm.

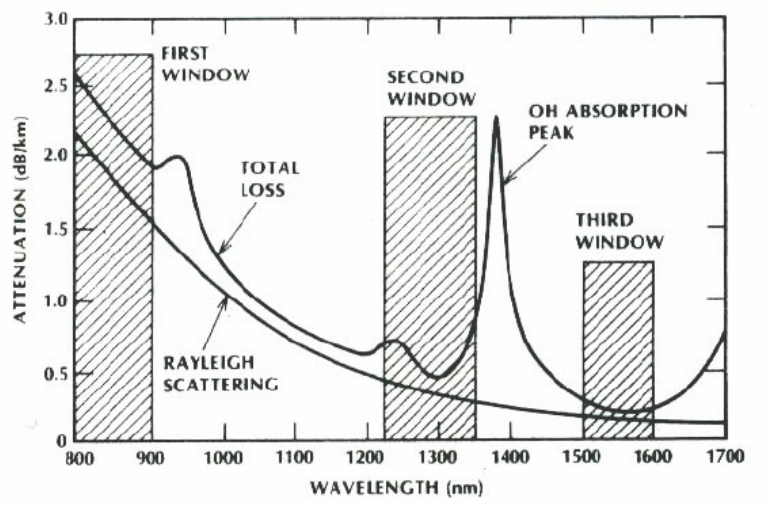

Fig 2.2 Total attenuation of an optical fiber [2]

2.2.2 Fiber chromatic dispersion

Different components of the signal travel at different group velocities within the fiber, and thereby fiber CD is often referred as to group-velocity dispersion (GVD). The CD parameter β_2 which is also named the second-order dispersion parameter as above governs the strength of the dispersive effects. It can be positive or negative relying on whether normal or anomalous dispersion is experienced. To simply study the effect from CD only, we set γ=0 and α =0 in Eq. (2.4) and obtain:

$$\frac{\partial A}{\partial z}+\frac{i\beta_2}{2}\frac{\partial^2 A}{\partial t^2}=0 \tag{2.7}$$

This linear equation can be solved with the Fourier-transform method and the general solution is given as follows:

$$A(z,t)=\frac{1}{2\pi}\int_{-\infty}^{\infty}\tilde{A}(0,\omega)\exp\left(\frac{i}{2}\beta_2 z\omega^2-i\omega t\right)d\omega \tag{2.8}$$

where $\tilde{A}(0,\omega)$ is the Fourier transform of $A(0,t)$:

$$\tilde{A}(0,\omega)=\int_{-\infty}^{\infty}A(0,t)\exp(i\omega t)dt \tag{2.9}$$

The phase factor $\exp\left(\frac{i}{2}\beta_2 z\omega^2\right)$ is responsible for the degradation.

The relationship between CD and wavelength is plotted in Fig 2.3, for various fibers. A typical value of CD in SMF at 1550nm is nearly 17ps/km/nm, while DSF has a CD value of nearly zero at 1550nm and is specially adapted for this low-loss window. Both low CD and low attenuation are obtained by employing DSF. However, FWM effect will be more likely appear because of the so-called phase-matching condition.

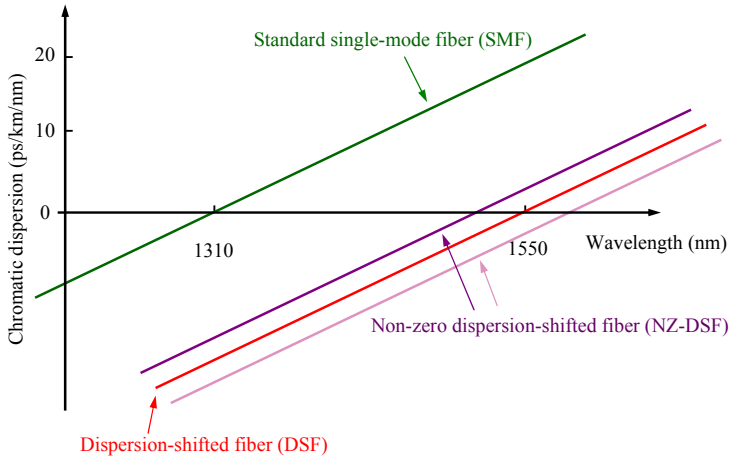

Fig 2.3 CD values of various fibers versus wavelength

2.3 Fiber nonlinear effects

Fiber nonlinear effects play a detrimental role during the optical signal propagation that leads to interference, distortion, and excess attenuation of the transmitted signals and thereby results in severe degradations on WDM systems, which is drawn in Fig 2.4. By signal propagation, S1 and S3 interfere with S2.

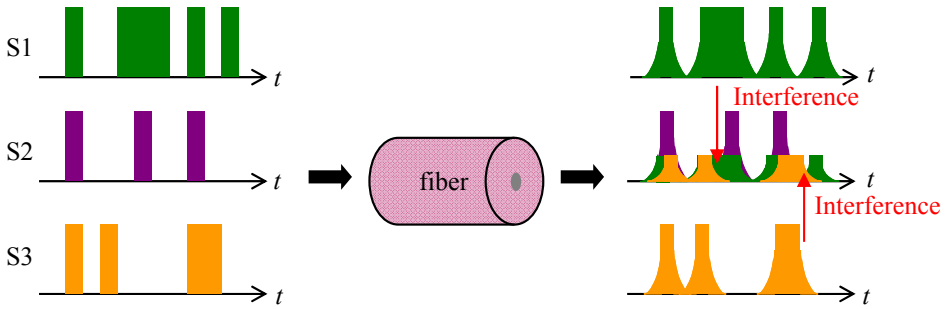

Fig 2.4 Multi-channel Interaction by propagation

The nonlinearities in optical fibers are commonly classified into two categories: One is nonlinear scattering effects including stimulated Brillouin scattering (SBS) and stimulated Raman scattering (SRS), the other is the optical Kerr effect comprising self-phase modulation (SPM), XPM as well as FWM [3]. These two categories arise from different mechanisms. The latter one is due to the changes in the refractive index expressed as:

$$n = n_0 + n_2 I = n_0 + n_2 \frac{P}{A_{eff}} \tag{2.10}$$

where n_0 is the ordinary refractive index. While stimulated scatterings are responsible for intensity dependent gain or loss [4], the nonlinear refractive index is responsible for intensity dependent phase shift of the optical signal. Moreover, a major difference between scattering effects and the Kerr effect is that stimulated scatterings have threshold power levels at which the nonlinear effects manifest themselves, while the Kerr effects don't have such a threshold.

Scattering effects will be neglected for the further discussion since SRS has a very high power threshold of around 500mW which is far above the powers that are utilized in optical communication applications [1]. The SBS threshold increases when short optical pulses propagate through the fiber, and modulation format can also increase the threshold power. They are also not involved in the above simplified NLSE. As a consequence, Kerr effects are viewed as the most detrimental factor and this section presents their relevant impairments, especially FWM, which is more prone to appear in dense WDM transmission systems.

2.3.1 Mathematical representation

The nonlinear term of the NLSE Eq. (2.4) is $\gamma|A|^2 A$. When the three-channel scenario

is taken into consideration, i.e.:

$$A = A_1 + A_2 + A_3 \tag{2.11}$$

The nonlinear term can be extended as [5, 6]:

$$\begin{aligned}
|A|^2 A &= A_1 A_1^* A_1 + A_1 A_1^* A_2 + A_1 A_1^* A_3 + A_1 A_2^* A_1 + A_1 A_2^* A_2 + A_1 A_2^* A_3 + A_1 A_3^* A_1 + A_1 A_3^* A_2 + A_1 A_3^* A_3 \\
&\quad + A_2 A_1^* A_1 + A_2 A_1^* A_2 + A_2 A_1^* A_3 + A_2 A_2^* A_1 + A_2 A_2^* A_2 + A_2 A_2^* A_3 + A_2 A_3^* A_1 + A_2 A_3^* A_2 + A_2 A_3^* A_3 \\
&\quad + A_3 A_1^* A_1 + A_3 A_1^* A_2 + A_3 A_1^* A_3 + A_3 A_2^* A_1 + A_3 A_2^* A_2 + A_3 A_2^* A_3 + A_3 A_3^* A_1 + A_3 A_3^* A_2 + A_3 A_3^* A_3 \\
&= |A_1|^2 A_1 + |A_2|^2 A_2 + |A_3|^2 A_3 + 2|A_1|^2 A_2 + 2|A_1|^2 A_3 + 2|A_2|^2 A_1 + 2|A_2|^2 A_3 \\
&\quad + 2|A_3|^2 A_1 + 2|A_3|^2 A_2 + A_1^2 A_2^* + A_1^2 A_3^* + A_2^2 A_1^* + A_2^2 A_3^* + A_3^2 A_1^* + A_3^2 A_2^* \\
&\quad + 2A_1 A_2 A_3^* + 2A_1 A_3 A_2^* + 2A_2 A_3 A_1^* \\
&= \underbrace{|A_1|^2 A_1 + |A_2|^2 A_2 + |A_3|^2 A_3}_{SPM} \\
&\quad + \underbrace{2|A_1|^2 A_2 + 2|A_1|^2 A_3 + 2|A_2|^2 A_1 + 2|A_2|^2 A_3 + 2|A_3|^2 A_1 + 2|A_3|^2 A_2}_{XPM} \\
&\quad + \underbrace{A_1^2 A_2^* + A_1^2 A_3^* + A_2^2 A_1^* + A_2^2 A_3^* + A_3^2 A_1^* + A_3^2 A_2^*}_{degenerate\ FWM} + \underbrace{2A_1 A_2 A_3^* + 2A_1 A_3 A_2^* + 2A_2 A_3 A_1^*}_{non\text{-}degenerate\ FWM}
\end{aligned} \tag{2.12}$$

From Eq. (2.12), it is quite easy to identify SPM, XPM and FWM. While the first three terms $|A_1|^2 A_1$, $|A_2|^2 A_2$ and $|A_3|^2 A_3$ provide SPM, the two groups of six terms in the middle of the Eq. (2.12) arise from XPM and degenerate FWM, respectively, and the last three terms $2A_1 A_2 A_3^*$, $2A_1 A_3 A_2^*$ and $2A_2 A_3 A_1^*$ represent non-degenerate FWM. We introduce each effect according to this representation in the followings as well as Appendix B.

2.3.2 Self-phase modulation

The optical phase increases linearly with z [7], then the γ term produces a nonlinear phase shift given by:

$$\phi_{NL} = \int_0^L \beta_{NL} dz = \int_0^L \gamma P(z) dz = \gamma P_0 L_{eff} \tag{2.13}$$

where L_{eff}=[1-exp(-αL)]/α is the effective fiber length. As shown in Eq. (2.12), this

nonlinear phase is modulated by itself, i.e., each channel distorts itself only, so this intra-channel phenomenon is referred to as SPM. The time-varying nonlinear phase shift results in a broadened spectrum of the optical signal. The broadened spectrum may cause a temporal broadening or narrowing of optical pulses in the presence of CD. However, the SPM becomes negligible near zero-dispersion wavelength in WDM systems.

2.3.3 Cross-phase modulation

Differing from SPM, the nonlinear phase shift of XPM depends on the power of other channels when two or more optical channels are transmitted simultaneously inside a fiber. Eq. (2.11) indicates that each channel suffers twice as much distortion as SPM, for the same amount of power.

2.4 Four-wave mixing

2.4.1 Brief introduction

When two or more optical channel wavelengths are transmitted simultaneously inside an identical fiber near the ZDW, some new components will be generated at frequencies:

$$\omega_{FWM} = \omega_i + \omega_j - \omega_k \tag{2.14}$$

Here, i, j, $k \in [1, N]$, and N is the number of channels. If $i=j=k$, the generated component is SPM; If $i=k$ or $j=k$, but $i\neq j$, the component is XPM; Otherwise, $k\neq i, j,$ this is the so-called FWM. The component is named degenerate FWM while $i=j$, and it is defined as non-degenerate FWM while $i\neq j$.

For the long-distance transmission in WDM system, a cumulative CD will undermine the system performance if the standard SMF is employed at 1550nm window. Due to

the GVD, different channels travel at different speeds. This makes the FWM efficiency low. However, it is clear that both low CD and low attenuation are obtained by using DSF near 1550nm shown in Fig 2.2 and Fig 2.3. Zero-dispersion means that different channels travel at approximately the same speed, which makes FWM effect becomes more likely appear because of the so-called phase-matching condition which will be involved in Section 2.4.3.

2.4.2 FWM degradation

For clear explanation, a three-channel WDM system is plotted in Fig 2.5 as an example. Both non-degenerate FWMs and degenerate FWMs are indicated in this figure. The FWM degradation affects system performance in two respects in general. First, during the FWM generation, the signal power will be transferred to the newly generated FWM frequencies, and the decrease of original-channel powers make it more difficult to detect the signals correctly after a long transmission. What's more, a more detrimental consequence is that the FWM components will coincide with the signal channels. For this case, the FWMs act as coherent crosstalk on signal channels and lead to even greater degradation of overall system performance.

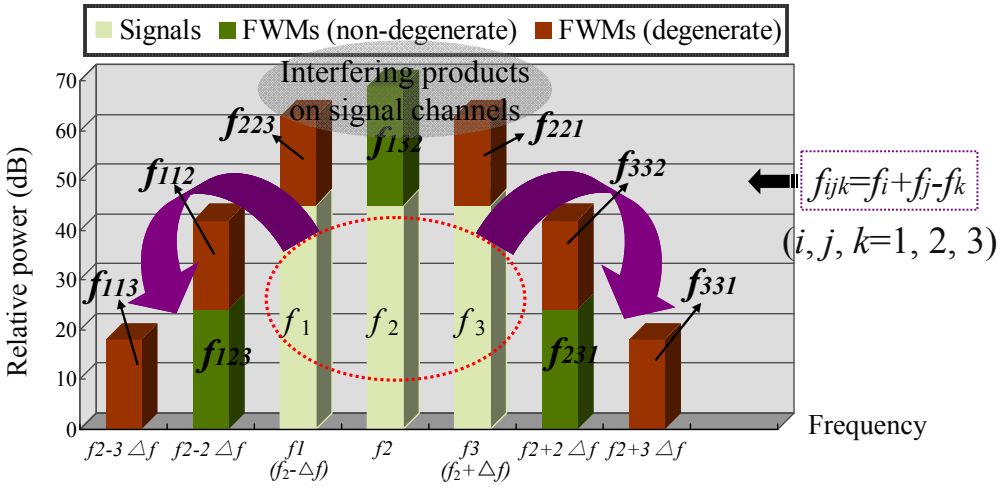

Fig 2.5 FWM generation in a three-channel WDM system

For a N-channel system, the total number of generated FWM products increases to $N^2(N\text{-}1)/2$ [8, 9], some of which fall on existing signal channels. Fig 2.6 plots the number of FWM products versus signal channels. When we assume the number of channels is even and the channels are equally spaced, the number of these FWM components on the m-th signal channel is expressed as [10]:

$$N_{FWM,m} = \frac{N^2}{4} + \frac{Nm}{2} - \frac{m^2}{2} - N + \frac{m}{2} \tag{2.15}$$

Therefore, the total number of the FWM components that fall on the signal channels can be calculated as:

$$\begin{aligned} N_{FWM,total} &= \sum_{m=1}^{N} N_{FWM,m} \\ &= N \cdot \frac{N^2}{4} + \frac{N(1+2+\cdots+N)}{2} - \frac{1^2+2^2+\cdots+N^2}{2} - N \cdot N + \frac{1+2+\cdots+N}{2} \\ &= \frac{N^3}{4} + \frac{N+1}{2} \cdot \frac{N^2+N}{2} - \frac{1}{12} N(N+1)(2N+1) - N^2 \\ &= \frac{1}{3}N^3 - \frac{3}{4}N^2 + \frac{1}{6}N \end{aligned} \tag{2.16}$$

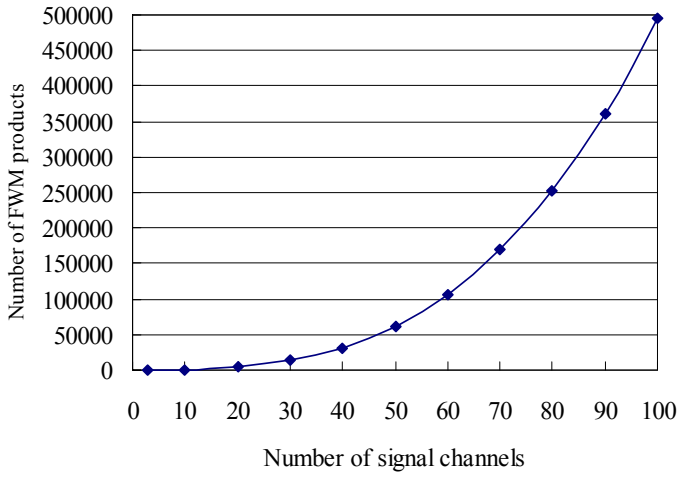

Fig 2.6 Number of FWM products & signal channels

2.4.3 Phase matching condition and FWM efficiency

The FWM is represented by [3]:

$$P_{ijk}(FWM)=\frac{3\varepsilon_0}{2}\chi_3\left[A_iA_jA_k\exp\left(i\theta_+\right)+A_iA_jA_k^*\exp\left(i\theta_-\right)+\cdots\right] \tag{2.17}$$

where ε_0 is the vacuum permittivity, χ_3 is the 3rd order nonlinear susceptibility.

$$\theta_+=\left(\beta_i+\beta_j+\beta_k-\beta_{ijk}\right)z+\left(\omega_i+\omega_j+\omega_k-\omega_{ijk}\right)t \tag{2.18}$$

$$\theta_-=\left(\beta_i+\beta_j-\beta_k-\beta_{ijk}\right)z+\left(\omega_i+\omega_j-\omega_k-\omega_{ijk}\right)t \tag{2.19}$$

where β_p (p=i, j, k, ijk) indicates the propagation constant. To realize the relative phase θ_+ and θ_-, two relationships can be referred to as the phase-matching condition and derived as:

$$\begin{cases}\Delta\beta=\beta_i+\beta_j+\beta_k-\beta_{ijk}=0\Rightarrow\beta_{ijk}=\beta_i+\beta_j+\beta_k\\ \omega_{ijk}=\omega_i+\omega_j+\omega_k\end{cases} \tag{2.20}$$

$$\begin{cases}\Delta\beta=\beta_i+\beta_j-\beta_k-\beta_{ijk}=0\Rightarrow\beta_{ijk}=\beta_i+\beta_j-\beta_k\\ \omega_{ijk}=\omega_i+\omega_j-\omega_k\end{cases} \tag{2.21}$$

It is difficult to realize the condition of (2.19) in optical fiber with high efficiencies since frequency range cannot be as wide as nearly three times of the input angular frequency. As a consequence, the condition of (2.20) is considered as the common case for FWM only and $\Delta\beta$ is named the phase-mismatching factor. The FWM process is completely phase matched when $\Delta\beta=0$. When β is expanded in Taylor series about f_m=c/λ_m, the phase-mismatching factor can be represented as [11, 12, Appendix C]:

$$\begin{aligned}\Delta\beta&=\frac{2\pi\lambda_m^2D_c}{c}\left(f_i-f_k\right)\left(f_j-f_k\right)+\frac{\pi\lambda_m^4}{c^2}\left(\frac{dD_c}{d\lambda}\right)\left(\left(f_i-f_m\right)+\left(f_j-f_m\right)\right)\left(f_j-f_k\right)\left(f_i-f_k\right)\\&=\frac{2\pi\lambda_m^2D_c}{c}\left(f_i-f_k\right)\left(f_j-f_k\right)+\frac{\pi\lambda_m^4}{c^2}\left(f_i-f_k\right)\left(f_j-f_k\right)\left(f_i+f_j-2f_m\right)S\end{aligned} \tag{2.22}$$

And when we set the f_m near to the zero-dispersion frequency f_0, i.e., D_c becomes zero, Eq. (2.21) can be rewritten as:

$$\Delta\beta = \frac{\pi\lambda_0^4}{c^2}\left(f_i - f_k\right)\left(f_j - f_k\right)\left(f_i + f_j - 2f_0\right)S \tag{2.23}$$

By viewing this equation, it is clear that when the zero dispersion frequency is located at the center of two signal frequencies, $\Delta\beta$ becomes zero and FWM components are most prone to be generated.

However, when f_m is far from f_0, the 2nd term can be ignored compared with the 1st term and Eq. (2.21) becomes:

$$\Delta\beta = \frac{2\pi\lambda_m^2 D_c}{c}\left(f_i - f_k\right)\left(f_j - f_k\right) \tag{2.24}$$

The efficiency of FWM depends on the phase-mismatching and can be expressed as:

$$\eta = \frac{\alpha^2}{\alpha^2 + \left(\Delta\beta\right)^2}\left[1 + \frac{4e^{-\alpha L}\sin^2\left(\Delta\beta L/2\right)}{\left\{1 - \exp\left(-\alpha L\right)\right\}^2}\right] \tag{2.25}$$

FWM efficiency takes the maximum value 1 while $\Delta\beta = 0$. For long-haul transmission systems, $e^{-\alpha L} \approx 0$ and therefore Eq. (2.24) becomes:

$$\eta = \frac{\alpha^2}{\alpha^2 + \left(\Delta\beta\right)^2} = \frac{1}{1 + \left(\dfrac{\Delta\beta}{\alpha}\right)^2} \tag{2.26}$$

Assuming the same channel spacing, $\Delta\beta$ can be modified as:

$$\Delta\beta = \begin{cases} \dfrac{2\pi\lambda_0^4}{c^2}\Delta f^2\left(f_i - f_0\right)S & \lambda_m \text{ is near } \lambda_0 \\ \dfrac{2\pi\lambda_m^2 D_c}{c}\Delta f^2 & \lambda_m \text{ is far from } \lambda_0 \end{cases} \tag{2.27}$$

Eq. (2.25) is deduced by substituting Eq. (2.26) into it, and the FWM efficiency is plotted in Fig 2.7. As the CD increases, the FWM becomes less efficient especially for the broader channel spacing.

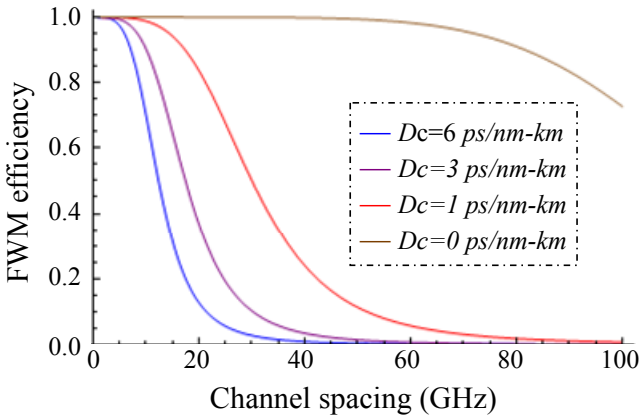

Fig 2.7 FWM efficiency versus channel spacing

2.5 Summary

The basic propagation equation NLSE is introduced in this chapter, which can be viewed as the principle of BP compensation method in Chapter 3. The linear degradation and fiber nonlinear effects, especially FWM and its related factors, such as phase matching condition and FWM efficiency, are explained so as to be utilized for the following discussion.

Reference

[1] G. P. Agrawal, "Lightwave technology: telecommunication systems," WILEY-INTERSCIENCE, Rochester, NY, 2005.

[2] Savera Tanwir, Attenuation- fiber communication systems, http://stanwir.seecs.nust.edu.pk/Lectures/FOCS/

[3] G. P. Agrawal, *Nonlinear Fiber Optics*, San Diego, CA: Academic Press, 2001.

[4] A. Singh, A. K. Sharma, and T. S. Kamal, "Investigation on modified FWM suppression methods in DWDM optical communication system," *Optics Communications*, Vol. 282, No. 3, pp. 392-395, Feb., 2009.

[5] N. H. Adams, “Explorations in modulation formats for nonlinear DWDM fiber optic communications,” Master’s thesis, University of Virginia, Aug., 2001.

[6] B. Xu, “Study of fiber nonlinear effects on fiber optic communication systems,” Ph.D. dissertation, University of Virginia, Aug., 2003.

[7] G. P. Agrawal, *Fiber-optics communication systems*, 3rd Edition, WILEY-INTERSCIENCE, Rochester, NY, 2002.

[8] R.W. Tkach, A. R. Chraplyvy, F. Forghieri, A. H. Gnauck, and R. M. Derosier, “Four-photon mixing and high-speed WDM systems,” *J. Lightw. Technol.*, Vol. 13, No. 5, pp. 841–849, May., 1995.

[9] B. Goebel, and N. Hanik, “Analytical calculation of the number of four-wave mixing products in optical multichannel communication systems,” *Technical report*, pp. 1-4, Oct., 2008.

[10] S. Song, “The number of four-wave mixing (FWM) waves in WDM systems and its applications,” in *Proc. LEOS 2001*, San Diego, CA, USA, Nov. 12-13, 2001, Paper TuS4.

[11] N. Shibata, R. P. Braun, and R. G. Waarts, “Phase-mismatch dependence of efficiency of wave generation through four-wave mixing in a single-mode optical fiber,” IEEE Journal of Quantum Electronics, Vol. QE-23, No. 7, pp.1205-1210, Jul., 1987.

[12] 島田 禎晉，柴田 宣，鳥羽 弘，ブロードバンド時代の光通信技術，新技術コミュニケーションズ，東京，2004.

Chapter3

FWM compensation using backward propagation method

3.1 General configuration of WDM Systems for FWM compensation

First, in order to clarify the FWM compensation feasibilities with BP method, the general configuration of WDM transmission system (total number of channel is *N*) for fiber nonlinearity compensation is shown in Fig 3.1 using digital coherent detection [1]. The compensation is performed in the digital domain after coherent detection. The WDM signals are transmitted over multi spans of fiber. The in-phase and quadrature components of each WDM channel are received by balanced photodetectors (PD). Analog-to-digital (A/D) conversion is followed by DSP to achieve post-compensation and data recovery. The polarization compensation, which is indispensable for coherent detection is not shown in Fig 3.1 for simplicity. Three aspects are emphasized as follows.

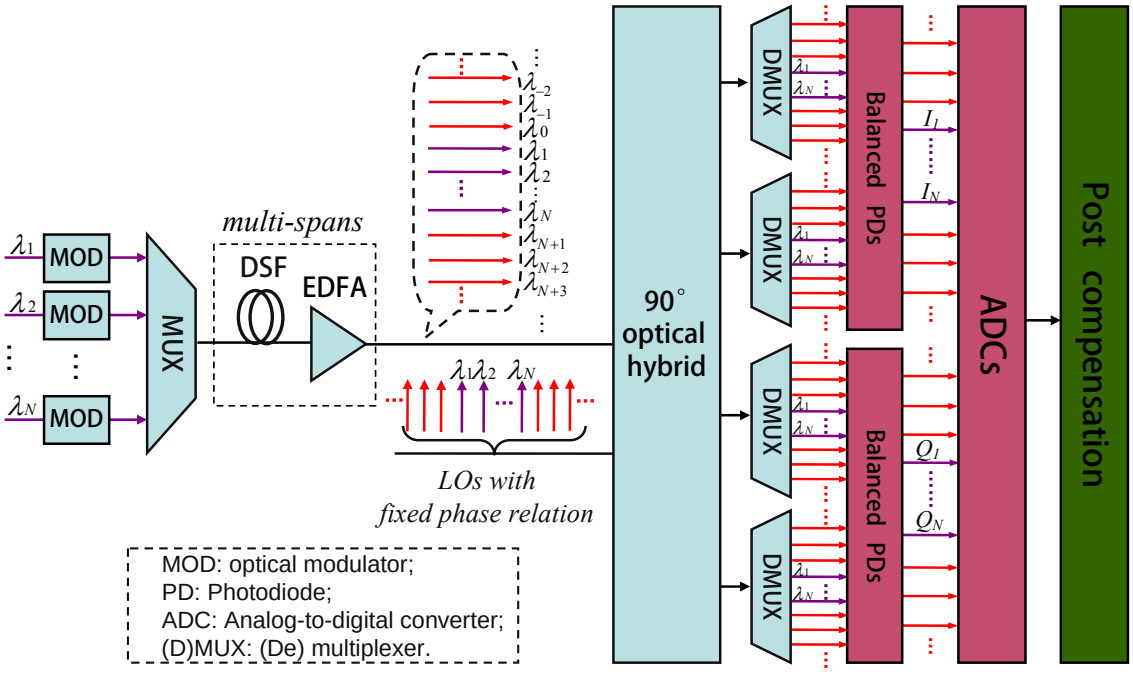

Fig 3.1 Configuration of WDM transmission system for fiber nonlinearity compensation using digital coherent detection. For FWMs: red line; for signals: purple line.

First, the signal distortions induced by fiber nonlinearities such as FWM, XPM are affected by other channels in WDM transmission system. Therefore, data information from other signal channels must be included for their compensation. Especially, FWM impairments compensation requires not only the powers from newly generated channels but also the phase information of each channel.

Additionally, the difficulties of FWM compensation are to convert optical signal information to electrical signal with remaining the phase relationship of individual channels. If individual transmitters and different LOs are employed in coherent detection, the detected electrical signals on different channels will have different phases and cannot be distinguished, i.e., the phase relationship between the received signals becomes random. Therefore, either individual transmitters or LOs should be controlled. If fixed phase relationship can be employed in the coherent detection, the post compensation can be realized.

Last but not least, the received signals are mixed in a 90 degree optical hybrid with a set of local oscillators (LOs), of which N LOs are aligned at the center of the N WDM channels. Additional LOs which are indicated as red color on both sides are also required to be arranged for FWM compensation since some of the FWM information is transferred from original signals to out-band channels (outside the WDM signals).

3.1.1 Digital coherent detection

Digital coherent detection is considered as a promising technique for future high-speed transmission [2-4] because it offers high receiver sensitivity and is capable of compensating for transmission impairments such as CD, polarization-mode dispersion,

and fiber nonlinearities.

On one hand, the digitized signal has the full information of the analog electric field, enabling DSP compensation to have no loss in performance compared to analog impairment compensation performed in either the optical or electronic domain. Digital compensation can be done either at the transmitter prior to up-conversion onto an optical carrier, or at the receiver after the optical signal has been down-converted to the electrical domain.

On the other hand, coherent detection has its own merit superior to direct detection, which will be explained in Section 3.1.2.

3.1.2 Characteristics of coherent detection

Coherent detection, in which a LO is brought in, is utilized rather than direct detection since signal phase will be lost with square-law detection. Additionally, phase coherence of optical carrier plays a significant role in optical communication systems, especially for FWM process. The optical signal is described using complex notation as:

$$E_S = A_S \exp\left[-i\left(\omega_S t + \phi_S\right)\right] \tag{3.1}$$

where A_S is the amplitude, ω_S is the carrier frequency, and ϕ_S is the phase. And the optical field of LO is given as:

$$E_{LO} = A_{LO} \exp\left[-i\left(\omega_{LO} t + \phi_{LO}\right)\right] \tag{3.2}$$

where A_{LO}, ω_{LO}, and ϕ_{LO} is the amplitude, frequency, and the phase of the LO, respectively. Since a PD responds to the optical intensity, the optical power incident at the PD is given by $P = K\left|E_S + E_{LO}\right|^2$, where K represents a constant of proportionality. Therefore, optical power incident at PD is deduced by substituting Eq. (3.1) and Eq. (3.2):

$$P(t) = P_S + P_{LO} + 2\sqrt{P_S P_{LO}} \cos(\omega_{IF} t + \phi_S - \phi_{LO}) \tag{3.3}$$

where $P_S = KA_S^2$, $P_{LO} = KA_{LO}^2$, $\omega_{IF} = \omega_F - \omega_{LO}$ represents the intermediate frequency (IF). Therefore, the photocurrent is described as:

$$I(t) = R(P_S + P_{LO}) + 2R\sqrt{P_S P_{LO}} \cos(\omega_{IF} t + \phi_S - \phi_{LO}) \tag{3.4}$$

where $R = \frac{\eta \lambda e}{hc}$ is the detector responsivity. The corresponding frequency relationship is shown in Fig 3.2.

For heterodyne detection, since $P_{LO} \gg P_S$ in practice and the direct-current term is nearly constant, the alternating-current is substituted for Eq. (3.4) and written as:

$$I(t) = 2R\sqrt{P_S P_{LO}} \cos(\omega_{IF} t + \phi_S - \phi_{LO}) \tag{3.5}$$

From Eq. (3.1), the signal frequency and phase information will be lost after the square-law detection of direct detection, so the FWM impairments compensation cannot be substituted. However, coherent detection conserves the optical field in the detected electrical signal. Amplitude, phase and frequency can be kept well after the detection. For the case of our FWM compensation with BP, the phase information can be utilized correctly.

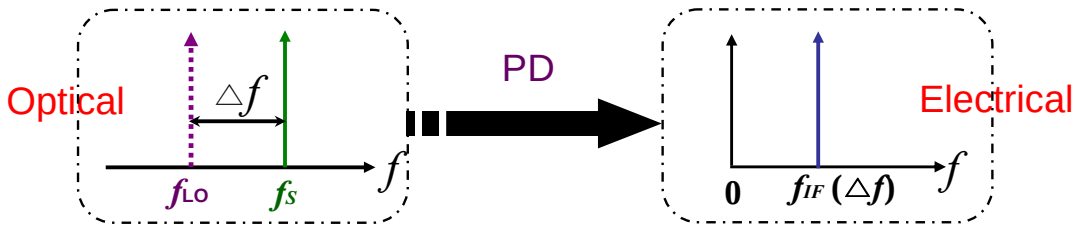

Fig 3.2 Frequency relationship between optical domain & electrical domain

3.1.3 Advantage of DPSK Modulation in transmission systems

DPSK modulation format is preferred in transmission systems, since it has 3-dB receiver sensitivity advantage over on-off-keyed (OOK) for balanced coherent detection

[5-7]. Moreover, the optical power is evenly distributed in every bit slot for DPSK, which reduces bit-pattern-dependent nonlinear effects and the peak power is 3-dB lower for DPSK than for OOK for the same average optical power [7]. This means that DPSK is more resilient and robust to fiber nonlinear effects compared to OOK [7, 8].

It is not surprising, then, that DPSK modulated signals are implemented in recent long-haul WDM transmission systems [8-10]. And we also compare these two formats in our experimental test in the following parts.

3.2 Backward propagation method for FWM impairments compensation

3.2.1 Principles of BP compensation scheme

BP method is an inverse process of signal propagation, which is described by Eq. (2.4). Therefore, the electrical field of BP can be represented as:

$$\frac{\partial A}{\partial z}+\frac{i\beta_2^{'}}{2}\frac{\partial^2 A}{\partial t^2}=i\gamma^{'}\left|A\right|^2 A-\frac{\alpha^{'}}{2}A \tag{3.6}$$

where $\alpha^{'}$, $\beta_2^{'}$, $\gamma^{'}$ are the fiber-loss coefficient, CD parameter and fiber nonlinear parameter, respectively, which are the opposite-sign values with respect to the signal propagation fiber.

BP method is achieved by solving Eq. (3.6). The numerical solution of split-step Fourier method (SSFM) is generally preferred for this purpose, and becomes the core of this method. To explain the BP method of the total-field comprising the compensation for fiber loss, CD and fiber nonlinearity, firstly, it is easier to understand the SSFM in signal propagation if Eq. (2.2) is reformed as:

$$\begin{aligned}\frac{\partial A}{\partial z}&=\left(i\gamma\left|A\right|^2-\frac{i\beta_2}{2}\frac{\partial^2}{\partial t^2}-\frac{\alpha}{2}\right)A\\&=\left(\hat{D}+\hat{N}\right)A\end{aligned} \tag{3.7}$$

where $\hat{D}$ and $\hat{N}$ are the linear (differential) and nonlinear operators and represented

as:

$$\hat{D} = -\frac{1}{2}\alpha - i\frac{\beta_2}{2}\frac{\partial^2}{\partial t^2} \tag{3.8}$$

$$\hat{N} = i\gamma |A|^2 \tag{3.9}$$

In a similar way, the inverse linear and nonlinear operators comprise the BP:

$$\frac{\partial A}{\partial z} = (\hat{N}^{-1} + \hat{D}^{-1})A \tag{3.10}$$

where

$$\hat{D}^{-1} = -\frac{1}{2}\alpha' - i\frac{\beta_2'}{2}\frac{\partial^2}{\partial t^2} \tag{3.11}$$

$$\hat{N}^{-1} = i\gamma' |A|^2 \tag{3.12}$$

The plot of signal propagation and backward propagation is shown in Fig 3.3. The use of the SSFM for BP may be viewed as distributed compensation of the deterministic impairments in the fiber link. Nondeterministic effects become the performance limiting factor when backward propagation is employed. The BP compensation process through SSFM gives us an approximation obtained by assuming that CD and fiber nonlinearities act independently with two main processes [11]:

1. The optical fiber span in BP is divided into several steps which are shown in Fig 3.4. That is to say, BP is considered as the concatenation of *N* steps which correspond to "×N" shown in Fig 3.4 and the specific process is plotted in Fig 3.5.

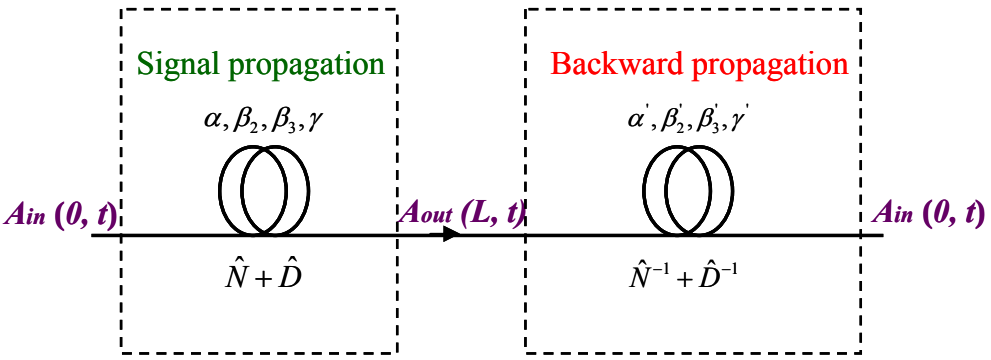

Fig 3.3 Signal propagation & BP in post compensation

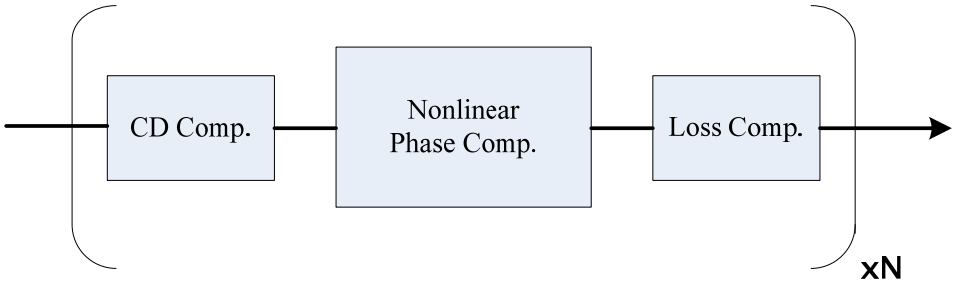

Fig 3.4 BP compensation process

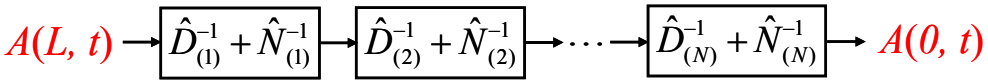

Fig 3.5 Specific process of N steps

2. In each step over a small length of h, the process is carried on by the following equation:

$$\begin{aligned} A(z,t) &= \exp\left(h\left(\hat{D}^{-1}+\hat{N}^{-1}\right)\right)A(z+h,t) \\ &\approx \exp\left(h\hat{D}^{-1}\right)\exp\left(h\hat{N}^{-1}\right)A(z+h,t) \\ &= \mathcal{F}^{-1}\left\{\exp\left(-\frac{\alpha' h}{2}\right)\exp\left(-i\frac{\beta_2'\omega^2 h}{2}\right)\mathcal{F}\left\{A(t,z)\exp\left(-i\gamma'\left|A(t,z)\right|^2 h\right)\right\}\right\} \end{aligned} \tag{3.13}$$

where $\mathcal{F}$ and $\mathcal{F}^{-1}$ stand for the Fourier and inverse Fourier transform. It is obvious that the solution from SSFM converges to the exact solution of Eq. (3.7) as the step size decreases to 0. For perfect BP in practice, very small step size is chosen in order that the maximum nonlinear phase shift does not exceed 0.005 rad (0.294 degree) [12], i.e., $\gamma\left|A(z,t)\right|^2 h < 0.005$ rad. In this case, each step corresponds to approximately the same phase shift induced by nonlinearity, and thereby fiber CD, fiber nonlinearity induced during fiber transmission and optical loss are compensated at each section. The results are assumed to be the exact solutions to NLSE throughout this dissertation. FWM compensation can be achieved through BP method after the above two main processes.

3.2.2 Experiment for investigating compensation performance by BP

In a practical realization of the configuration, a digital circuit should be required by Field-Programmable Gate Array (FPGA) or digital signal processor (DSP) chips, and both analog-to-digital converters (ADC) and DSP will be included in this circuit. However, in our experimental test of the following parts, we introduce the multi-channel oscilloscope as ADC, and then implement an off-line digital signal processing by software (Mathematica) on computer to realize the FWM compensation. And the coherent detection refers to heterodyne detection, and this is applicable to most of our experimental conditions except for Section 3.2.2.2.

In reality, different-wavelength signals should be detected by different receivers and demodulated. These received signals should be fixed phase relationship in IF band. However, this configuration is complicated to realize, since the individual detection includes the optical and electrical devices characteristics and phase relation ambiguity of LOs. In order to demonstrate the compensation possibilities experimentally and clarify the performance of BP compensation only, firstly we focus on a simplified experimental scheme in which all the transmitted wavelengths are received simultaneously by one receiver.

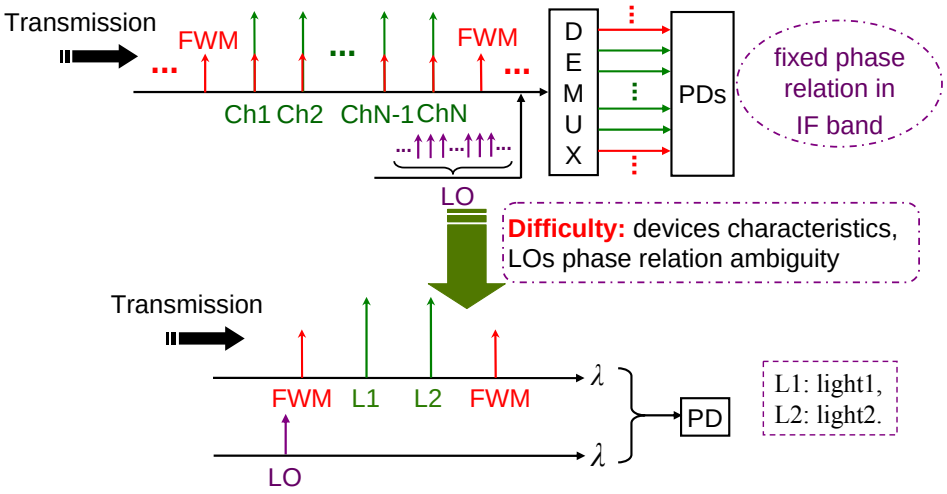

Fig 3.6 Scheme simplification

3.2.2.1 Experiment with heterodyne detection

Here, we investigate the simplified scheme, in which the transmitted lights and the generated FWM components are simultaneously detected by one detector with a LO through coherent detection, and thereby the compensation performance can be studied conveniently. Fig 3.6 shows the idea for the scheme simplification. It is difficult to appraise directly whether there is improvement on the system performance or not for transmitted signals by CW lights in this simplified scheme. However, the compensation performance can be evaluated by the signal-to-FWM crosstalk ratio. The FWM here is referred to the one that falls out of the light frequency, e.g., FWM1 and FWM2 which are shown in Fig 3.7, which is illustrated for a clear explanation of the compensation principle in the simplified scheme. When we consider a three-channel system and assume there is another transmitted light (L3) locating at the frequency of $2f_2$-f_1, the frequency of generated FWM2 (f_{221}) will coincide with L3 by the FWM process and result in degradation on it (Other FWMs are neglected here). If the crosstalk ratio between L2 and FWM2 is improved, that is, the degradation on L3 will be improved by this compensation method for this case. In a similar way, other FWM components that locate at the same frequency with f_1 and f_2 should also be suppressed simultaneously if FWM1 and FWM2 are compensated, because the phase matching condition is realized more completely.

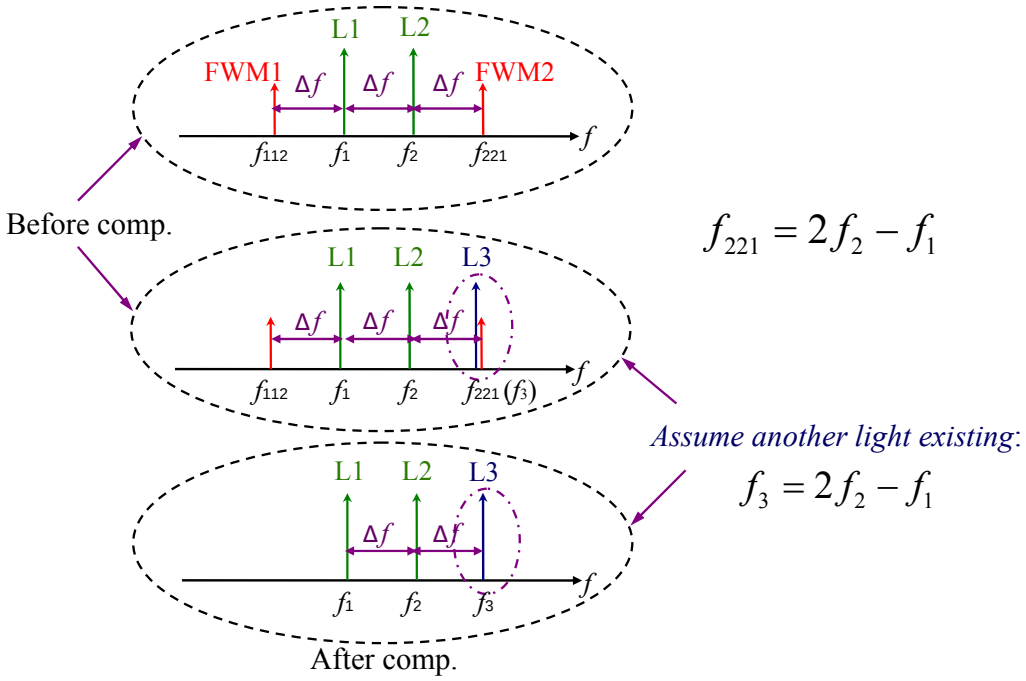

Fig 3.7 Compensation principle in simplified scheme

Figure 3.8 shows the experimental setup with heterodyne detection [13, 14]. Two CW lights whose wavelengths are around 1549nm are used as optical sources. The frequency difference between these two lights is set near 600MHz. The frequency difference between the optical lights and the ZDW of the DSF is less than 100GHz so as to generate FWM components efficiently. Through an optical coupler (OC), the coupled two lights of co-polarization are amplified by an EDFA and transmitted through 20km DSF. FWM components are induced as shown in Fig 3.8(a). Transmitted optical lights and the generated FWMs are detected simultaneously by the heterodyne detection with one LO. The frequency arrangement is given in Fig 3.8(b). The detected coupled lights are received by a photodiode (PD) and sampled with an ADC at a sampling frequency of 20 Gsample/s. The converted signals are processed with off-line digital signal processing (DSP) through BP.

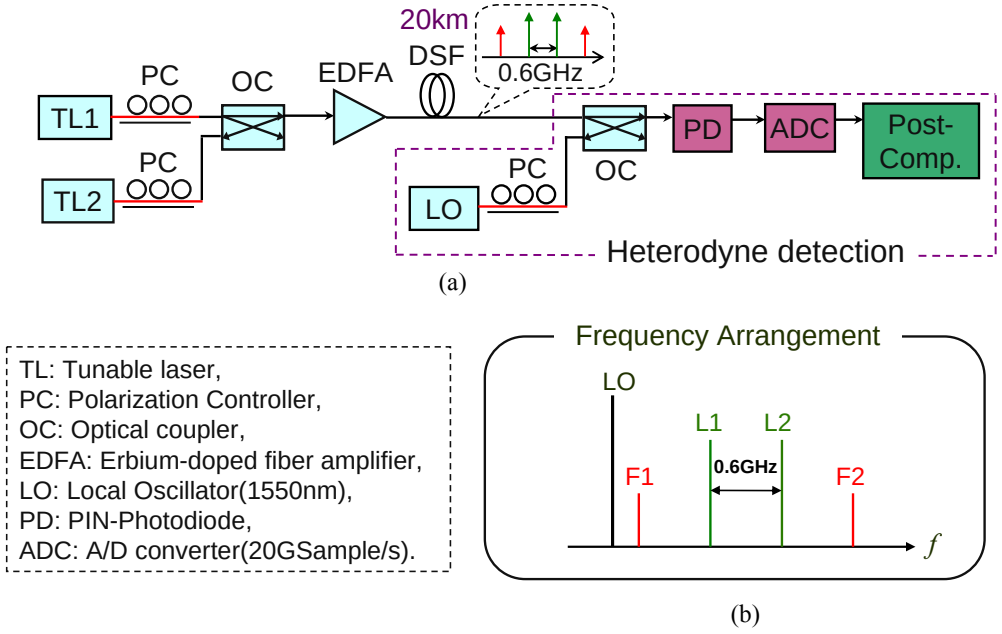

Fig 3.8 Experimental setup for jointly detected lights with the heterodyne detection: (a) Experimental setup; (b) Frequency arrangement.

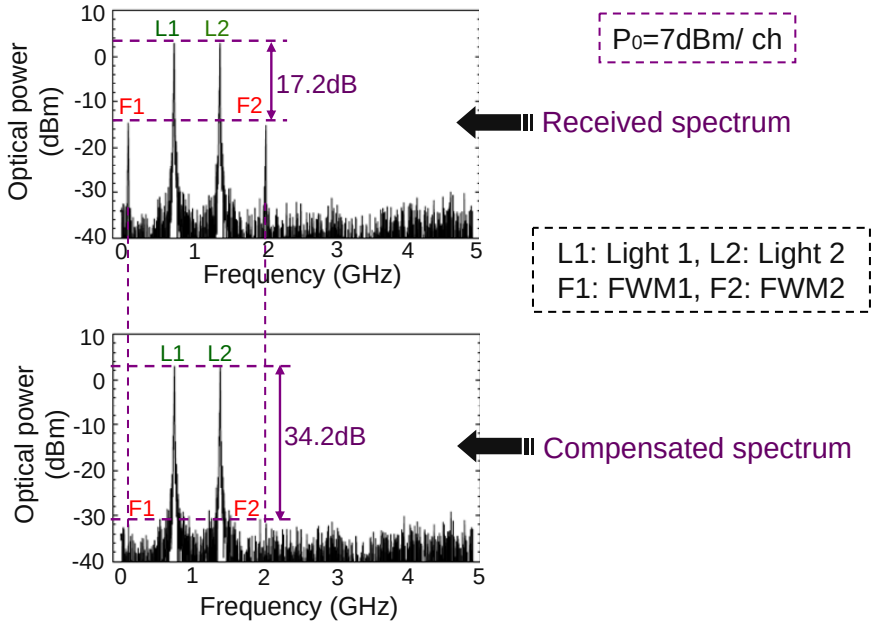

Fig 3.9 Spectra w/o compensation & w/ compensation at P_0=10dBm

We increase the fiber input power to generate more efficient FWM. Fig 3.9 shows the spectra at the total fiber input power P_0 of 10dBm. The signal-to-FWM crosstalk ratio becomes 17.2dB before compensation, whereas the FWM powers diminish to the noise

level after the post-compensation and the signal-to-FWM crosstalk ratio is improved to more than 34dB. These results mean that by heterodyne detection the induced FWM components can be suppressed effectively, and the degradation after compensation becomes negligible [15].

3.2.2.2 Experiment with Phase diversity detection

The possibilities of the electrical post-compensation through BP with phase diversity detection are confirmed definitely in this dissertation [16].

Evidently, a “zero IF” receiver that avoids the need for phase locking is the most desirable [17, 18]. The advantage of baseband processing can be retained by employing phase diversity detection which requires quite low bandwidth. The frequency relationship of heterodyne detection and phase diversity detection between signals and FWMs are shown in Fig 3.10. In the two-phase case, phase diversity is constructed by coupler and polarization beam splitter (PBS). Signals and LO light are combined, and the outputs are converted into two mutually orthogonal baseband signals then received by I-arm with the same phase and Q-arm with 90 degree phase difference. This is, therefore, named 90° hybrid.

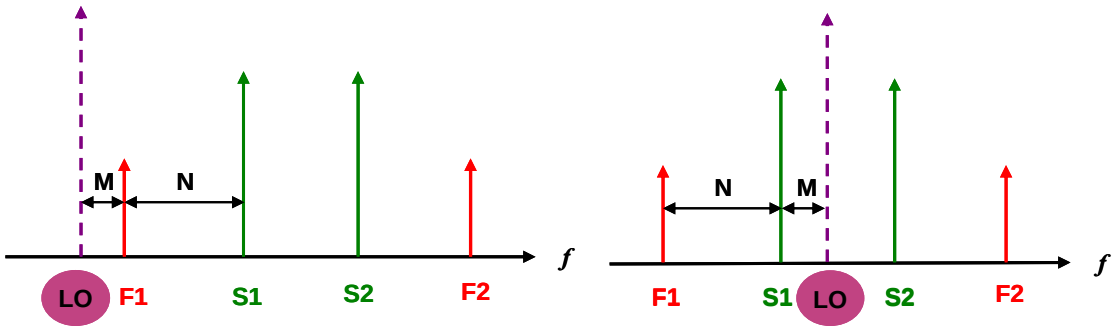

(a1) (b1)

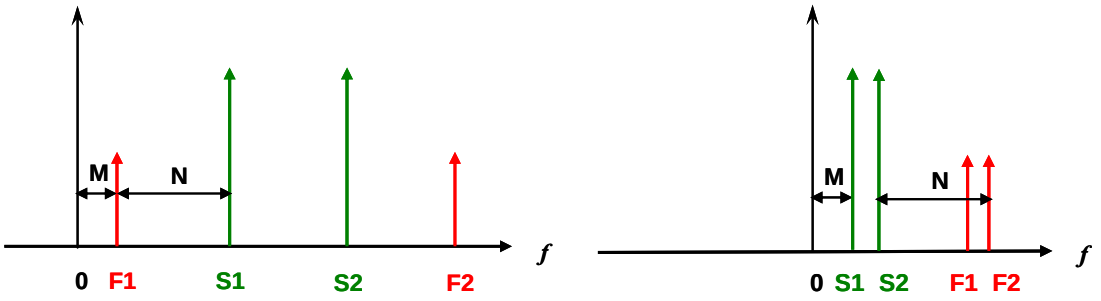

(a2) (b2)

Fig 3.10 Frequency relationship of heterodyne and phase diversity between signals and FWMs: a1) and a2) are the frequency relationship for heterodyne detection, a1) optical domain, a2) electrical domain; b1) and b2) are the frequency relationship for phase diversity detection, b1) optical domain, b2) electrical domain.

The I-arm signal is described as:

$$\begin{aligned} I &= R_I\left(\sum_0^{n+1} E_i e^{i\omega_i t} + E_l e^{i\omega_l t}\right)\left(\sum_0^{n+1} E_i^* e^{-i\omega_i t} + E_l^* e^{-i\omega_l t}\right) \\ &\simeq R_I \sum_0^{n+1} E_l E_i^* e^{i(\omega_i-\omega_l)t} + R_I \sum_0^{n+1} E_l E_i^* e^{-i(\omega_i-\omega_l)t} \end{aligned} \tag{3.14}$$

where R_I is the responsivity of the I-arm photo-detector, E_i (i=1, 2, …, n) are the electrical field of the signals, E_0 and E_{n+1} are the electrical field of induced FWMs, E_l is the electrical field of LO, ω_i and ω_l corresponds to the optical angular frequency of the signals and LO, respectively, * denotes complex conjugation. In this calculation, we assume that $|E_i|^2 \ll |E_l|^2$.

The Q-arm signal is described as:

$$\begin{aligned} Q &= R_Q\left(\sum_0^{n+1} E_i e^{i\omega_i t} + E_l e^{i\omega_l t + i(\pi/2+\varphi)}\right)\left(\sum_0^{n+1} E_i^* e^{-i\omega_i t} + E_l^* e^{-i\omega_l t - i(\pi/2+\varphi)}\right) \\ &\simeq R_Q \sum_0^{n+1} E_i E_l^* e^{i(\omega_i-\omega_l)t - i(\pi/2+\varphi)} + R_Q \sum_0^{n+1} E_l E_i^* e^{-i(\omega_i-\omega_l)t + i(\pi/2+\varphi)} \\ &= R_Q \sum_0^{n+1} (-i) E_i E_l^* e^{i(\omega_i-\omega_l)t - i\varphi} + R_Q \sum_0^{n+1} i E_l E_i^* e^{-i(\omega_i-\omega_l)t + i\varphi} \end{aligned} \tag{3.15}$$

where R_Q is the responsivity of the Q-arm photo-detector.

Therefore, the combined signal can be represented as:

$$\begin{aligned} I+iQ &= \left(R_I + R_Q e^{-i\varphi}\right)\sum_0^{n+1} E_i E_l^* e^{i(\omega_i-\omega_l)t} + \left(R_I - R_Q e^{i\varphi}\right)\sum_0^{n+1} E_l E_i^* e^{-i(\omega_i-\omega_l)t} \\ &= R_I\left(1+re^{-i\varphi}\right)\sum_0^{n+1} E_i E_l^* e^{i(\omega_i-\omega_l)t} + R_I\left(1-re^{i\varphi}\right)\sum_0^{n+1} E_l E_i^* e^{-i(\omega_i-\omega_l)t} \end{aligned} \tag{3.16}$$

where $r = R_Q / R_I$.

If r=1 and $\varphi=\pi$, the 1st term is eliminated. And the other way round, if r=1 and φ=0, the 2nd term vanishes. The frequency difference of combined signal is the same as optical domain. By applying the BP method, the fiber nonlinearity can be compensated. The tolerance of amplitude and phase is investigated here. If the 2nd term is considered to be eliminated, the suppression ratio is defined as:

$$S_r = \left|\frac{1+re^{-i\varphi}}{1-re^{i\varphi}}\right| \tag{3.17}$$

If we assume φ=0, or r=1, it is deduced that

$$\frac{S_r-1}{S_r+1} \le r \le \frac{S_r+1}{S_r-1}, \text{ or } \; -2\tan^{-1}\frac{1}{S_r} \le \varphi \le 2\tan^{-1}\frac{1}{S_r} \tag{3.18}$$

For instance, when $S_r = \sqrt{1000}$ which corresponds to the suppression of 30dB, r should be 1 ± 0.065 and $-0.063 \le \varphi \le 0.063$. Therefore, more than 4bit resolution of AD converter is required. And likewise, if the 1st term is considered to be removed, the suppression ratio is defined as:

$$S_r = \left|\frac{1-re^{i\varphi}}{1+re^{-i\varphi}}\right| \tag{3.19}$$

If we assume $\varphi=\pi$, or r=1, and $S_r = \sqrt{1000}$, r should be 1 ± 0.065 and $\pi - 0.063 \le \varphi \le \pi + 0.063$.

Figure 3.11 shows the experimental setup for FWM compensation with the phase diversity detection. In this experiment, two tunable lasers (TL) with the wavelengths around 1549nm are used as optical sources without modulation. The frequency difference is set nearly 0.5GHz. These two optical sources are controlled to the same optical power and polarization by adjusting polarization controllers (PC). The coupled lights are amplified, and transmitted through the 20km DSF. The transmitted lights and generated FWMs pass through an optical filter (OF) with 0.35nm bandwidth to reject the optical amplified spontaneous emission (ASE) noise. They are detected by the phase diversity detection with one LO, whose frequency is set between the frequencies of two lights. The coupled lights go through a PBS and are received simultaneously by two PDs which are indicated "I-arm" and "Q-arm" in Fig 3.11. The output signals are sampled at a rate of 10 Gsample/s by an ADC. The converted signals are processed with off-line digital signal processing to realize the post-compensation.

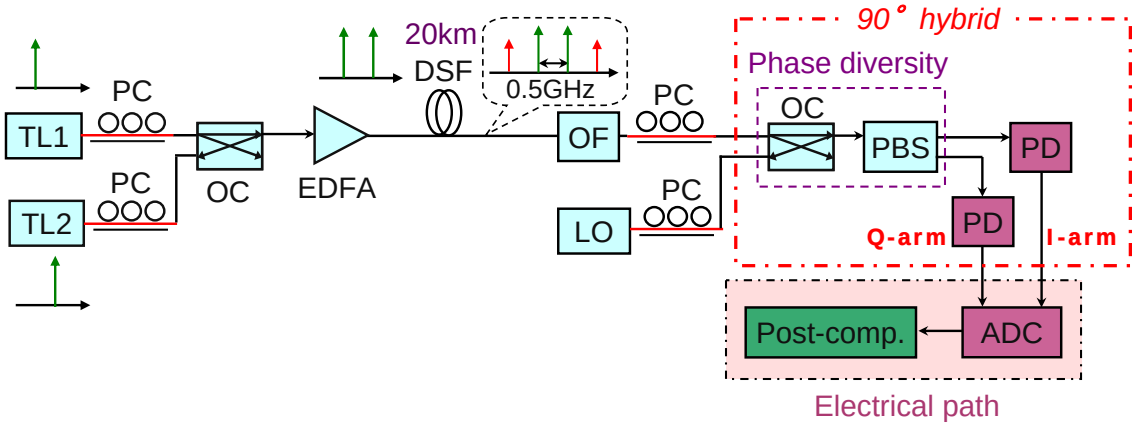

Fig 3.11 Experimental setup for jointly detected lights with phase diversity detection. LD: Tunable laser, PC: Polarization controller, OC: Optical coupler (1:1), EDFA: Erbium doped fiber amplifier, DSF: Dispersion-shifted fiber, OF: optical filter, LO: Local oscillator (1549nm), PBS: Polarization beat splitter, PD: PIN-Photodiode, ADC: A/D converter (10GSample/s).

In electrical post-compensation, it is necessary to satisfy the condition of $\varphi=\pi$ or $\varphi=0$

as mentioned above, in order that the first term or the second term in Eq. (3.14) can be eliminated by adding the signals of I-arm to Q-arm by a 90-degree phase hybrid. However, it is difficult to make one term vanish completely, and thereby it is convenient to adjust amplitude and phase difference by off-line signal processing.

The received spectrum of I-arm with total input power of 6dBm is shown in Fig 3.12. The sampling rate is 10GS/s and the number of sample points is 4096 which corresponds to 0.4μs. Therefore, the frequency difference of each point corresponds to 2.44MHz. Two peaks around 1GHz are the two optical CW lights. Another two peaks around 4GHz are the generated powers induced by FWM process. 1st and 2nd terms are indicated in Fig 3.12.

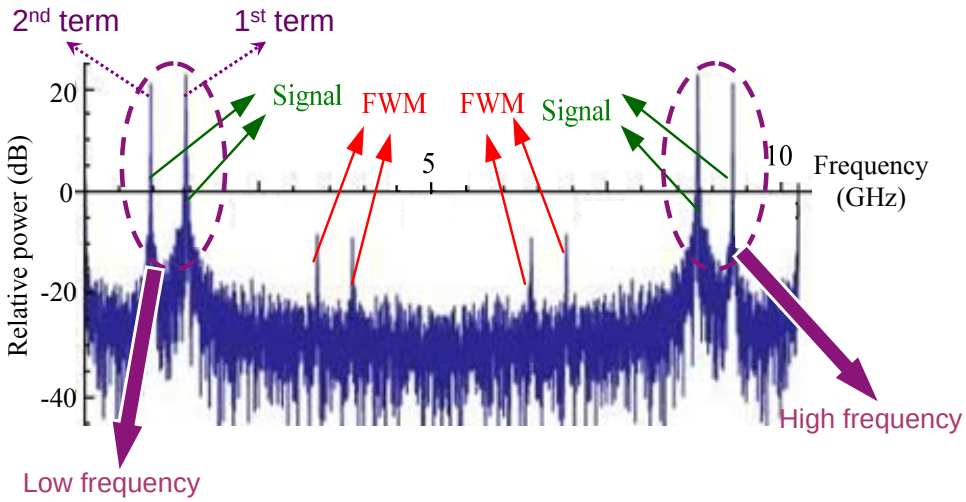

Fig 3.12 Received spectrum of I-arm.

We make the peak of 1st term suppressed by adjusting the amplitude and phase as Eq. (3.19). The suppression is measured by the difference between the values of peak level in low frequency region and high frequency region. When r=1 and $\varphi=\pi$, 1st term can not vanish completely. The suppression dependence on amplitude and phase is shown in Fig 3.13 (a) and (b), respectively, by adjusting a minute deviation. Two curves in the figures correspond to low frequency and high frequency, respectively. In order to make sure

that 1st term of both low frequency and high frequency can be suppressed simultaneously, the value of the intersection point is chosen: r=1.0, φ=3.2.

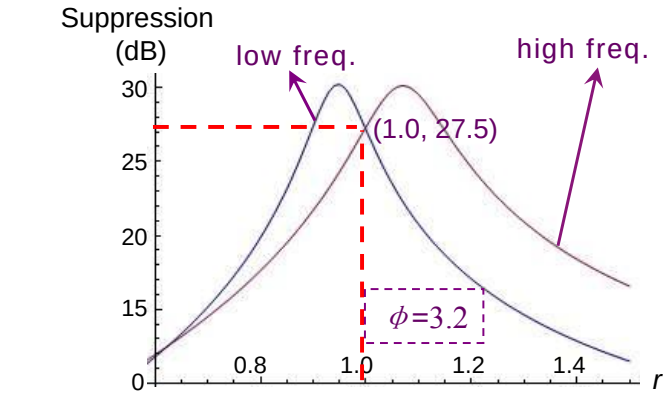

(a)

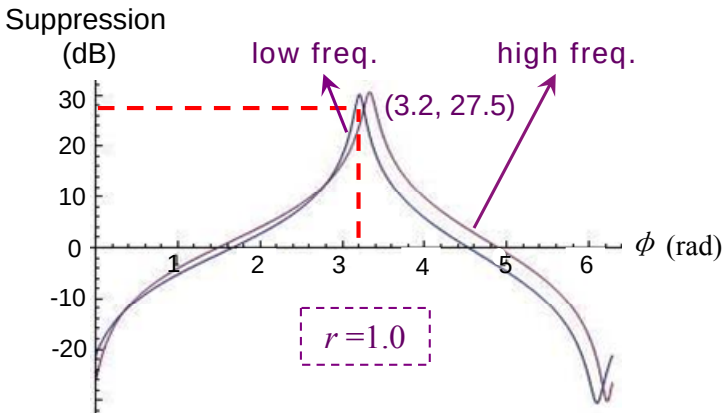

(b)

Fig 3.13 Suppression dependence on amplitude & phase: (a) amplitude; (b) phase.

The suppressed spectrum at r=1.0, φ = 3.2 is shown in Fig. 3.14(a) and compensated spectrum is given in Fig 3.14(b). The FWM components are diminished after compensation and the power difference between the signal and FWM is improved from 29dB to 37dB. Actually, this power difference can be increased by changing above parameters at the expense of the appearance of other signals near FWM, which is also likely to influence the performance of WDM systems. After compensation, the other unavoidably appeared components that are relatively far from signals can be rejected by low pass filter.

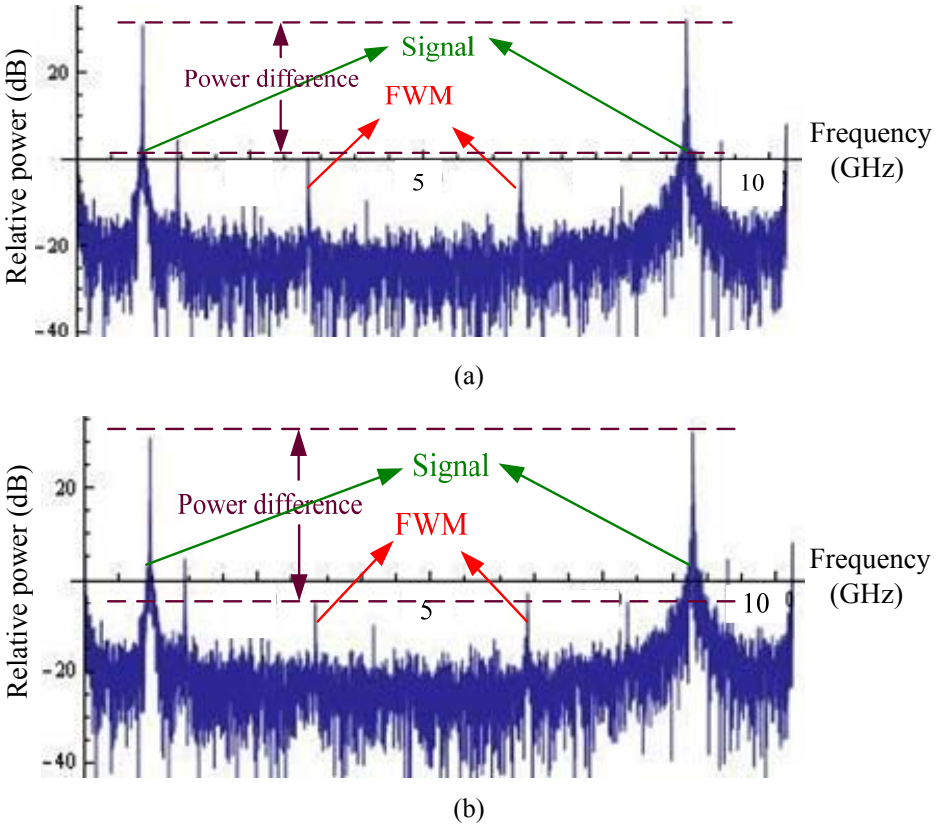

Fig 3.14 Spectrum of *I*+*iQ*: (a) without compensation; (b) with compensation.

Figure 3.15 shows the power difference between transmitted lights and FWM powers (signal-to-FWM crosstalk ratio). It is obvious that the power difference decreases gradually with the fiber input power increases. By compensation, more than 7dB improvement of power difference is obtained when the fiber input power increases from 2dBm and 11dBm. In the low power region, FWM power is very low and thereby it is difficult to implement the compensation since FWMs are liable to be confused with noise. However, these FWM components don't degrade the system performance. In the higher power region, FWM powers cannot be compensated perfectly. The reasons for this are considered that other FWM powers should be included in this compensation, but these FWM powers are out of receiver bandwidth or image components. However, after compensation, the power difference is improved to 30dB, so the FWM powers

don't degrade the system performance.

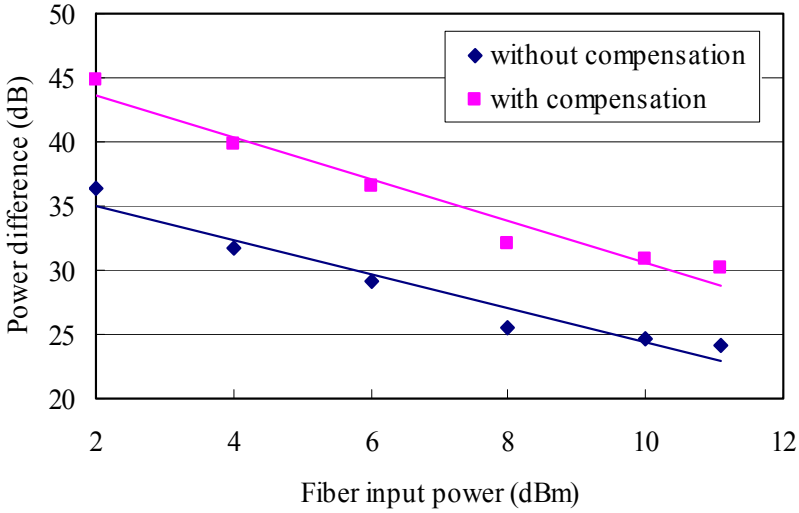

Fig 3.15 Power difference between transmitted lights and FWMs

3.3 FWM compensation using individual receivers and phase modulated LOs

3.3.1 Phase-locked LOs for our experimental condition

Here we consider the compensation for FWM components by using individual PDs. In this part, our purpose is to verify the feasibility of the phase-locked LOs for individual coherent detectors, and to directly observe the degradation improvement on modulated signals. The compensation performance is evaluated by both signal-to-FWM crosstalk ratio as well as eye penalty. The configuration of our experimental condition in WDM transmission system is given in Fig 3.16. Balanced receivers are not utilized here due to the limitation of our experimental devices. The difficulties of FWM compensation for individual channels are to convert optical signal information to electrical signal with remaining the phase relation of individual channels. If individual transmitters and LOs are used, the phase relationship of the received IF signals becomes random. Therefore, one of them should be controlled. We modulate a LO light using a phase modulator so as to realize fixed phase relationship among LOs, which is named phase locked LOs,

then the relationship of the individual IF signals can be kept unchanged when coherent detected. This is the prerequisite for FWM nonlinear compensation by electrical signal processing. The combined individual detected signals are compensated using the previously developed compensation method.

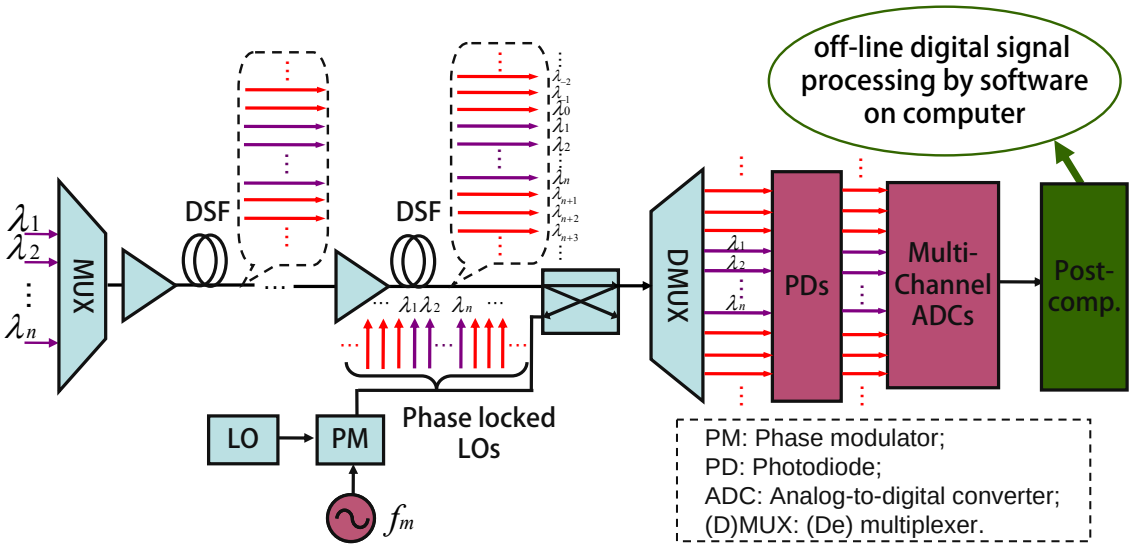

Fig 3.16 Configuration of our experimental condition with BP method in WDM transmission system

The phase modulation signal can be represented as [19, 20]:

$$\begin{aligned} E_{LO} &= E_{LO}\cos\left(\omega_{LO}t + m_p \sin\omega_m t\right) \\ &= E_{LO}\left\{\cos\omega_{LO}t\cdot\cos\left(m_p\sin\omega_m t\right) - \sin\omega_{LO}t\cdot\sin\left(m_p\sin\omega_m t\right)\right\} \end{aligned} \tag{3.20}$$

where ω_m is equal to the channel spacing between each channels in above configuration, m_p is modulation index, and

$$\begin{cases} \cos\left(m_p\sin\omega_m t\right) = \sum_{n=-\infty}^{\infty} J_n\left(m_p\right)\cos n\omega_m t \\ \sin\left(m_p\sin\omega_m t\right) = \sum_{n=-\infty}^{\infty} J_n\left(m_p\right)\sin n\omega_m t \end{cases} \tag{3.21}$$

where $J_n(m_p)$ is Bessel function of the 1st kind, which is plotted in Fig 3.17 while n=0, 1, 2, 3, 4. When $n<0$, $J_{-n}(m_p)=(-1)^n J_n(m_p)$. Therefore, the Eq. (3.20) can be rewritten as:

$$E_{LO} = E_{LO} \sum_{n=-\infty}^{\infty} J_n\left(m_p\right)\cos\left(\left(\omega_{LO} + n\omega_m\right)t\right) \tag{3.22}$$

Therefore, the phase relation between each sideband of LOs can be plotted in Fig. 3.18, and thereby the fixed phase relationship of individual IF signals can be achieved after coherent detection.

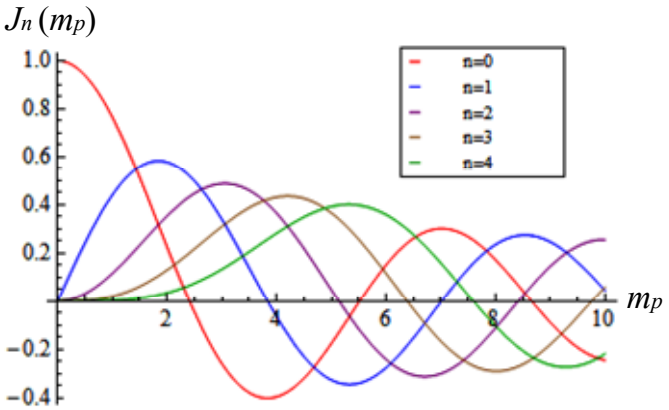

Fig 3.17 Bessel function of the 1st kind

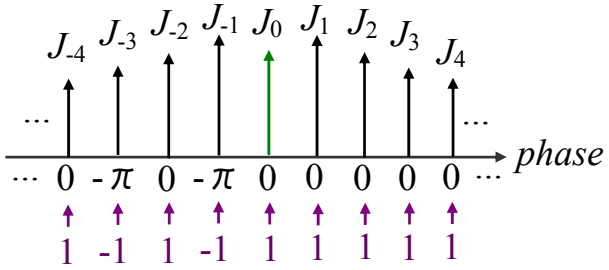

Fig 3.18 Phase relation between each sideband of LOs

3.3.2 Experiment of ASK modulated transmission for two-channel degenerate case

Firstly, we obverse the compensation performance of degenerate FWM by two-channel case of ASK modulation [21], since ASK is more vulnerable to FWM nonlinear effect and the transmitted signals are more liable to be degraded in this two-channel system. And the purpose in this part is to verify the feasibility of the phase-locked LOs for individual coherent detectors, and to evaluate the FWM degradation improvement by signal-to-FWM crosstalk ratio. Therefore, both signals as well as FWM components are

detected.

Figure 3.19 shows the experimental setup for inter-channel FWM compensation with coherent detection. Two TL with 23-GHz channel spacing are employed as WDM signal sources whose wavelengths are 1549.68nm and 1549.86nm, respectively. These two channel signals are ASK modulated using two Mach-Zehnder intensity modulators (MZM) driven at a bit rate of 0.8Gbps by individual pulse pattern generator (PPG) with a pseudo-random bit sequence (PRBS) of 2^{11}-1 length. The modulated signals are combined by a 3-dB OC, amplified by an EDFA, and subsequently fed to a 20-km DSF whose zero-dispersion wavelength is nearly 1549nm. PC is inserted appropriately that both channels are co-polarized. The transmitted signals and the induced FWM components are detected by each individual heterodyne detection receiver. The LO is modulated by a $LiNbO_3$ phase-modulator (LN-PM), so the phase relationship between all of the phase-modulated LOs can be kept constant when the IF signals are detected by each individual channel. The carrier wavelength is set near Sig2 to ensure the IF is about 1.6-GHz for heterodyne detection. The modulating frequency f_m is set as 23-GHz and the modulation index m_p is adjusted to about 1.75, so as to achieve sideband power as close to equivalent as possible if n=0, 1, 2 is involved only, which is obviously seen from Fig 3.17.

The modulated LOs are amplified and then coupled with the transmitted signals and FWM components by 3dB OC. These coupled signals are then split by the optical demultiplexer which consists of a Mach-Zehnder interferometer (MZI), optical circulator, and a couple of fiber Bragg gratings (FBG) with 3-dB bandwidth of 0.18nm. The configuration of the optical demultiplexer is given in Appendix E. The optical spectra of modulated LOs, the signals and FWMs after demultiplexer are illustrated in

Fig 3.20. The received signals are sampled by four ADC at a rate of 5Gsample/s.

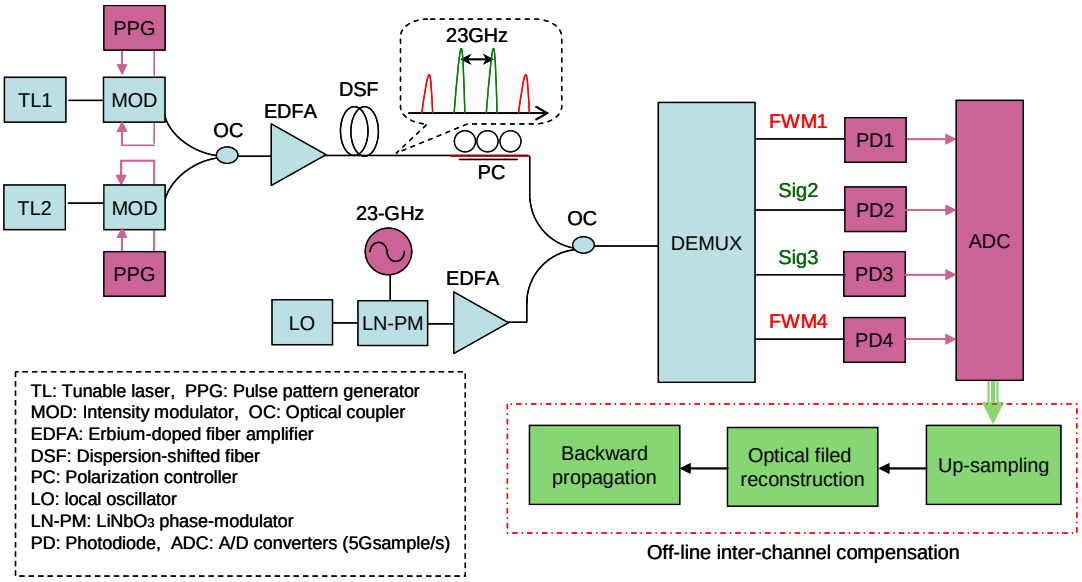

Fig 3.19 Experimental setup

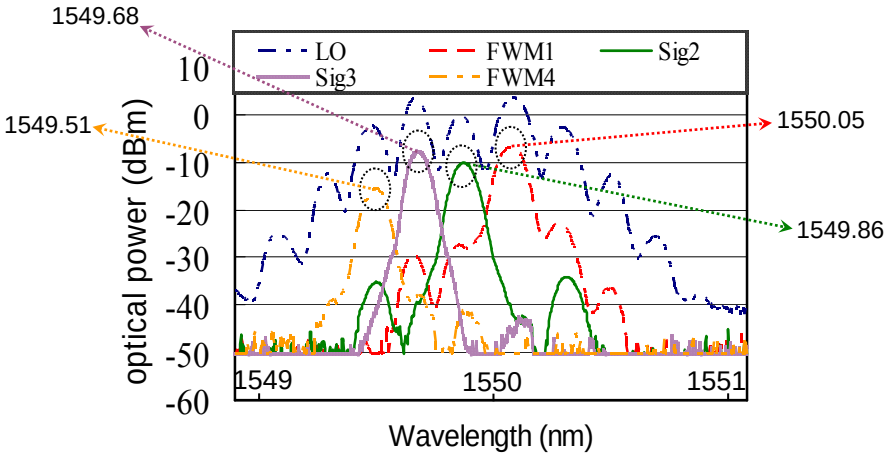

Fig 3.20 Optical spectrum of LO and demultiplexer

The converted signals are processed by an off-line calculation, which are shown in Fig 3.21. Each of the ASK signals/ FWMs are first filtered by Hilbert filters to eliminate half of the signals which are in higher-frequency and up-sampled to a total bandwidth of 4×46-GHz. The up-sampled signals are combined with the channel spacing of 23-GHz for optical field reconstruction. The phase differences between the LO sidebands are considered when the received signals are combined. The individual optical powers are

compensated to the fiber output powers which are measured before combining LOs. The combined signals are post-compensated through BP introduced above.

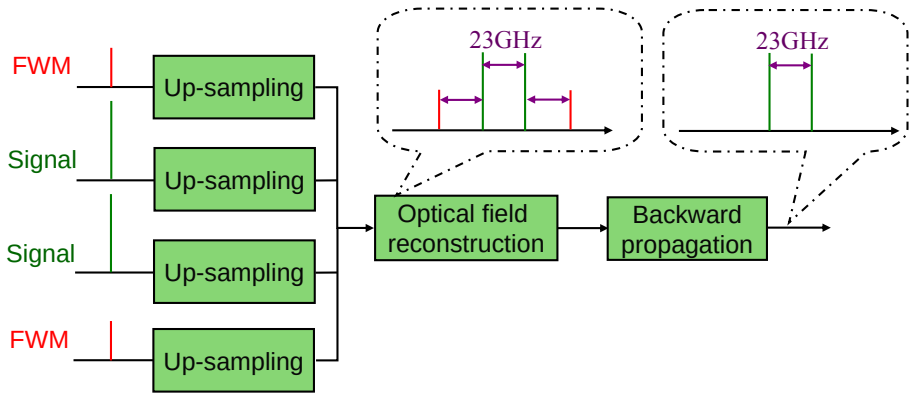

Fig 3.21 Off-line compensation process

Figure 3.22(a) and (b) give the spectra without and with compensation, respectively, for ASK signal when P_0=6.5dBm/ch. The inset in this figure indicates the spectrum of IF signals before up-sampling. By compensation, the signal-to-FWM crosstalk ratio is increased from 16.7dB to more than 34dB. New components, with the same channel spacing of 23GHz, are induced by the inverse nonlinearities from BP after compensation. However, the crosstalk ratio between signals and new components is below 30dB.

While the electrical post-compensation is implemented for individual channels, the phase relationship between each channel is considered. From Fig 3.18, the phases of each detected channels are $-\pi$, 0, 0, 0, respectively, since the carrier frequency of LO is set near f_2 in the experiment. $-\pi$ should be adjusted to 0 to restore the phase relation between each original channel for the compensation. Some slight deviation on phase may be induced by the imperfect delay adjustment, which can be corrected by our off-line process.

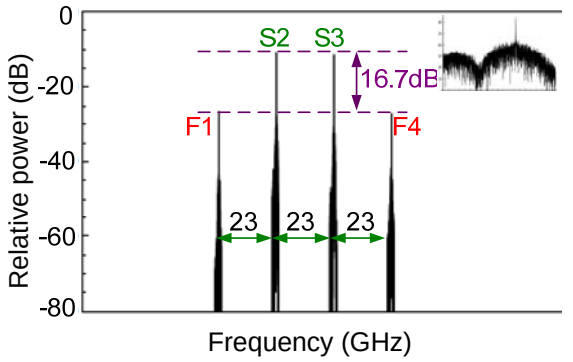

(a)

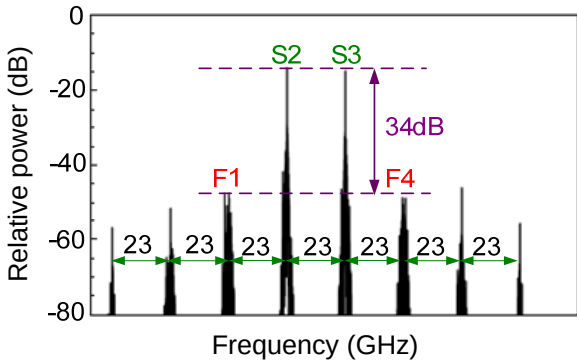

(b)

Fig 3.22 Spectra (a) w/o comp; (b) w/ comp.

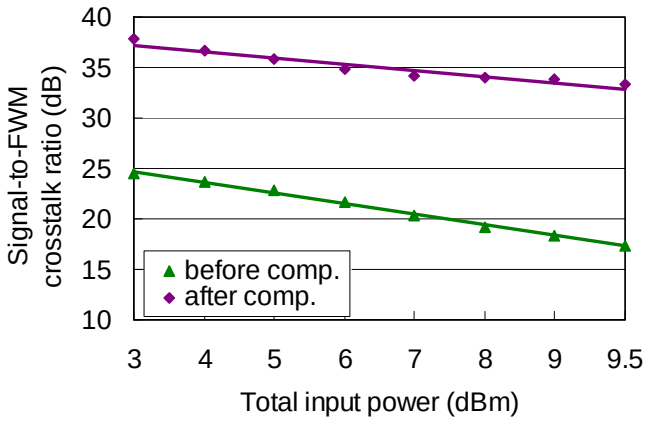

Fig 3.23 Signal-to-FWM crosstalk ratio versus optical input power

Figure 3.23 plots the signal-to-FWM crosstalk ratio as a function of launched power for transmitted ASK-modulated signals. The signal-to-FWM ratio gradually decreases as P_0 increases from 3dBm to 9.5dBm for each channel. There is more than 12.5dB

improved after compensation and the signal-to-FWM crosstalk ratio becomes more than 32dB after compensation in this range of the fiber input power. The degradation on system performance can be neglected.

3.3.3 Experiment of DPSK modulated transmission for three-channel non-degenerate case

In this part, we directly observe the degradation improvement on transmitted DPSK modulation signals on three-channel non-degenerate case. The compensation performance is evaluated by improved eye penalty after demodulation.

By longer transmission or higher optical input power, more FWM components will be accumulated (more than $N^2(N\text{-}1)/2$ for N-channel system) by the frequency mixing from not only the transmitted signals but also other generated FWMs, which is illustrated in Fig 3.24(a). We measure the optical spectra with multi-repeaters and higher optical power in Fig 3.24(b) and (c), respectively. In these cases, more detectors should be required for FWM compensation on signal channels. However, in order to demonstrate the compensation possibility by detecting only signal channels, the optical power can be controlled not too high and no more repeaters are inserted to ensure the FWM products are generated by the frequency mixing from transmitted signals only.

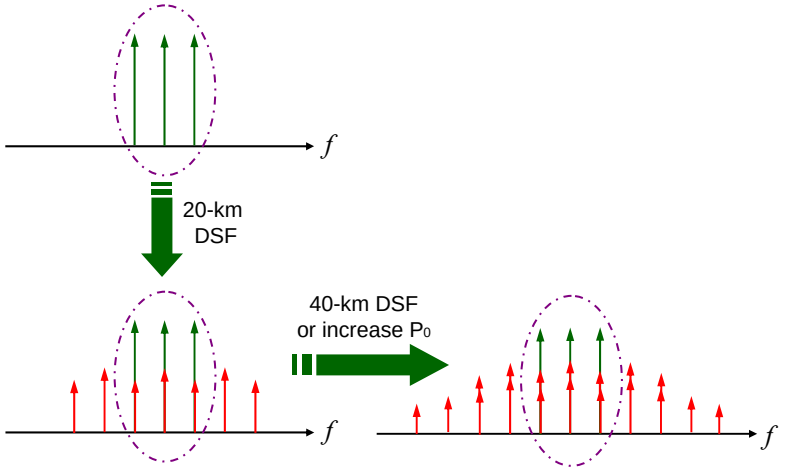

(a)

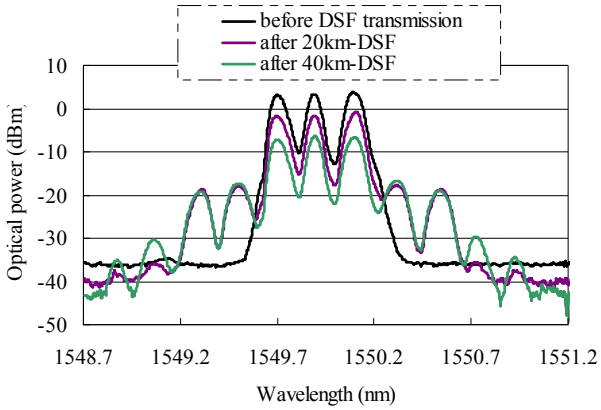

(b)

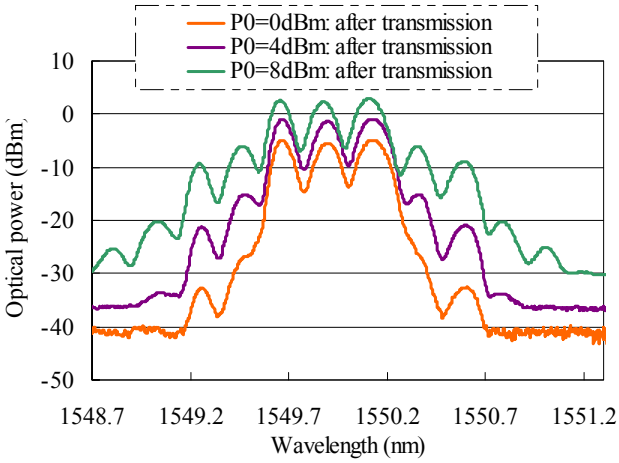

(c)

Fig 3.24 FWM generation: (a) Process of more FWM generation; (b) spectra with multi-repeaters; (c) spectra with higher optical power.

The configuration of experimental setup is given in Fig 3.25 which is nearly similar as previous experiment except that three optical sources are utilized and the transmitted signal channels are detected only for compensation. DPSK modulation is utilized since it is more adequate due to the influence of SBS effect. (The measurements of CW light, ASK and PSK modulated optical signals under our experimental situation are shown in Appendix G.) By transmission, both partially degenerate FWM and completely non-degenerate FWM appear simultaneously on signal channels.

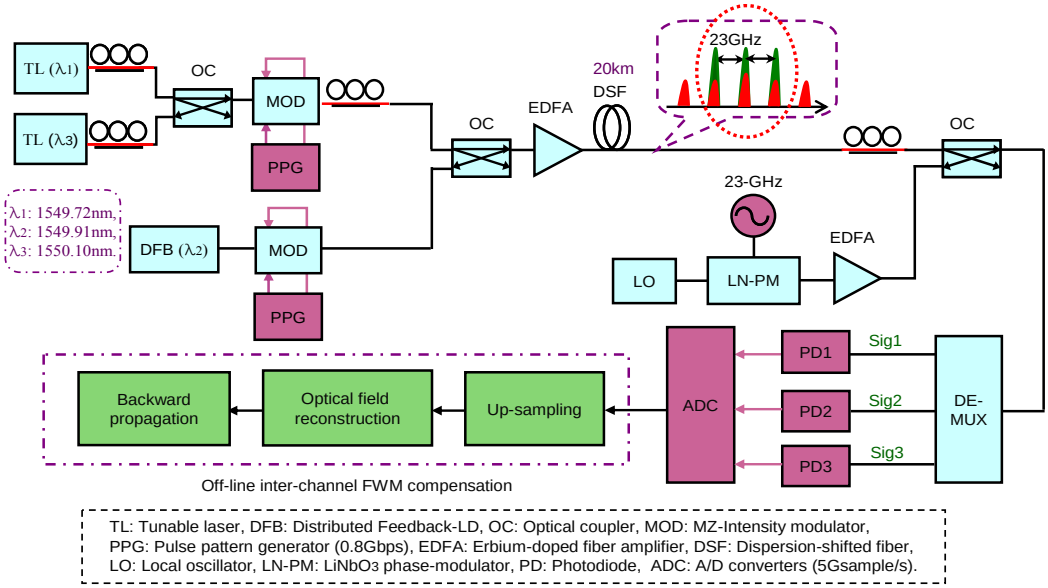

Fig 3.25 Experimental setup

The center channel is degraded severely due to the frequency mixing from non-degenerate case of FWM. Figure 3.26 gives the electrical spectra of the IF signals which are measured by multi-channel oscilloscope. The purple, red, green spectra denote the three detected signal channels, respectively. The brown denotes the spectrum of FWM components when another PD is used for viewing the frequency relation. In order to observe the FWM components clearly, the frequency of center-channel signal (red signal) is adjusted to f+2Δ in the electrical domain as shown in Fig 3.26 (a). By frequency adjustment of the red signal f_2', the FWM components f_{223}', f_{132}', f_{221}' locate at f+3Δ, f-2Δ, f+5Δ, respectively. The signals and induced FWMs power influenced by polarization can be observed clearly and controlled easily. The components f_{223}', f_{132}', f_{221}' will fall in f_1, f_2, f_3 respectively when the red signal is adjusted to the center frequency f, while the components of f_{123} and f_{112} coincide with each other as shown in Fig 3.26 (b).

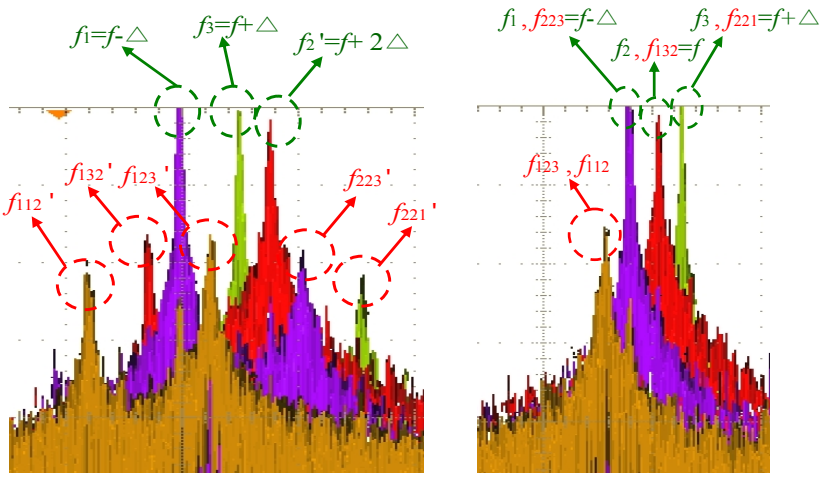

(a) (b)

Fig 3.26 Electrical spectrum of IF signals on ADC: (a) spectrum for observing FWM components; (b) spectrum after adjusting frequency allocation

The parameters for the compensation are chosen as follows: DSF fiber loss α, chromatic dispersion D_c, dispersion slope S and fiber nonlinear coefficient γ at 1550nm are 0.22dB/km, 0.07ps/km/nm, 0.07ps/km/nm^2, 3.04/W/km, respectively. The fiber is divided into 15 sections for this compensation.

Figure 3.27 (a) and (b) show the eye diagrams of sig1 w/o and w/ compensation of P_0=8dBm/ch, respectively. The eye-closure penalty can be calculated by:

$$\delta_{eye} = -20\log_{10}\left(\frac{eye\ opening\ after\ transmission}{eye\ opening\ before\ transmission}\right) \tag{3.23}$$

After compensation, the eye penalty of each signal is improved by more than 3dB.

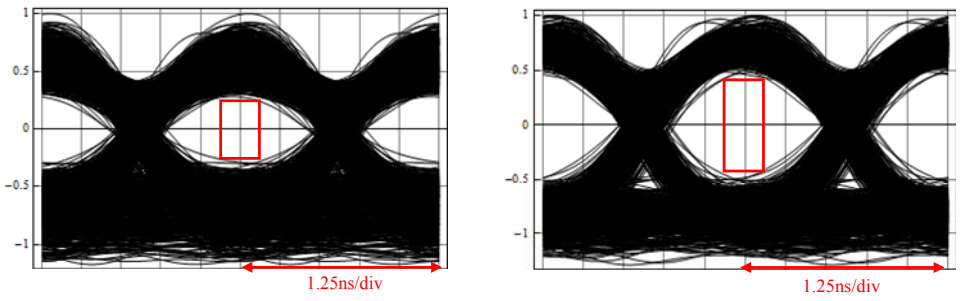

(a) (b)

Fig 3.27 Eye diagrams of individual signal for a1), a2), a3) 20-km transmission w/o comp.; b1), b2), b3) 20-km transmission w/ comp. with P_0=8dBm/ch.

3.3.4 Compensation possibility by reducing number of processed signals in BP

The transmitted signals can be compensated completely by increasing the number of detectors up until the same as the number of frequencies that new generated FWM components locate on. However, here we consider the compensation performance for individual signal by reducing number of processed signals in BP in off-line processing. For our experimental case of three channels, only the sig1 and sigl3 can be compensated since they are degraded by the degenerate FWM induced by the frequency mixing from only two signals. Take sig1 for example. The FWM degradation on signal1 is induced by the frequency mixing of sig2 and signal3 which is shown in Fig 3.28(a). Here Δf indicates the equal channel spacing. "+" represents the FWM appear during fiber propagation. Only signal2 and signal3 are involved in BP compensation process and FWM $f_{223(-)}$ is generated on f_1 which is shown in Fig 3.28(b). The symbol "-" represents the opposite phase. $f_{223(+)}$ on f_1 can be cancelled by combining with $f_{223(-)}$, which is shown in Fig 3. 28(c), i.e., sig1 is compensated. The eye diagram of sig1 after compensation by using only signal2 and signal3 with P_0=8dBm/ch is nearly equivalent to Fig 3.27 b). In a similar way, sig3 can also be compensated to the same degree by using only sig1 and sig2.

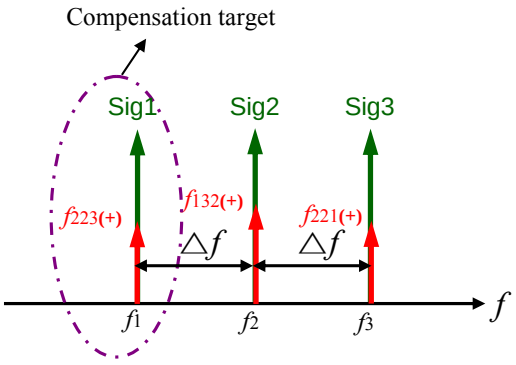

(a)

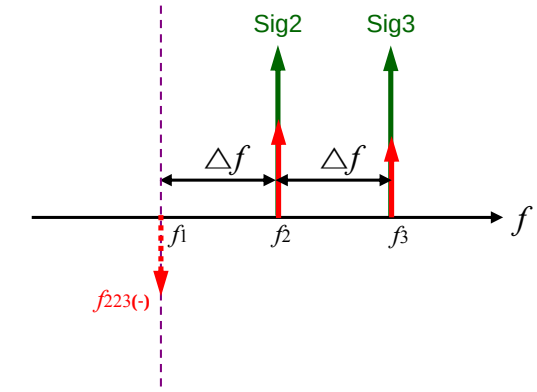

(b)

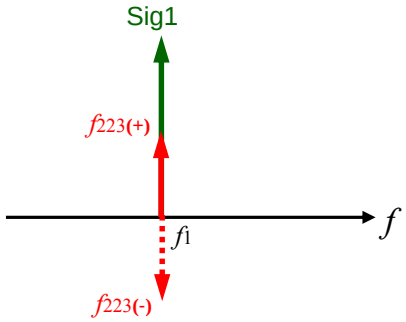

(c)

Fig 3.28 Principle of compensation for individual signal: (a) after transmission, (b) BP compensation process by using only sig2 and sig3, (c) sig1 compensation by combination.

We also simulate based on a 4-ch system with P_0=7dBm in order to demonstrate the applicability of reducing number of processed signals in BP in multi-channel system. Signal2 is considered as the compensation target by utilizing signal1, 3 and 4 through BP method. Four-detector compensation on signal2 can remove the FWM component f_{132}, f_{143} as well as f_{334}, while only f_{143} and f_{334} is compensated by three-detector compensation. The spectrum of detected signals before compensation is given in Fig 3.29 (a). Fig 3.29 (b) shows the spectrum of after BP compensation process using only sig1, sig3 and sig4, while sig2 compensation after combination are given in Fig 3.29 (c).

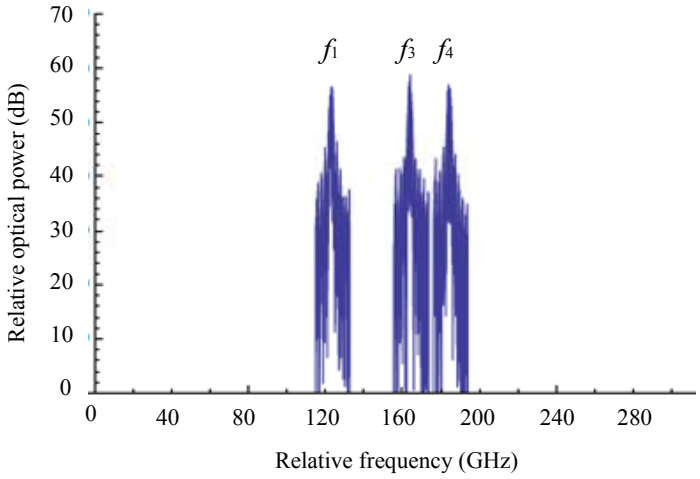

(a)

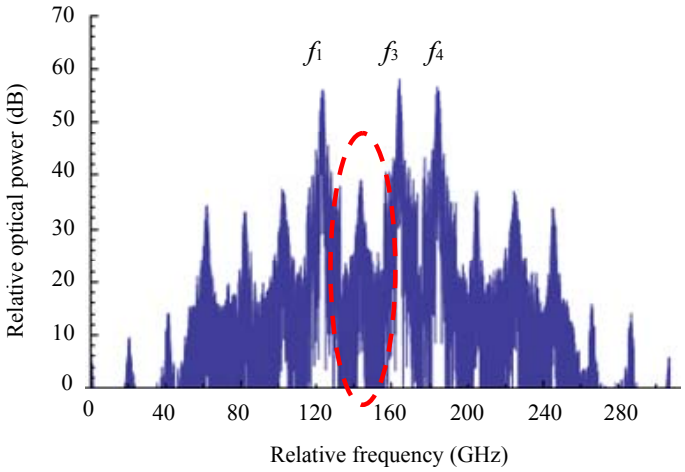

(b)

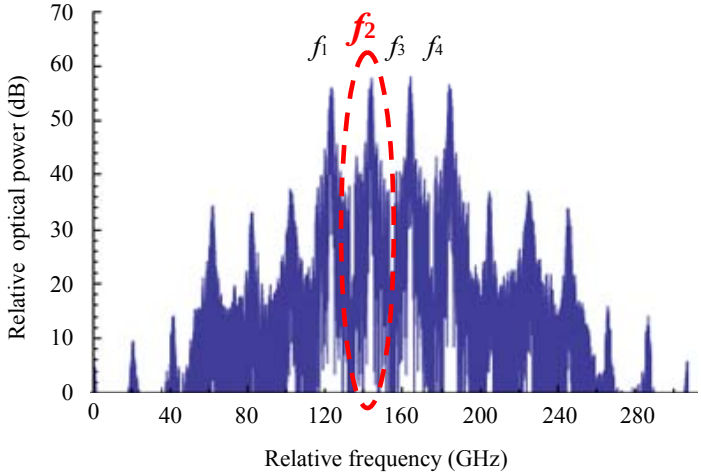

(c)

Fig 3.29 Spectra of signal2 compensation in 4-ch system with P_0=7dBm: (a) detected signals before

compensation, (b) BP compensation process using only sig1, sig3 and sig4, (c) sig2 compensation after combination.

The eye diagrams before compensation and after compensation using three signals in BP are shown in Fig 3.30(a), (b), respectively. Figure 3.30(c) corresponds to the eye diagram by processing all these four signals in BP. The eye penalty is improved by nearly 2dB and 3.5dB, respectively, in Fig 3.30(b), (c). This result indicates that it is possible to improve FWM impairments by processing less number of signals in BP, however more detectors are required to realize optimum compensation for multi-channel systems.

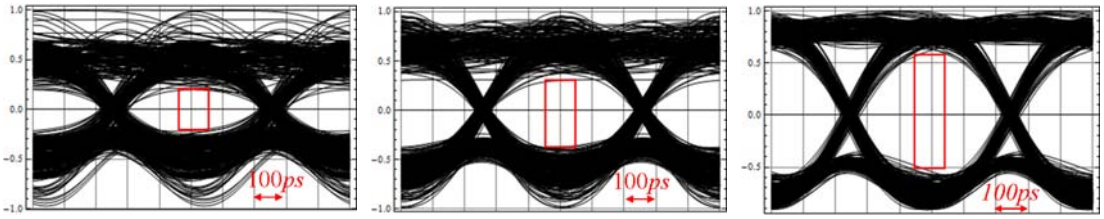

(a) (b) (c)

Fig 3.30 Eye penalty of signal2: (a) after transmission, (b) after compensation by detecting sig1, sig3 and sig4, (c) after compensation by detecting four signals.

3.4 Simulation for observing the number of required detectors

Simulation is performed for observing the number of required detectors for different number of signal channels. We calculate, firstly, the different eye penalty on different number of signal channels when the number of detectors is increased. The parameters are chosen as Table 3-1. The obtained eye penalty of center channel is shown in Fig 3.31. It is obvious that the eye penalty is improved to near 1dB using 3 detectors (N detectors) for 3-channel system, whereas the equivalent compensation can be obtained using 13 detectors (5+8 detectors) for 5-channel system. What's more, the eye penalty can be improved to nearly 5.5dB by 14 detectors (6+8 detectors) for 6-channel system. This

result indicates that great number of detectors must be employed in multi-channel systems.

Table 3-1 Simulation parameters

Modulation format	DPSK
Bit rate	2 Gbps
Channel spacing Δf	20 GHz
Transmission length L	20 km
Fiber loss α	0.2 dB/km
ZDW	1550 nm
Dispersion slope S	0.07 ps/km/nm^2
Nonlinear coefficient γ	1.5 /W/km
Optical power /ch	7 dBm
Line-width	1 MHz
Intermediate frequency	5 GHz

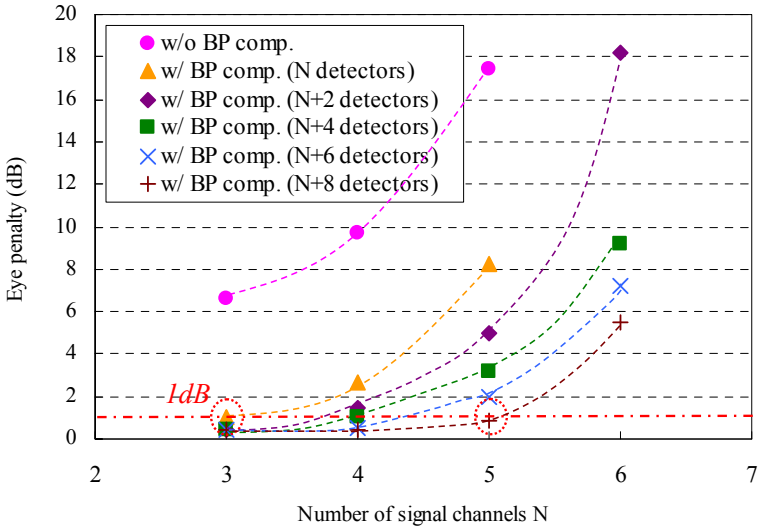

Fig 3.31 Eye penalty versus number of signal channels with different numbers of detectors

In order to clarify the eye penalty dependence on optical input power, we also plot the eye penalty versus optical input power in a 4-channel system with different numbers of detectors in Fig 3.32. When the optical input power is 5.5dBm/ch, the eye penalty can be improved to nearly 1dB by utilizing only 4 detectors, however 12 detectors (4+8 detectors) are employed to obtain the equivalent compensation performance with the input power P_0=8.5dBm/ch. For perspicuous understanding, the spectra before transmission, after transmission, after compensation with 4 detectors and 12 detectors, with P_0=8.5dBm/ch, are shown in Fig 3.33(a)-(d), respectively. The out-of-band FWMs cannot be suppressed after compensation with 4 detectors since only the transmitted signals are detected, however the compensation performance is improved compared with that of before compensation by viewing the eye diagrams which are given in Fig 3.34.

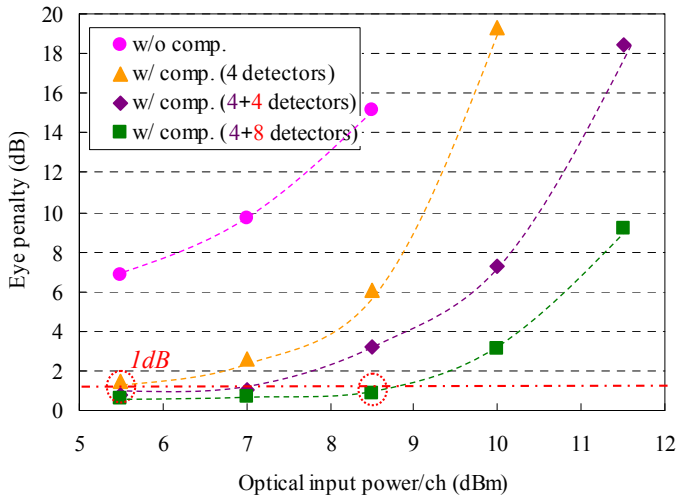

Fig 3.32 Eye penalty versus optical input power in 4-ch system with different numbers of detectors

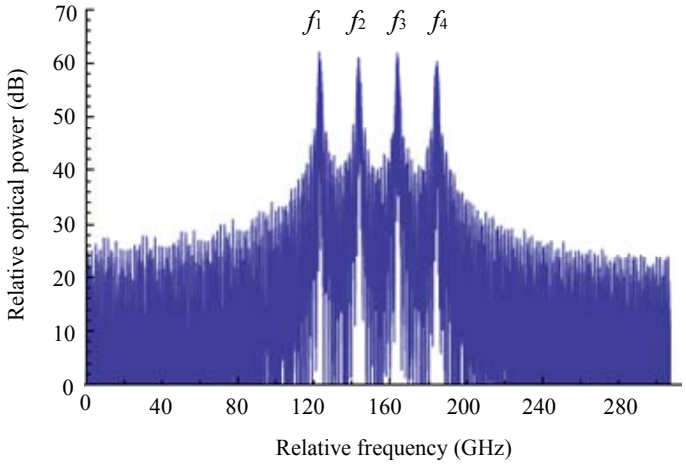
f_1 f_2 f_3 f_4
Relative optical power (dB)
0 10 20 30 40 50 60 70
0 40 80 120 160 200 240 280
Relative frequency (GHz)

(a)

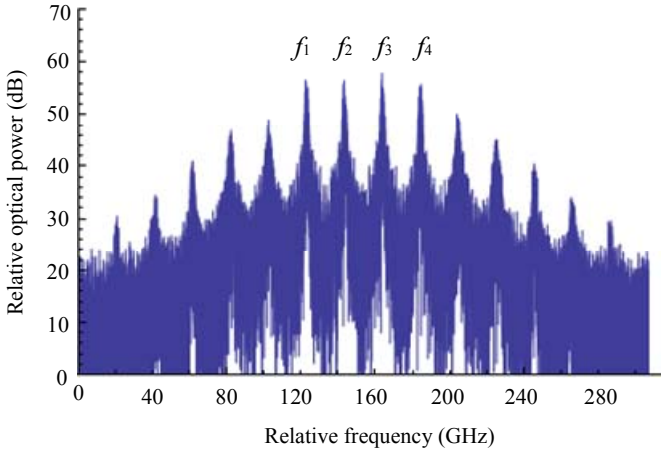
f_1 f_2 f_3 f_4
Relative optical power (dB)
0 10 20 30 40 50 60 70
0 40 80 120 160 200 240 280
Relative frequency (GHz)

(b)

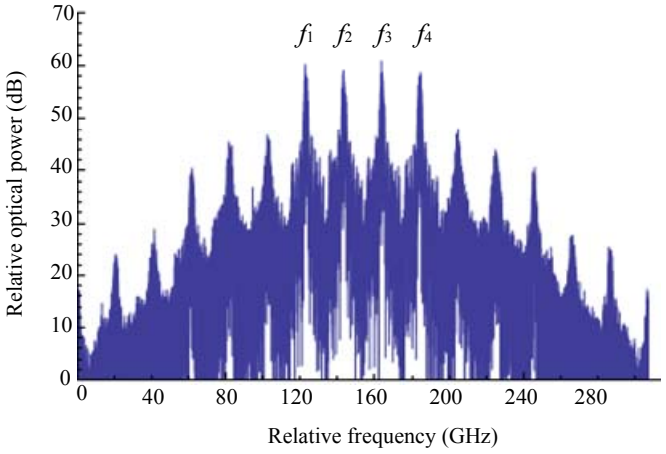
f_1 f_2 f_3 f_4
Relative optical power (dB)
0 10 20 30 40 50 60 70
0 40 80 120 160 200 240 280
Relative frequency (GHz)

(c)

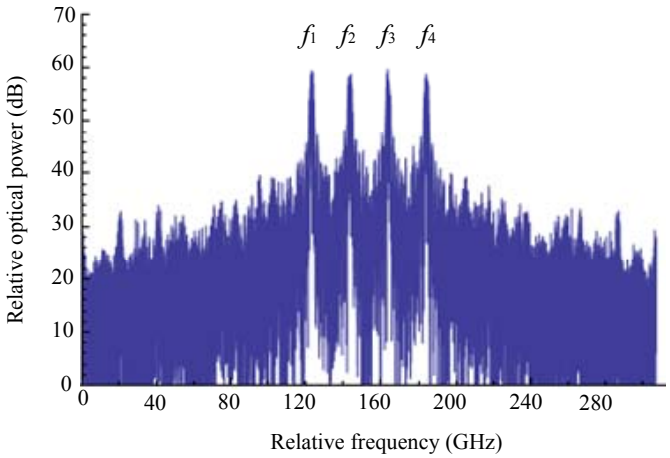

(d)

Fig 3.33 Spectra of 4-channel system with P_0=8.5dBm/ch: (a) before transmission, (b) after transmission, (c) after compensation with 4 detectors, (d) after compensation with 12 detectors.

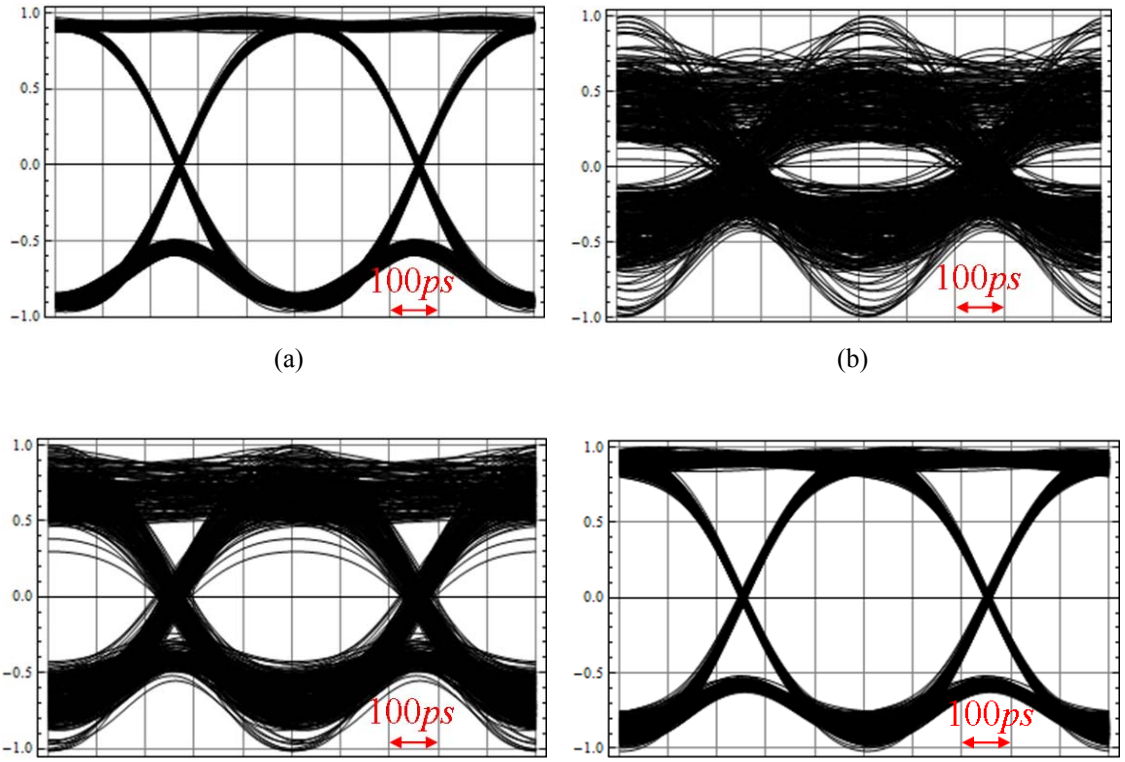

(a) (b)

(c) (d)

Fig 3.34 Eye diagram with P_0=8.5dBm/ch: (a) before transmission, (b) after transmission, (c) after compensation with 4 detectors, (d) after compensation with 12 detectors.

The eye penalty is improved to nearly 9dB with 12 detectors when the input power increases to 11.5 dBm. This result indicates that great number of detectors must be

employed when the optical input power is increased even in the systems with few number of signal channels.

3.5 Summary

The configuration of WDM transmission system for fiber nonlinearity compensation with digital coherent detection is provided in this chapter. Advantage of digital coherent detection as well as the characteristics of coherent detection compared with direct detection is pointed out.

Additionally, we introduce the method for achieving the fixed relationship between individual IF signals when coherent detected. A LO light is phase modulated by referring to Bessel function so as to realize phase locked LOs.

Principles of BP compensation scheme as well as SSFM are given in this chapter. Experiments based on overall optical lights with heterodyne detection as well as phase diversity detection are implemented. FWM products are suppressed when simultaneously detected with digital coherent detection and the compensation possibility is demonstrated experimentally by BP method off-line. Therefore, it is possible to implement this compensation method for individual detectors.

We also consider the compensation for FWM components by using individual PDs. The feasibility of the phase-locked LOs for individual coherent detectors is verified in this part. The degradation improvement is observed directly on both ASK and DPSK modulated signals. The compensation performance is evaluated by eye closure penalty as well as signal-to-FWM crosstalk ratio. It is possible to improve FWM impairments by reducing the number of processed signals in BP, however large number of detectors is necessary for optimum compensation in multi-channel systems.

Simulation for observing the number of required detectors is performed on different

number of signal channels as well as optical input power. The result indicates that great number of detectors must be employed when the optical input power is increased even in the systems with few number of signal channels.

Reference

[1] X. Li, X. Chen, G. Goldfarb et al, "Electronic post-compensation of WDM transmission impairments using coherent detection and digital signal processing," *Opt. Express*, Vol.16, No.2, pp. 880-888, Jan., 2008.

[2] S. J. Savory, "Digital filters for coherent optical receivers," *Opt. Express*, Vol. 16, No. 16, pp. 804-817, 2008.

[3] X. Liu, S. Chandrasekhar, B. Zhu, and D. W. Peckham, "Efficient digital coherent detection of a 1.2-Tb/s 24-carrier no-guard-interval co-OFDM signal by simultaneously detecting multiple carriers per sampling," *OFC 2010*, Paper OWO2, Mar., 2010.

[4] M. Kuschnerov, F. N. Hauske, K. Piyawanno et al., "DSP for coherent single-carrier receivers," *J. Lightw. Technol.*, Vol. 27, No. 16, pp. 3614-3622, Aug., 2009.

[5] P. A. Humblet, and M. Azizoglu, "On the bit error rate of lightwave systems with optical amplifiers," *J. Lightw. Technol.*, Vol. 9, No. 11, pp. 1576- 1582, Nov., 1991.

[6] C. Weber "Electronic pre-compensation of dispersion and nonlinearities in fiber-optic transmission systems," Ph.D. dissertation, Technische Universität Berlin, Jan., 2010.

[7] A. H. Gnauck, and P. J. Winzer, "Optical phase-shift-keyed transmission," *J. Lightw. Technol.*, Vol. 23, No. 1, pp. 115-130, Jan., 2005.

[8] G-W Lu, K. Chan, L-K Chen, C-K Chan, “Robustness of DPSK-WDM systems against nonlinear polarization fluctuation,” *IEEE Photon. Technol. Lett.*, Vol. 16, No. 3, pp. 927-929, Mar., 2004.

[9] J. X. Cai, D. G. Foursa, C. R. Davidson, Y. Cai et al, “A DWDM demonstration of 3.73 Tb/s over 11 000 km using 373 RZ-DPSK channels at 10 Gb/s,” in *Proc. OFC 2003*, Atlanta, GA, 2003, Postdeadline paper PD22.

[10] C. Y. Lin, M. R. Asif, M. Holtmannspoetter, B. Schmauss, “Evaluation of Nonlinear Phase Noise in DPSK Transmission for Different Link Designs,” *Physics Procedia*, Vol. 5, Part. 2, pp. 697-701, 2010.

[11] E. Ip, and J. M. Kahn, “Nonlinear impairment compensation using back propagation,” in: Optical Fiber, New Developments, In-Tech., Vienna, Austria (Invited Chapter), pp. 467-493, 2010.

[12] D. Yang, S. Kumar, M. Nakazawa, “Investigation and comparison of digital backward propagation schemes for OFDM and single-carrier fiber-optic transmission systems,” *Optical Fiber Technology*, Vol. 17, pp. 84-90, 2011.

[13] J. Liang and K. Iwashita, “Electrical compensation of FWM impairment by heterodyne detection using backward propagation,” *OECC 2009*, Hong Kong, Jul., 2009, Paper Tuk6.

[14] J. Liang and K. Iwashita, “Experimental investigation of post-compensation for FWM impairments considering inter-channel nonlinear crosstalk with digital coherent detection,” *IEICE TRANS. COMMUN.*, Vol. E94-B, No.2, pp. 558-561, Feb., 2011.

[15] T. Ohara, H. Takara, T. Yamamoto, H. Masuda et al., “Over-1000-channel ultra-dense WDM transmission with supercontinuum multicarrier source,” *J. Lightw.*

Technol., Vol. 24, No. 6, pp. 2311-2317, Jun., 2006.

[16] J. Liang and K. Iwashita, "Electrical compensation of FWM impairment by phase diversity detection via backward propagation," in *Proc. SPIE-OSA-IEEE*, Vol. 7632, pp. 76321E-1~76321E-7, 2009.

[17] A. W. Davis, M. J. Pettitt, J. P. King, and S. Wright, "Phase diversity techniques for coherent optical receivers," *J. Lightw. Technol.*, Vol. LT-5, No. 4, pp. 561-572, Apr., 1987.

[18] L. G. Kazovsky, "Phase- and polarization-diversity coherent optical techniques," *J. Lightw. Technol.*, Vol. 7, No.2, pp. 279-292, Feb., 1989.

[19] 木村磐根，通信工学概論，オーム社，東京，1998.

[20] H. Taub and D. L. Schilling, *Principles of Communication Systems*, 2nd Edition, MacGraw-Hill, New York, 1986.

[21] J. Liang, K. Nishiuchi, K. Iwashita, "Inter-channel FWM impairments compensation of ASK transmission with digital coherent detection," *ECOC 2010*, Turin, Italy, Sep., 2010, Paper P3.04.

Chapter 4

Proposed estimation method for FWM impairments compensation

4.1 Comparison of estimation method and BP method

Digital coherent detection can compensate for fiber transmission degradation, including fiber nonlinearity impairments. However, there are drawbacks. Firstly, the post compensation methods through BP need extra detectors for out of band information produced by the nonlinearity [1]. Additionally, great computation power is required since many compensation steps are necessary in the segmenting of the transmitted fibers for processing. Therefore, we propose a novel compensation method based on FWM estimation. The number of detectors is reduced in our estimation method since only signal channels need to be detected and information of other FWM channels are deduced based on these detected channels. As a consequence, less computation power is required than in the BP method. The configuration of WDM systems for FWM compensation with estimation method is shown in Fig 4.1. Both the number of LOs as well as PDs are reduced compared with the BP method in Fig 3.16. The difference of the compensation process between these two methods is illustrated as Fig 4.2. In BP method, up-sampling is indispensable for each detected channels including signals as well as FWMs, and optical field reconstruction is realized by combining all these channels as equal channel spacing. Furthermore, individual filters are required after great number of steps through SSFM in order to obtain individual signals. In contrast,

optical field reconstruction is unnecessary in estimation method, and re-sampling is implemented so as to obtain the eye diagrams in estimation method. Individual signals can be obtained directly after 1st and 2nd round estimation compensation.

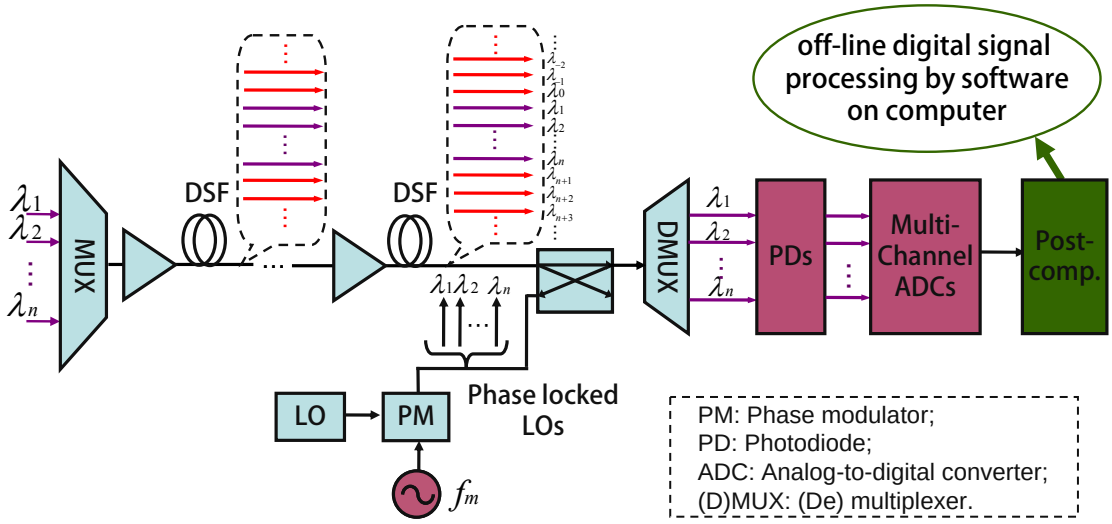

Fig 4.1 Configuration of our experimental condition with estimation method in WDM system

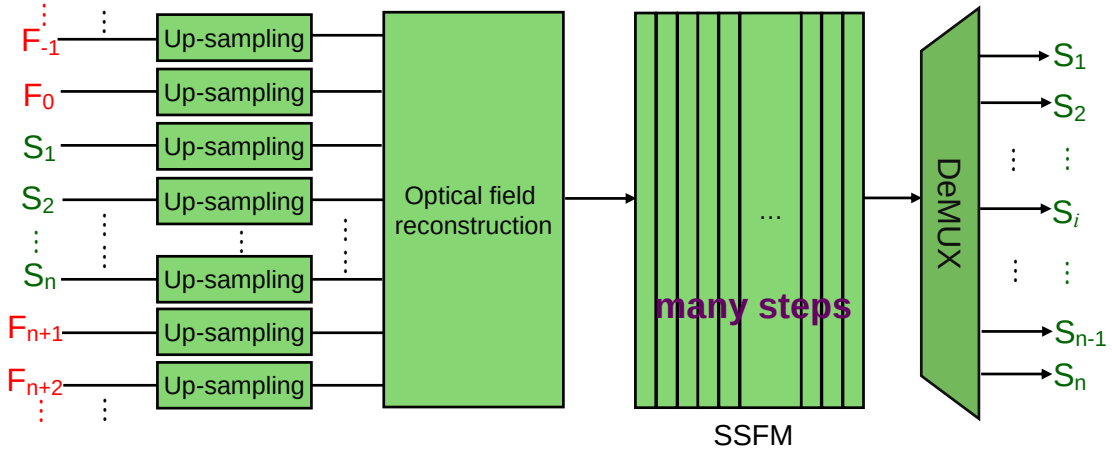

(a)

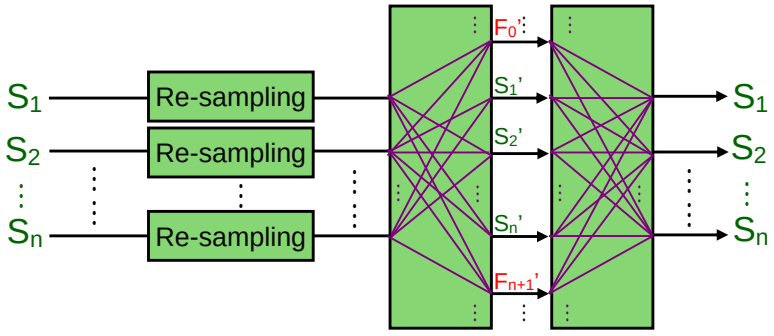

1st, 2nd round estimation

(b)

Fig 4.2 Difference of the compensation process between these two methods: (a) BP method, (b) estimation method

4.2 Proposal of Estimation compensation method

4.2.1 Principle of the method

Our proposed FWM impairments compensation method is based on estimating FWM components and then substituting the estimated components for the generated ones. Direct detection is square-law detection so the impairments cannot be substituted. However coherent detection conserves the optical field in the detected electrical signal and this signal can be compensated. The FWM components can be calculated by nonlinear propagation, but this requires great computation power. We propose, therefore, to utilize the calculations which are given by equations [2], [3].

The thought of the proposed compensation method is shown in Fig 4.3 based on a three-channel system for brevity. The equal difference between frequency $f_{-1}, f_0, \ldots, f_4, f_5$ is Δf. In the case of equal channel-spacing, the generated new frequencies coincide with the existing frequencies, leading to coherent in-band crosstalk and degrading system performance severely. The compensation process consists of the following steps. Figure 4.3(a) shows the 1st round FWM calculation. Only the in-band FWM components are applied to the compensation process in this step. E_{223}, E_{132}, E_{221} are suppressed by generating FWM E_{223}', E_{132}', E_{221}' which are estimated from initially detected waveforms w_{01}, w_{02}, w_{03}. The FWM components below the coordinate axis signify out of phase (opposite sign). However, other out-of-band components also generate new FWMs that can not be compensated by 1st round FWM compensation. The reasons for this incomplete compensation are considered as follows. One reason is

other FWM components are induced by this nonlinearity which is induced by the above FWM components. The other reason is due to the assumption of the derived equation without considering the power depletion and the FWM components are contained in the initially detected signal components.

The components E_{F1}, E_{F2}, and E_{F3} represent the residual components. For 2nd round FWM compensation, 1st round compensated waveforms w_{11}, w_{12}, w_{13} which are shown in Fig 4.3 (b) are utilized for further calculation. Firstly, out-band FWM components which appear during 1st round FWM process are calculated by w_{11}, w_{12}, w_{13} (indicated by ②), since these FWMs are necessary for calculating 2nd round FWM; secondly, E_{F1}', E_{F2}', and E_{F3}' are calculated using both signals and already calculated out-band FWMs (indicated by ③).

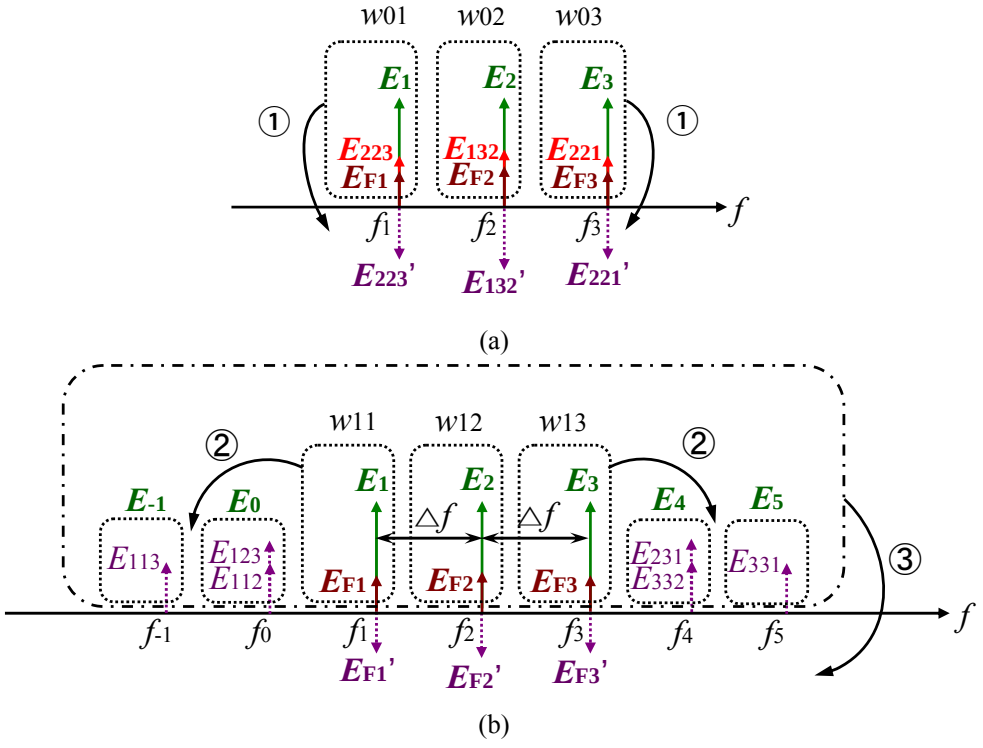

Fig 4.3 Compensation process: (a) 1st round FWM compensation; (b) 2nd round FWM compensation.

4.2.2 Equation derivation for Estimation

A. 2nd round compensation:

The differential equation for an induced FWM component E_{ijk} is expressed as follows [2]:

$$\frac{d}{dz}E_{ijk}(z) = -\frac{1}{2}\alpha E_{ijk}(z) + i\gamma D E_i(z) E_j(z) E_k^*(z) \exp(i\beta_{ijk} z) \tag{4.1}$$

where α is the fiber attenuation coefficient, and z is fiber length, respectively. $\gamma(=\omega_{ijk} n_2 / cA_{eff})$ is the nonlinear parameter, here ω_{ijk} is optical carrier angular frequency at $f_{ijk}=f_i+f_j-f_k$, n_2 is nonlinear index, c is light velocity at vacuum, A_{eff} is effective area, D is degeneracy factor which has value 3 or 6 for degenerate or non-degenerate terms, respectively. E_p (z) ($p=i, j, k$) represents the electrical fields of the input signal, β_{ijk} is the propagation constant for E_{ijk}. The amplitude of each electrical field is diminished solely by fiber attenuation and represented as:

$$E_p(z) = E_p \exp\left(-\frac{1}{2}\alpha z - i\beta_p z\right) \tag{4.2}$$

The frequency relation between the induced FWM E_{ijk} and signal E_i, E_j, E_k is $f_{ijk}=f_i+f_j-f_k$. The induced FWM can be derived as:

$$E_{ijk}(z) = i\gamma D E_i E_j E_k^* \frac{\exp(-\alpha z + i\Delta\beta z) - 1}{i\Delta\beta - \alpha} \exp\left(-\frac{1}{2}\alpha z\right) \tag{4.3}$$

where $\Delta\beta=\beta_i+\beta_j-\beta_k-\beta_{ijk}$ is the phase matching difference. This can be rewritten as the transmitted electrical field at the length L:

$$E_{ijk}(L) = i\gamma D E_i(L) E_j(L) E_k^*(L) \frac{\exp(-\alpha L + i\Delta\beta L) - 1}{i\Delta\beta - \alpha} \exp(\alpha L) \tag{4.4}$$

In the 2nd round, the estimated FWM (indicated by ② in Fig 4.3) will act as input components that induce new FWM components on signal channels. We derive applied equations for two cases. E_{ijk} (z) is generated along the fiber transmission and varies with the fiber length. We assume it as the following expression:

$$E_{ijk}(z) = E_{ijk0}(z)\exp\left(-\frac{1}{2}\alpha z - i\beta_{ijk} z\right) \tag{4.5}$$

where E_{ijk0} (z) represents the electrical field once the FWM appears.

By substituting Eq. (4.5) into Eq. (4.1) as one of the signals, we can obtain differential equation of 2nd round FWM:

$$\frac{d}{dz}E_{Fn}(z) = -\frac{\alpha}{2}E_{Fn}(z) + i\gamma' D' E_{ijk}(z)E_l(z)E_m^*(z)\cdot\exp\left(-\alpha z + i\Delta\beta_{Fn} z\right) \tag{4.6}$$

where γ' is the nonlinear parameter for E_{Fn}, D' is degradation factor for this process. Then, we obtain:

$$E_{Fn}(z) = i\frac{1}{2}\gamma' D' E_{ijk} E_l E_m^* \exp\left(-\frac{1}{2}\alpha z\right)\frac{\exp(-\alpha z + i\Delta\beta' z) - 1}{i\Delta\beta' - \alpha} \tag{4.7}$$

where $\Delta\beta' = \beta_{ijk} + \beta_l - \beta_m - \beta_{Fn}$. This can also be rewritten as the transmitted electrical field length L:

$$E_{Fn}(L) = i\frac{1}{2}\gamma' D' E_{ijk}(L)E_l(L)E_m^*(L)\exp(\alpha L)\frac{\exp(-\alpha L + i\Delta\beta' L) - 1}{i\Delta\beta' - \alpha} \tag{4.8}$$

The opposite sign FWM E_{Fn}' in 2nd round compensation is calculated using E_{Fn} (z).

B. Residual components:

The received signal w_{01}, w_{02}, w_{03} include not only signal but also FWM components. These components affect the FWM estimation at the 1st round. If we assume that w_{02} consists of E_2 and E_{132}, the 2nd round components which are induced by the FWM components inside the signal is produced E_{F2}, then the components can be cancelled.

Power depletion is another factor which is introduced in Section 4.4.1.

4.3 Simulation performance based on estimation compensation method

4.3.1 Demonstration in un-equal channel spacing system

In order to demonstrate the possibility of this compensation method, a five-channel transmission system distributed around 1550nm with lower optical power and un-equal

channel spacing is taken as an example. The input optical power P_0 is chosen at 4dBm/ch. The channel spacing between each signal is 14GHz, 21GHz, 28GHz, 37GHz, respectively. Signal on each channel is DPSK modulated at 2 Gbit/s. The transmission of WDM signals over dispersion-shifted fiber (DSF) of 20km is simulated. The fiber loss, CD, dispersion slope and fiber nonlinear coefficient are 0.2 dB/km, 0.01 ps/km/nm, 0.07 ps/km/nm^2, 1.5 /W/km, respectively. Figure 4.4 (a) (b) (c) gives the spectra of before transmission, without compensation and with compensation at P_0=4dBm/ch, respectively. Some FWM components are generated after transmission shown in Fig 4.4(b) by comparing with Fig 4.4(a). For the case of un-equal channel spacing, nearly all the FWM components fall out of signal channels, therefore the compensation possibilities can be easily seen by the cancellation of the FWM components. It is obviously seen from Fig 4.4(c) that the generated FWM components are cancelled by calculating the estimated FWMs with opposite sign using Eq. (4.3).

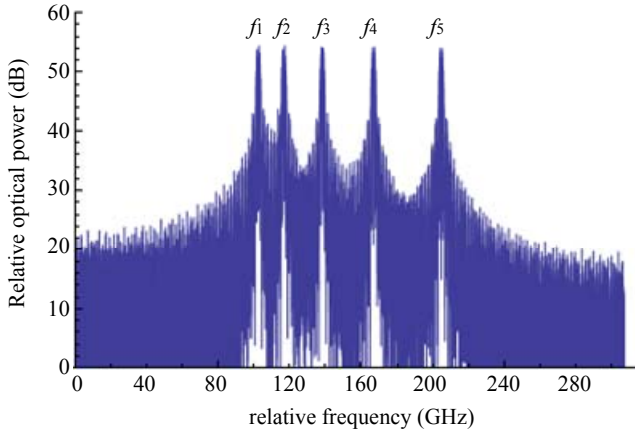

(a)

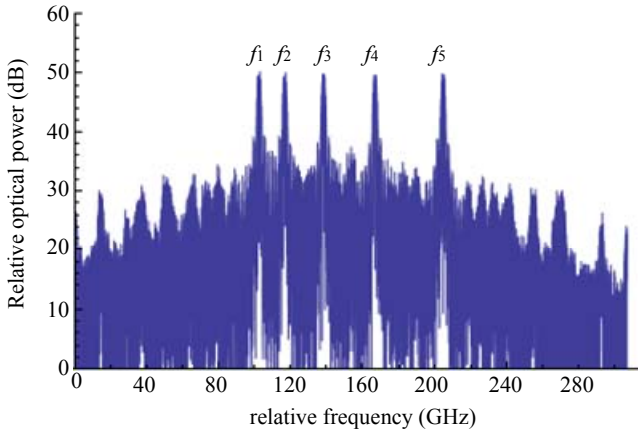

(b)

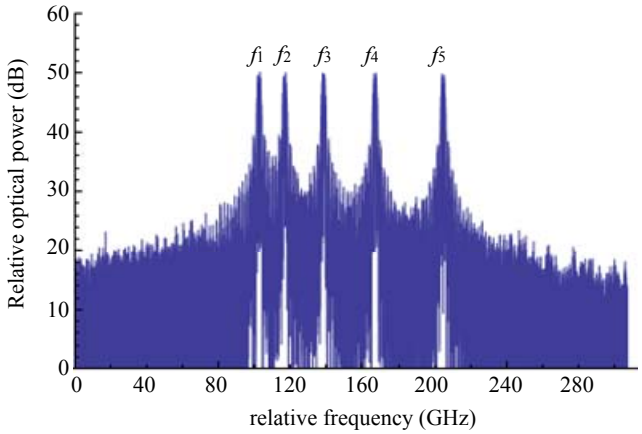

(c)

Fig 4.4 Spectra of five-channel transmission system with un-equal channel spacing: (a) before transmission, (b) after transmission & w/o compensation, (c) after transmission & w/ compensation

4.3.2 Compensation possibility in equal channel spacing system

Simulation is also performed on a five-channel WDM system with equal channel spacing of 20GHz. The bit length is 2^9. The spectra of before/after transmission at P_0=7dBm are shown in Fig 4.5. Decisive FWM products are generated after fiber transmission. The transmitted signals are heterodyne detected with phase-modulated LOs. The demultiplexed signals are received by individual receivers and processed. Other parameters are set the same as above. Under our numerical condition, the phase difference between all of the phase-modulated LOs keeps unchanged. Therefore, the

phase relationship of the intermediate frequency (IF) signals can be kept fixed when heterodyne detected by individual receivers. The carrier frequency of LO is set near f_3 and the phases of the five detected signal channels f_1, f_2, f_3, f_4, f_5 are 0, -π, 0, 0, 0, respectively. Then -π is adjusted to 0 for the compensation. Other considered channels are calculated based on these five channels. The eye diagrams of center channel before and after estimation compensation with P_0=4dBm, 5.5dBm, 7dBm are given in Fig 4.6, respectively. By compensation, there is a distinct improvement on the eye openings.

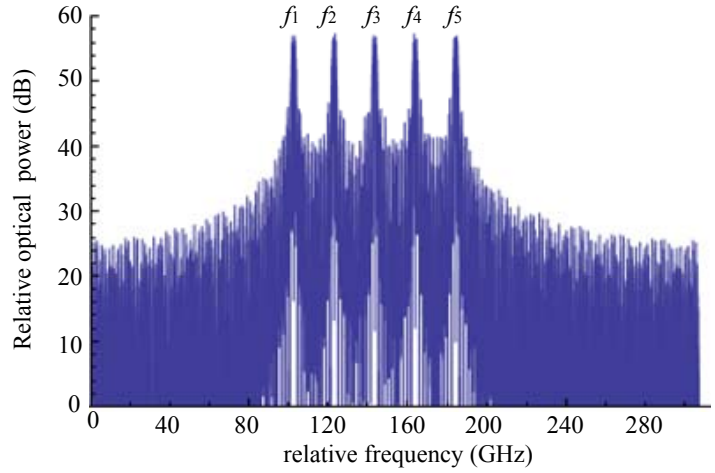

(a)

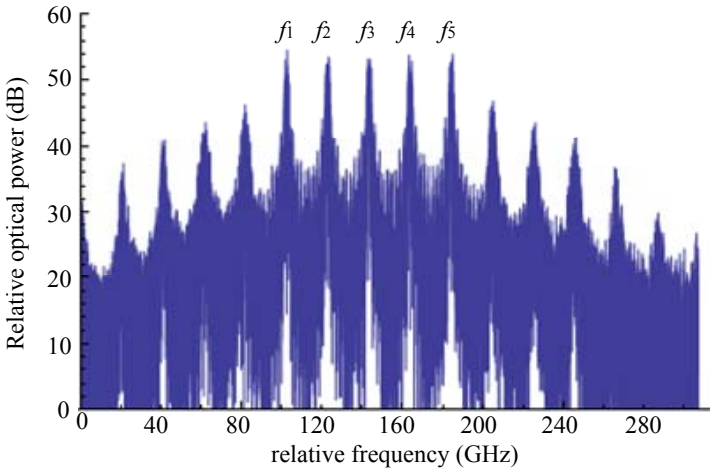

(b)

Fig 4.5 Spectra of five-channel transmission system with channel spacing of 20GHz: (a) before transmission, (b) after transmission

	Before compensation	After compensation
4dBm	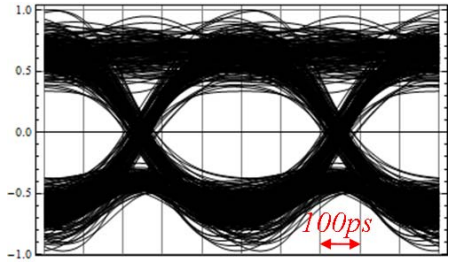	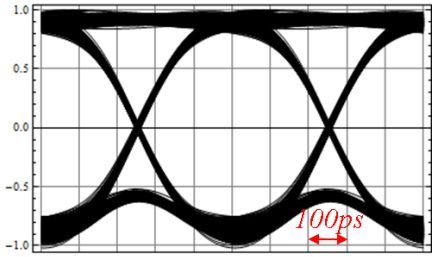
5.5dBm	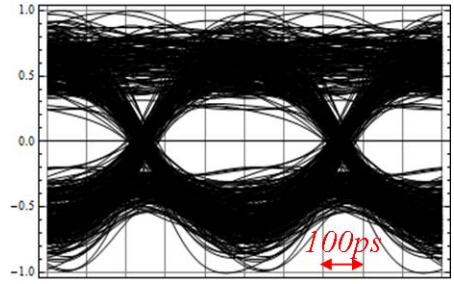	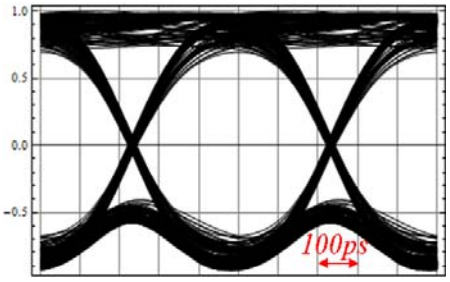
7dBm	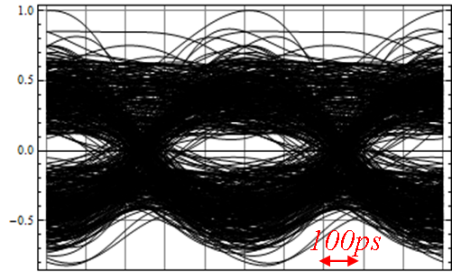	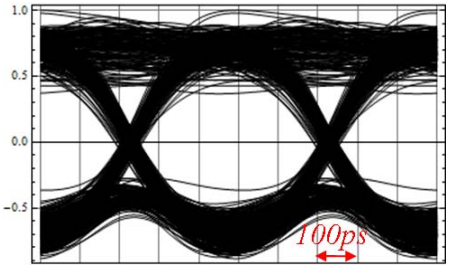

Fig 4.6 Eye diagrams of center channel before and after compensation by estimation method with P_0=4dBm, 5.5dBm, 7dBm in five-channel WDM system.

4.4 Power adjustment and limitation

4.4.1 Power adjustment

The in-band FWMs are ignored in the electrical fields of the detected signals during above derivation. However, the detected waveforms include not only signals but also these FWM components fall on the signal channels as shown in Fig 4.3, especially for the scenario of higher power. Furthermore, the powers of signals are decreased not only by the fiber loss but also by their depletion induced through frequency conversion from signals to FWMs. Therefore, the powers of signals should be adjusted due to the above

composite factor. Therefore, a coefficient K_p (p=…, i, j, k,...,l, m, n,...) is assumed as adjustment factor of each signal, which is used for approximately estimating the difference between the detected power P_{Det} with equal separation and non-depletion P_p, in which the degradation stems from fiber loss only. Fig 4.7 shows the contrast between P_p and P_{Det}.

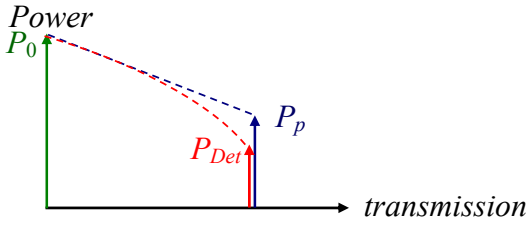

Fig 4.7 Power contrast between P_p and P_{Det}

For simplicity, the channel powers of depletion case (with equal and unequal separation) as well as only loss case in three-channel system are illustrated in Fig 4.8 so as to observe the power difference induced by depletion. K_p is represented as:

$$K_p = \sqrt{\frac{P_p}{P_{Det}}} \tag{4.9}$$

where $P_p = P_0 e^{-\alpha L}$, P_{Det}= P_p-P_{tr}+$P_{F\text{-}on}$. Here, P_{tr} represents the depletion due to the power transfer from original signal channels to FWM frequencies during the FWM generation, and $P_{F\text{-}on}$ denotes the power of FWM components that locate on each signal channels. The electrical fields of detected signals utilized for estimating FWM, therefore, can be adjusted as $K_p \cdot E_{Det}(z)$.

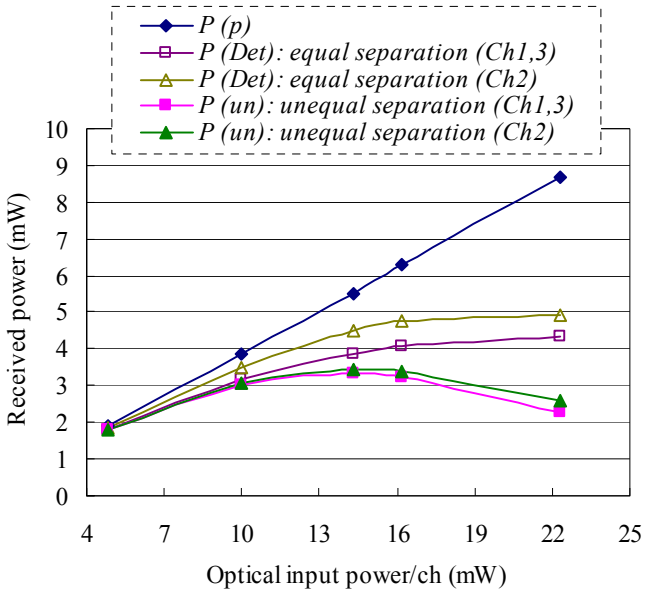

Fig 4.8 Channel power difference in three-channel system

In order to observe the improvement on compensation performance, power adjustment is carried out on the five-channel case of Fig 4.6 with P_0=4dBm and 7dBm, and the corresponding eye diagrams are obtained as Fig 4.9. The improved eye penalty is nearly equivalent in the case of P_0=4dBm, whereas 1.9dB is improved in the case of P_0=7dBm after power adjustment. And K_p (p=1, 2, 3, 4, 5) is 1.09, 1.08, 1.06, 1.06, 1.11, respectively.

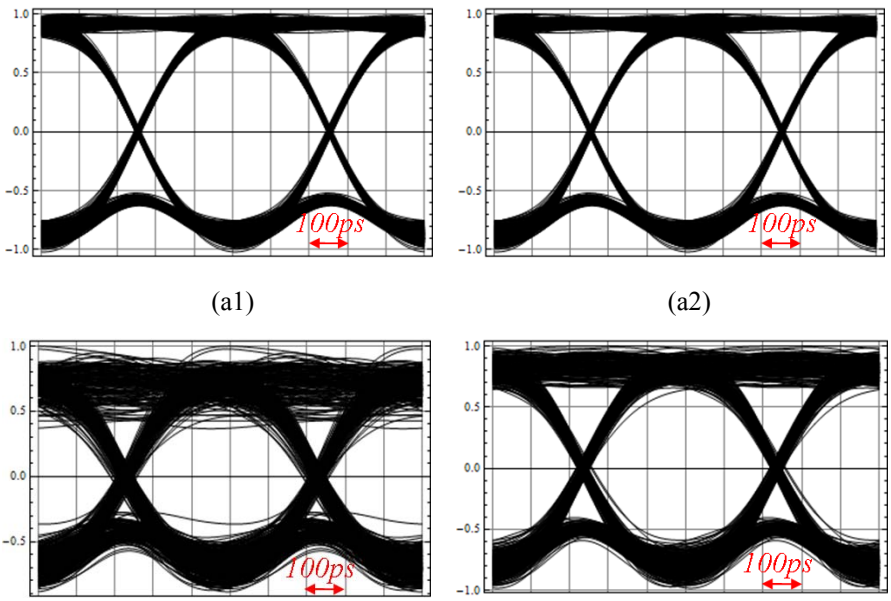

(a1) (a2)

(b1) (b2)

Fig 4.9 Eye diagrams: (a1) after compensation without power adjustment (P_0=4dBm), (a2) after compensation by power adjustment (P_0=4dBm); (b1) after compensation without power adjustment (P_0=7dBm), (b2) after compensation by power adjustment (P_0=7dBm).

4.4.2 Limitation

The 1st and 2nd round can be utilized for FWM compensation by estimation with this method. However, the 1st and 2nd round will become ineffective when the optical power becomes higher that the FWMs overwhelm the transmitted signals. This is the limitation of this method and the reason for the inadequate compensation in higher input power region. For the three-channel system, the power of equal separation approaches twice of that of unequal separation after transmission when the input optical power P_0 increases to nearly 22mW (13.5dBm)/ch as shown in Fig 4.8, where $P_{un}= P_p-P_{tr}$. This means the power of newly generated FWMs on signal channels becomes considerable and equivalent to the signal power. In this case, the eye penalty becomes hardly improved. However, 2nd round estimation is unnecessary to be carried on in the multi-channel systems which will be discussed in the following part.

4.5 Compensation performance of estimation method in comparison with that of BP method

In order to compare the compensation performance of BP method corresponding to different number of detectors with that of our estimation method, we also simulate for BP compensation on five-channel scenario. The optical input power and other parameters are chosen the same as above. Figure 4.10 shows the eye penalty variation while the optical input power varies from 2dBm/ch to 7.5dBm/ch for brevity. The solid marks stand for estimation method, while the hollow marks correspond to BP method, in which 5 detectors are for 5 signals and additional detectors are aligned symmetrically to the

signal-channel detectors.

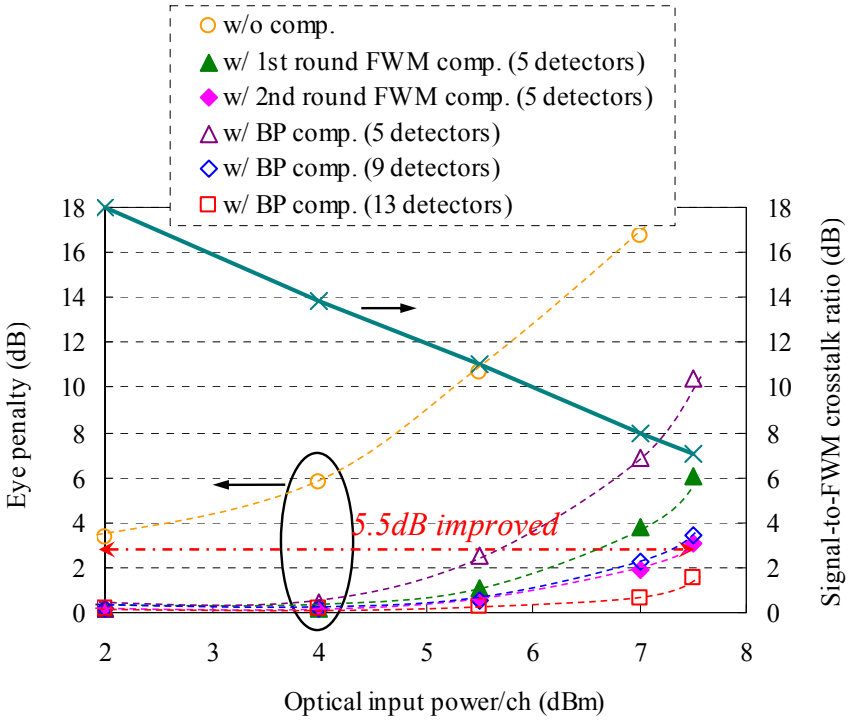

Fig 4.10 Eye penalty versus optical input power

The compensation performance of estimation method after 2nd round FWM compensation is between that of BP method with 9 detectors and 13 detectors. The compensation results indicate that the input optical power tolerance is improved by nearly 5.5dB at 3dB eye penalty, which is designated by red dashed line in Fig 4.10.

4.6 Discussion in multi-channel systems

This compensation method is also effective in multi-channel systems. The computation power augments with the number of channels increasing. For a three-channel system, the number of calculations of 1st and 2nd round compensation is only 3 and 14, respectively. However, the computation power, i.e., number of calculations for 1st and 2nd round FWM compensation rise higher in a WDM system with *N*-channel, where the number of calculations depends exclusively on the number of

channels. When we assume the number of channels is even, the number of FWM components on *m*-th signal channel is expressed as [4]:

$$N_{FWM,m} = \frac{N^2}{4} + \frac{Nm}{2} - \frac{m^2}{2} - N + \frac{m}{2} \tag{4.10}$$

Therefore, the total number of 1st round FWM on signal channels can be obtained while *m* varies from 1 to *N* by the following equation:

$$\begin{aligned} N_{FWM,total} &= \sum_{m=1}^{N} N_{FWM,m} \\ &= N \cdot \frac{N^2}{4} + \frac{N\left(1+2+\cdots+N\right)}{2} - \frac{1^2+2^2+\cdots+N^2}{2} - N \cdot N + \frac{1+2+\cdots+N}{2} \\ &= \frac{1}{3}N^3 - \frac{3}{4}N^2 + \frac{1}{6}N \end{aligned} \tag{4.11}$$

However, FWM are hardly generated on the channels which are further from ZDW due to the phase mismatch in WDM system with large number of channels. Therefore, not all of theoretically calculated FWMs can be generated for a large *N*. The number of 2nd round FWMs is also limited. We focus on the center channel for the worst-case scenario in multi-channel WDM systems to roughly estimate the channel threshold value of FWM involved by observing the total FWM efficiency η. Each FWM efficiency η with respect to phase mismatch is calculated as [5]:

$$\eta = \frac{\alpha^2}{\alpha^2 + \Delta\beta^2}\left(1 + \frac{4e^{-\alpha L}\sin^2\left(\Delta\beta L/2\right)}{\left(1-e^{-\alpha L}\right)^2}\right) \tag{4.12}$$

where α is fiber loss, L is transmission length, $\Delta\beta$ is the phase-mismatching factor which is introduced in Section 2.4.3:

$$\begin{aligned} \Delta\beta &= 2\pi\lambda^2 D_c / c\left(f_k - f_i\right)\left(f_k - f_j\right) + \pi\lambda^4 / c^2\left(f_k - f_i\right)\left(f_k - f_j\right)\left(f_i + f_j - 2f\right)S \\ &= 2\pi\lambda^2 D_c / c\left(k-i\right)\left(k-j\right)\Delta f^2 + \pi\lambda^4 / c^2\left(k-i\right)\left(k-j\right)\Delta f^2\left(f_i + f_j - 2f\right)S \end{aligned} \tag{4.13}$$

where c is the light velocity, D_c is the chromatic dispersion, S is the dispersion slope, Δf is the channel spacing, f_i, f_j, f_k are the frequencies of three signals whose relationship is

represented as:

$$f = f_i + f_j - f_k \tag{4.14}$$

Assuming the channel spacing is 100GHz, the dispersion slope S=0.07 ps/km/nm^2, and other parameters are chosen the same as above. The total efficiencies of each FWM components that coincide with center signal channel are summarized and obtained in Fig 4.11. We consider the ZDW locates on both the center of all the channels as well as relatively further, which are indicated by solid marks. When the total efficiency tends towards flat, it can be viewed as that FWMs are hardly generated. By our calculation, the range that is vulnerable to FWM impairments covers from nearly 20 channels to 40 channels as center channel becomes further from ZDW. The sharp rise is by virtue of that the phase matching condition for the special completely non-degenerate case is satisfied [Appendix C]. In actual fiber transmissions, however, ZDW is non-uniform for the combination of individual fibers, even for the entire length of a fiber itself, the ZDW fluctuates along the fiber length [5]. We consider that the fibers consist of two segments with non-uniform ZDW for brevity. In this case, the FWM efficiency is not simply a summation of the values for each segment, but an interference appearing between the FWM generations in each fiber segment. The efficiency is deduced as [5]:

$$\eta = \frac{\eta'}{\eta'\left(\Delta\beta_1 = \Delta\beta_2 = 0\right)} \tag{4.15}$$

where

$$\eta' = \left| \frac{\exp\left[\left(-\alpha + i\Delta\beta_1\right)L_1\right] - 1}{i\Delta\beta_1 - \alpha} + \exp\left[\left(-\alpha + i\Delta\beta_1\right)L_1\right] \cdot \frac{\exp\left[\left(-\alpha + i\Delta\beta_2\right)L_2\right] - 1}{i\Delta\beta_2 - \alpha} \right|^2 \tag{4.16}$$

When L_1=L_2=10km is assumed, the non-uniform ZDW cases are plotted in Fig 4.11,

which are indicated by hollow mark. The sharp rise is improved by any combination of different ZDW, especially when the ZDW is relatively closer to the center.

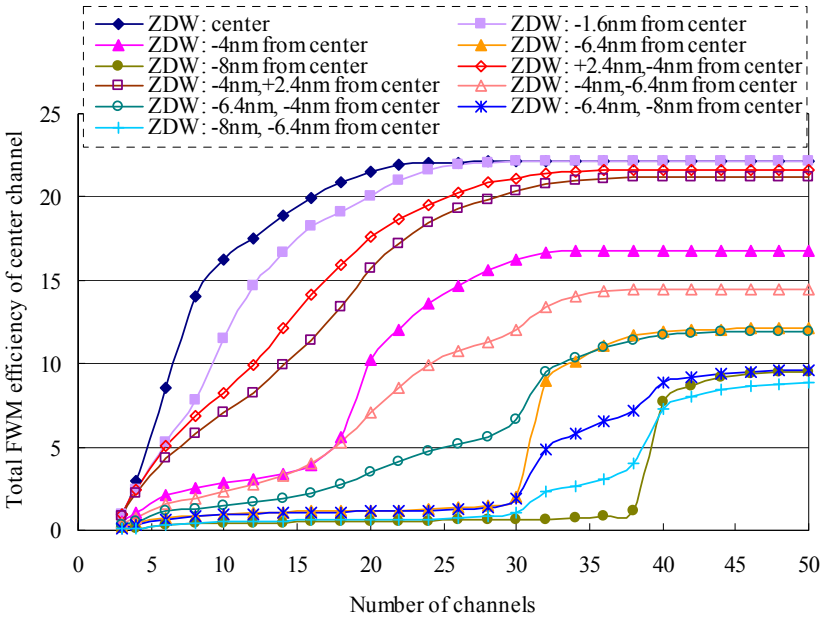

Fig 4.11 Total FWM efficiency of worst channel with different ZDW

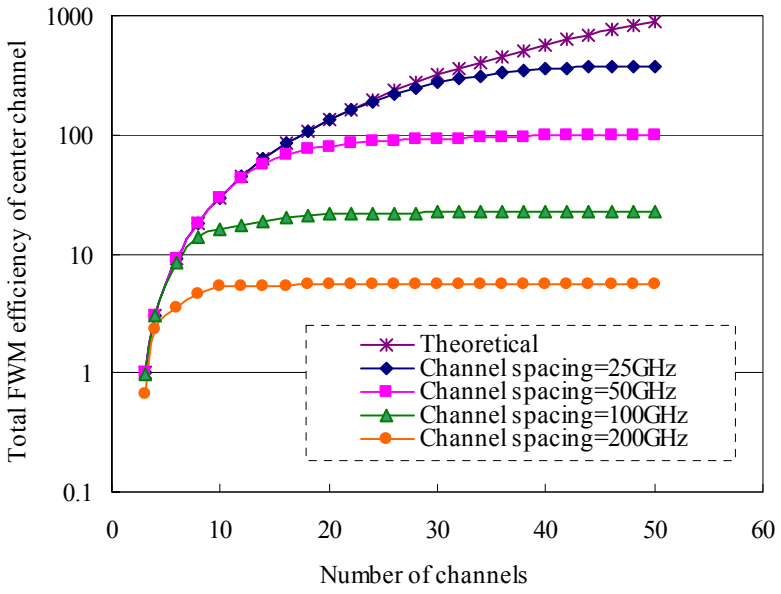

Fig 4.12 Total FWM efficiency of center channel with different channel spacing

The total efficiency with respect to different channel spacing is also plotted in Fig 4.12 by assuming ZDW locates on the center of the channels. The purple curve corresponds to the theoretical value calculated by Eq. (4.10), i.e., the efficiencies of all the FWMs locate

on center channel equal to 1. The number of channels that are vulnerable to FWM decreases as the channel spacing increases. When the channel spacing is 25GHz, the signal channels are probably hardly affected by FWM from out of 40 channels, however only 10 channels are involved while the channel spacing increases to 200GHz.

We take 100GHz channel spacing for example, for a rough estimate of the worst-case scenario on center channel, assuming 30 channels are involved. The efficiency of each FWM that locates on the 15th channel is plotted in Fig 4.13, in which $i+j-k=15$. This figure covers some reduplicate FWM products (e.g., notation of f_{ijk} and f_{jik}). For a larger number of channels $N \geqq 30$, the number of calculations remains unchanging under this condition.

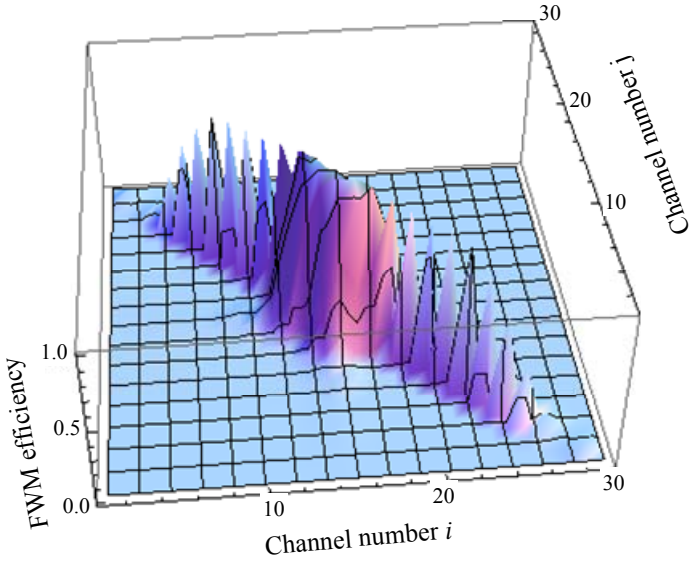

Fig 4.13 Efficiency of each FWM locates on channel 15 in a 30-channel system.

The superiority of our estimation method is mainly based on: 1) Fewer detectors are employed since only signal channels are required to be detected and FWM information of other channels are estimated based on the detected channels; 2) While the number of calculations required depends on the number of channels involved, our method uses only two steps. In contrast, the BP compensation method requires many more steps per

channel as each transmitted fiber must be segmented. Our method is preferable in terms of less computation power, and smaller number of actual circuits involved.

4.7 Experimental verification

The compensation method is verified experimentally. The number of required detectors will be doubled for phase diversity detection. Therefore, heterodyne detection is chosen due to the limitation of our experimental devices. The experimental setup for FWM estimation compensation is identical to that of BP method except the off-line process, shown in Fig 4.14. Two tunable lasers (TL) and a distributed feedback (DFB) laser with 23-GHz channel spacing are employed as WDM signal sources whose wavelengths are around 1550nm. The line-widths of both signal optical sources and LO are nearly 1MHz. They are DPSK modulated using dual Mach-Zehnder intensity modulator driven at a bit rate of 0.8Gbps by individual PPG with the pseudo-random bit sequence of 2^9-1 length. The combined signals are amplified, and subsequently fed to a 20-km DSF whose ZDW is around 1549nm. Some of the generated new FWM components fall in the signal channels. The signal-to-FWM (adjacent FWM) crosstalk ratio is nearly 8dB. Only the transmitted signals are heterodyne detected with phase-modulated LOs. The modulation index is adjusted to approximately 1.5, so as to bring sideband power as close to equivalent as possible. The phase relationship between modulated LOs and signals in optical domain is shown in Fig 4.15. The black dashed lines denote modulated LOs, whose center carrier is set nearly 1.6GHz frequency difference with Sig2, i.e., the IF is set nearly 1.6GHz. These coupled signals are demultiplexed by the optical demultiplexer. The 3-dB bandwidth of the optical demultiplexer is nearly 0.18nm. The received signals are sampled by three ADC at a rate of 5Gsample/s and the converted signals are processed off-line. The optical field reconstruction is unnecessary in the off-line digital signal

processing in estimation method as mentioned above. Re-sampling is followed by differential demodulation with one bit delay. The demodulated signals are then sent through low-pass filters.

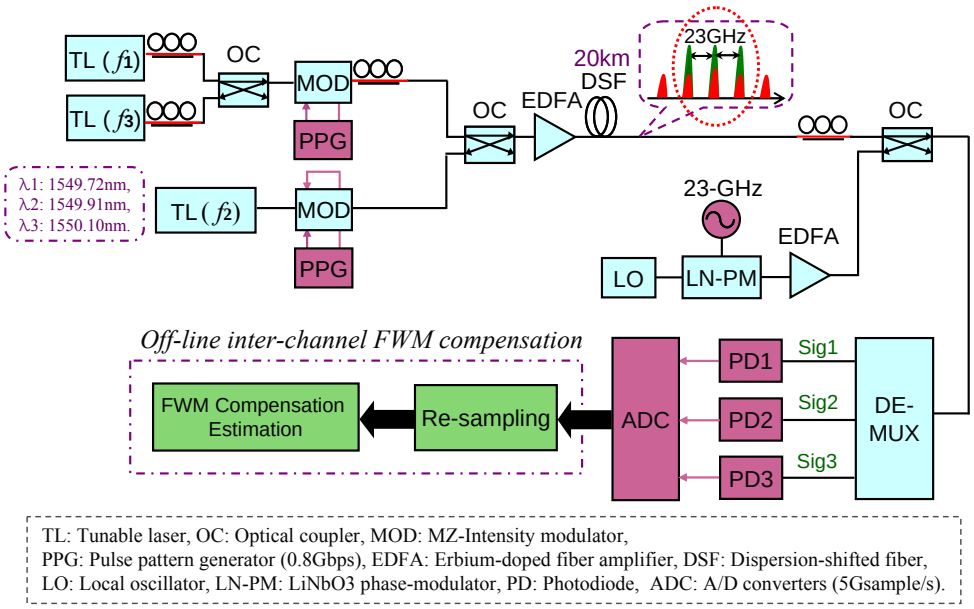

Fig 4.14 Experimental setup

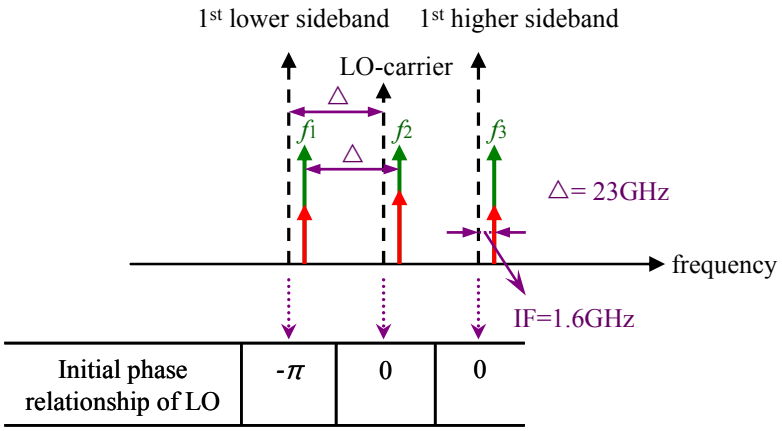

Fig 4.15 Phase relationship between LOs and signals

The optical spectra before transmission and after transmission with the fiber input power P_0=8dBm/ch are shown in Fig 4.16.

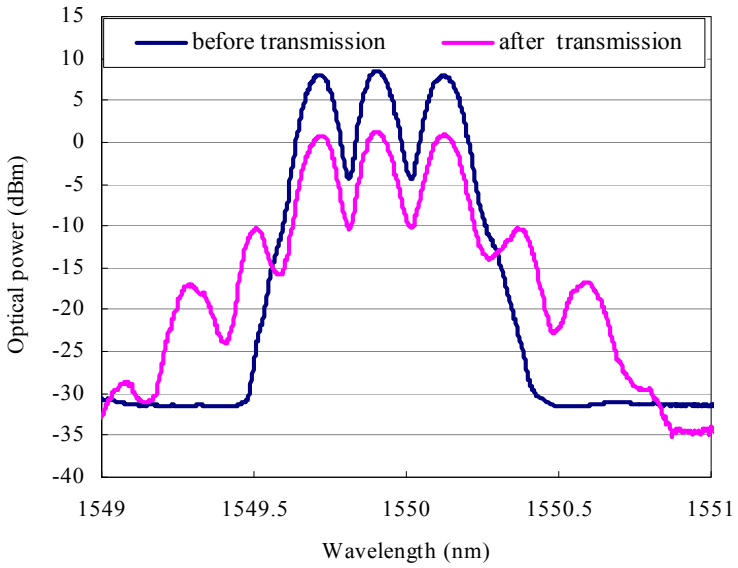

Fig 4.16 Optical spectra of transmitted signals with P_0=8dBm/ch.

Figure 4.17 a1), a2), a3) give the obtained eye diagrams of individual signals before compensation, while Fig 4.17 b1), b2), b3) plot the ones after 1st round and 2nd round FWM compensation. The eye penalty of each signal is improved by 3.5dB, 5.8B, 5dB, respectively, with our compensation.

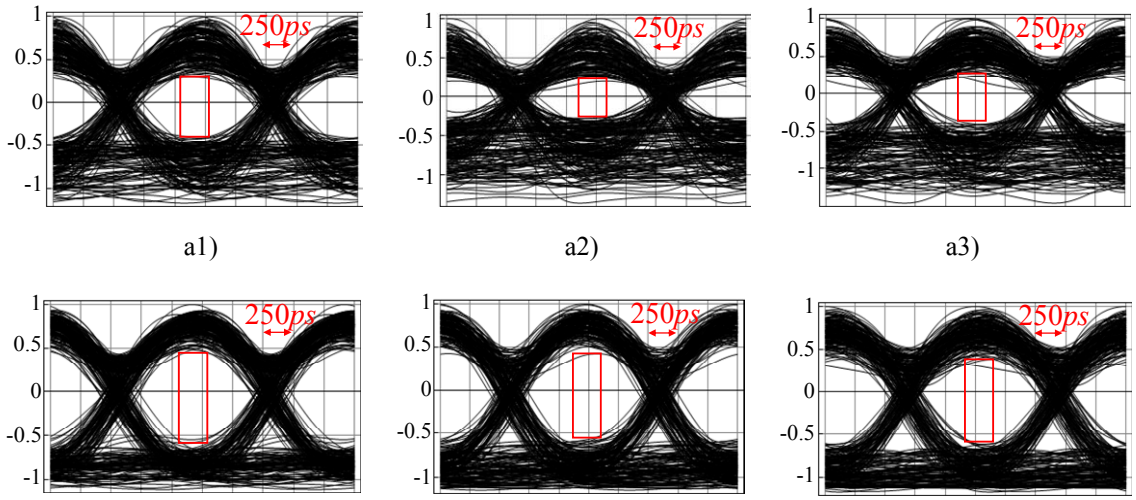

Fig 4.17 Eye openings of individual signal for a1), a2), a3) 20-km transmission w/o comp.; b1), b2), b3) w/ 1st & 2nd round FWM comp. method with P_0=8dBm/ch.

The eye penalty variation while the optical input power varies from 4dBm/ch to

9dBm/ch is shown in Fig 4.18. The eye penalty is improved to nearly 3dB in this range of the optical input power after estimation compensation. And the optical power tolerance is improved by nearly 4dB at 3dB eye penalty.

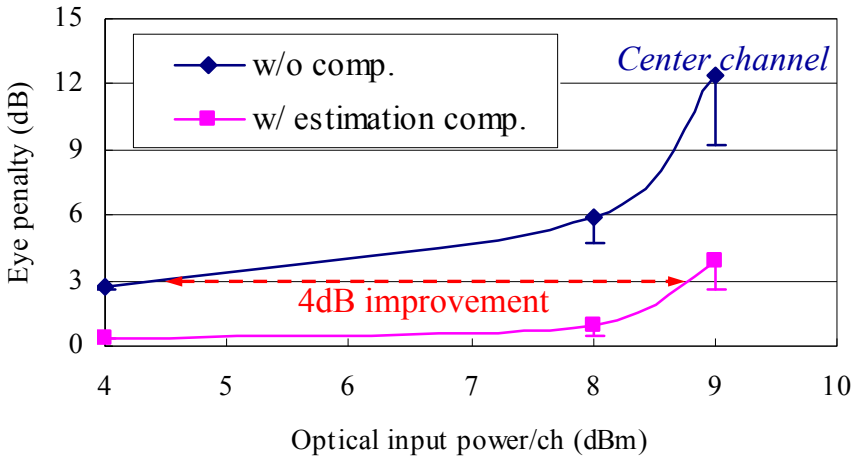

Fig 4.18 Eye penalty variation

4.8 Summary

Compared with BP method, fewer detectors are employed since only signal channels are required to be detected and FWM information of other channels are estimated based on the detected channels in our estimation method. Additionally, while the number of calculations required depends on the number of channels involved, the BP compensation method requires many more steps per channel as each transmitted fiber must be segmented. In contrast, the estimation algorithm uses only two steps and it is preferable in terms of less computation power, and smaller number of actual circuits involved.

The novel algorithm for FWM compensation is based on estimating FWM components and then substituting the estimated components for the generated ones. The principle of this algorithm is introduced and the equation derivation utilized for 1st and 2nd round estimation is given in this chapter. The 1st and 2nd round will become ineffective when the optical power becomes higher that the in-band FWMs overwhelm

the transmitted signals. This is the limitation of this method.

In order to demonstrate the possibility of this compensation method, simulation is performed firstly based on a 5-ch un-equal channel spacing system. The 5-ch system with equal channel spacing is simulated subsequently. After compensation, the eye penalty is improved by estimation method, which is also compared with BP method. The compensation results indicate that the input optical power tolerance is improved by nearly 5.5dB at 3dB eye penalty.

This compensation method is also effective in multi-channel systems, which is discussed in this part. Furthermore, the compensation method is verified experimentally. The eye penalty is improved effectively.

Reference

[1] X. Li, X. Chen, G. Goldfarb, E. Mateo, I. Kim, F. Yaman, and G. Li, "Electronic post-compensation of WDM transmission impairments using coherent detection and digital signal processing," Opt. Express, OSA, Vol. 16, No. 2, pp. 880-888, Jan., 2008.

[2] K. O. Hill, D. C. Johnson, B. S. Kawasaki, and R. I. MacDonald, "CW three-wave mixing in single-mode optical fibers," *J. Appl. Phys.*, Vol. 49, No. 10, pp. 5098–5106, Oct., 1978.

[3] G. P. Agrawal, *Nonlinear Fiber Optics*, Academic Press, San Diego, CA, 1989.

[4] S. Song, "The number of four-wave mixing (FWM) waves in WDM systems and its applications," in *Proc. LEOS 2001*, San Diego, CA, USA, Nov. 12-13, 2001, Paper TuS4.

[5] K. Inoue, “Four-wave mixing in an optical fiber in the zero-dispersion wavelength region,” *J. Lightw. Technol.*, Vol. 10, Vo. 11, pp. 1553–1561, Nov., 1992.

Chapter 5

Summary and Conclusions

We propose to demonstrate experimentally the feasibility of electrical post compensation using digital coherent detection with BP method in this dissertation, firstly. Post-compensation is more adaptive since feedback is unnecessary and demodulation process is done at the receiver side. Moreover, this method offers great flexibility to transmission length, fiber characteristics. Various fiber propagation degradations may be digitally compensated, relieving the need for complex and expensive optical solutions. The difficulties of FWM electrical compensation are to convert optical signal information to electrical signal with remaining the phase relation of individual channels. In order to realize fixed phase relationship among LOs when coherent detected by individual detectors, we modulate a LO light using a phase modulator. Both ASK and DPSK transmissions are verified in our experiments. The combined individual detected signals are compensated and the original signals can be retrieved off-line by observing the signal-to-FWM crosstalk ratio as well as the eye penalty.

Simulation is also performed for observing the number of required detectors for different number of signal channels as well as optical input power. The result indicates that great number of detectors must be employed when the optical input power is increased even in the systems with few number of signal channels.

Digital coherent detection can compensate fiber transmission degradation, including fiber nonlinearity impairments. However, for complete compensation in BP method, the extra detectors for out of band information produced by FWM are required. Additionally,

great computation power is required since many compensation steps are necessary in the segmenting of the transmitted fibers for processing. As a consequence, we propose a novel FWM impairments compensation method based on estimating FWM components and then substituting the estimated components for the generated ones. Equation derivation for estimation method is described in this dissertation for both 1st and 2nd round compensation.

With estimation method, the number of detectors is reduced since only signal channels are detected and information of other FWM channels is deduced based on these detected channels. Simulation is performed based on a five-channel WDM system, in which compensation performance is compared between our estimation method and BP method. The compensation performance is evaluated by eye penalty of each signal. The compensation results indicate that the input optical power tolerance is improved by nearly 5.5dB. The compensation performance is also verified experimentally. This method is preferable in terms of fewer employed detectors, less computation power, and fewer actual circuits involved. This method is also effective in multi-channel systems.

The limitation of this method is also discussed in higher input power region. The 1st and 2nd round will become ineffective when the power of newly generated FWMs on signal channels becomes considerable and equivalent to the signal power.

Appendix A

List of Abbreviations

WDM: wavelength division multiplexing

FWM: four-wave mixing

EDFA: erbium-doped fiber amplifier

XPM: cross-phase modulation

SPM: self-phase modulation

NLSE: nonlinear Schrödinger equation

SBS: stimulated Brillouin scattering

SRS: stimulated Raman scattering

CD: chromatic dispersion

SMF: single-mode fiber

ADC: analog-to-digital converter

BP: backward propagation

ASK: amplitude-shift keying

DPSK: differential phase-shift keying

GVD: group velocity dispersion

CW: continuous-wave

DSF: dispersion-shifted fiber

LD: laser diode

PD: photodiode

OC: optical coupler

LO: local oscillator

PC: polarization controller

ASE: Amplified spontaneous emission

DCF: dispersion compensation fiber

DSP: digital signal processing

PBS: polarization beam splitter

MZM: Mach–Zehnder modulator

PPG: pulse pattern generator

NLSE: nonlinear Schrödinger equation

FBG: Fiber Bragg grating

SSFM: split-step Fourier method

PMD: polarization mode dispersion

PRBS: pseudo-random binary sequence

LN-PM: $LiNbO_3$ phase-modulator

FPGA: Field-Programmable Gate Array

Appendix B

Partially degenerate FWM & completely non-degenerate FWM

Degenerate case:

In Section 2.4.2, we utilize the degenerate and non-degenerate FWM directly. Here, we give the explanation about the definition. For simplicity, a two-channel system is plotted in Fig A.1. As shown in Eq. (2.11), the two-channel scenario is a particular case, in which these two channels are not interfered by the FWM terms that induced by only two signal frequency mixing (However, multi-channel system will be undermined). This is named as degenerate FWM. In this case, the signal powers are depleted from the original channels to the generated extraneous degenerate FWM frequencies located at $2\omega_1$-ω_2 (f_{112}) and $2\omega_2$-ω_1 (f_{221}). The situation becomes more complicated as signal channels or optical power increases, and more FWMs will be generated. Degenerate FWMs are generated in multi-channel systems likewise.

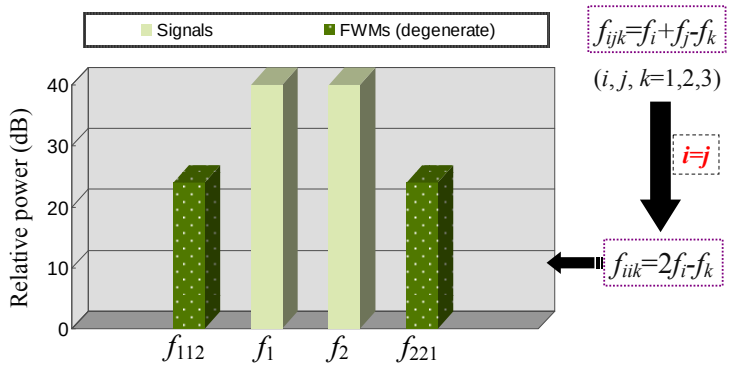

Fig A.1 Frequency allocation of degenerate FWM in a two-channel system

Non-degenerate case:

Different from degenerate case, FWM terms that induced by the frequency mixing from three signals are called completely non-degenerate FWM. The components can be viewed clearly in Fig 2.5.

Appendix C

β expansion in Taylor series and phase mismatching factor

In order to find the relationship between phase mismatching factor $\Delta\beta$ and chromatic dispersion D_c, the propagation constant β is expanded in Taylor series about $\omega=\omega_m=2\pi c/\lambda_m$ as follows:

$$\begin{aligned}\beta(\omega) &= \beta(\omega_m)+(\omega-\omega_m)\left(\frac{d\beta}{d\omega}\right)_{\omega=\omega_m}+\frac{1}{2}(\omega-\omega_m)^2\left(\frac{d^2\beta}{d\omega^2}\right)_{\omega=\omega_m}+\frac{1}{6}(\omega-\omega_m)^3\left(\frac{d^3\beta}{d\omega^3}\right)_{\omega=\omega_m}\\ &= \frac{\omega_m}{v_p}+\frac{\omega-\omega_m}{v_g}+(\omega-\omega_m)^2\frac{\lambda_m^2 D_c}{4\pi c}+(\omega-\omega_m)^3\frac{\lambda_m^4}{24\pi^2c^2}\frac{dD_c}{d\lambda}\end{aligned} \tag{A-1}$$

where v_p and v_g is the phase velocity and group velocity of HE_{11} mode, respectively. And $\beta_1=\left(\frac{d\beta}{d\omega}\right)_{\omega=\omega_m}$, $\beta_2=\left(\frac{d^2\beta}{d\omega^2}\right)_{\omega=\omega_m}$, $\beta_3=\left(\frac{d^3\beta}{d\omega^3}\right)_{\omega=\omega_m}$, respectively. β_1 is related inversely to v_g, β_2 and β_3 are named as second- and third-order dispersion parameters, respectively. Therefore, $\Delta\beta=\beta_i+\beta_j-\beta_k-\beta_{ijk}$ in Eq. (2.20) can be deduced as:

$$\begin{aligned}\Delta\beta &= \beta_{ijk}+\beta_k-\beta_i-\beta_j\\ &= \frac{\omega_m}{v_p}+\frac{\omega_{ijk}-\omega_m}{v_g}+(\omega_{ijk}-\omega_m)^2\frac{\lambda_m^2 D_c}{4\pi c}+(\omega_{ijk}-\omega_m)^3\frac{\lambda_m^4}{24\pi^2c^2}\frac{dD_c}{d\lambda}\\ &\quad+\frac{\omega_m}{v_p}+\frac{\omega_k-\omega_m}{v_g}+(\omega_k-\omega_m)^2\frac{\lambda_m^2 D_c}{4\pi c}+(\omega_k-\omega_m)^3\frac{\lambda_m^4}{24\pi^2c^2}\frac{dD_c}{d\lambda}\\ &\quad-\left\{\frac{\omega_m}{v_p}+\frac{\omega_i-\omega_m}{v_g}+(\omega_i-\omega_m)^2\frac{\lambda_m^2 D_c}{4\pi c}+(\omega_i-\omega_m)^3\frac{\lambda_m^4}{24\pi^2c^2}\frac{dD_c}{d\lambda}\right\}\\ &\quad-\left\{\frac{\omega_m}{v_p}+\frac{\omega_j-\omega_m}{v_g}+(\omega_j-\omega_m)^2\frac{\lambda_m^2 D_c}{4\pi c}+(\omega_j-\omega_m)^3\frac{\lambda_m^4}{24\pi^2c^2}\frac{dD_c}{d\lambda}\right\}\end{aligned}$$

$$
\begin{aligned}
&= \frac{\omega_{ijk}+\omega_k-\omega_i-\omega_j}{v_g} + \left\{\left(\omega_{ijk}-\omega_m\right)^2+\left(\omega_k-\omega_m\right)^2-\left(\omega_i-\omega_m\right)^2-\left(\omega_j-\omega_m\right)^2\right\}\frac{\lambda_m^2 D_c}{4\pi c} \\
&\quad + \left\{\left(\omega_{ijk}-\omega_m\right)^3+\left(\omega_k-\omega_m\right)^3-\left(\omega_i-\omega_m\right)^3-\left(\omega_j-\omega_m\right)^3\right\}\frac{\lambda_m^4}{24\pi^2c^2}\frac{dD_c}{d\lambda} \\
&= \left(\omega_{ijk}{}^2+\omega_k{}^2-\omega_i{}^2-\omega_j{}^2\right)\frac{\lambda_m^2 D_c}{4\pi c} + 3\left(\omega_k-\omega_i\right)\left(\omega_k-\omega_j\right)\left(\omega_i+\omega_j-2\omega_m\right)\frac{\lambda_m^4}{24\pi^2c^2}\frac{dD_c}{d\lambda} \\
&= \left(\omega_{ijk}{}^2+\omega_k{}^2-\omega_i{}^2-\omega_j{}^2\right)\frac{\lambda_m^2 D_c}{4\pi c} + 3\left(\omega_k-\omega_i\right)\left(\omega_k-\omega_j\right)\left(\omega_i+\omega_j-2\omega_m\right)\frac{\lambda_m^4}{24\pi^2c^2}\frac{dD_c}{d\lambda} \\
&= \left(\omega_k-\omega_i\right)\left(\omega_k-\omega_j\right)\frac{\lambda_m^2 D_c}{2\pi c} + \left(\omega_k-\omega_i\right)\left(\omega_k-\omega_j\right)\left(\omega_i+\omega_j-2\omega_m\right)\frac{\lambda_m^4}{8\pi^2c^2}\frac{dD_c}{d\lambda}
\end{aligned}
\tag{A-2}
$$

where the frequency relation $\omega_{ijk}+\omega_k-\omega_i-\omega_j=0$ is utilized. We consider whether the wavelength locates near the zero-dispersion wavelength λ_0 or not. If it is far from λ_0, the 2nd term of Eq. (A-2) can be neglected and becomes:

$$
\Delta\beta = \left(\omega_k-\omega_i\right)\left(\omega_k-\omega_j\right)\frac{\lambda_m^2 D_c}{2\pi c} = \left(f_k-f_i\right)\left(f_k-f_j\right)\frac{2\pi\lambda_m^2 D_c}{c} \tag{A-3}
$$

Otherwise, if it locates near λ_0 (i.e., $\omega_m=\omega_0$), D_c is nearly zero and the 1st term approaches zero. In this case, Eq. (A-2) becomes:

$$
\begin{aligned}
\Delta\beta &= \left(\omega_k-\omega_i\right)\left(\omega_k-\omega_j\right)\left(\omega_i+\omega_j-2\omega_0\right)\frac{\lambda_m^4}{8\pi^2c^2}\frac{dD_c}{d\lambda} \\
&= \left(f_k-f_i\right)\left(f_k-f_j\right)\left(f_i+f_j-2f_0\right)\frac{\pi\lambda_m^4}{c^2}\frac{dD_c}{d\lambda}
\end{aligned}
\tag{A-4}
$$

When we assume the equal channel spacing, i.e., $f_i=f_j$, Eq. (A-4) is rewritten as:

$$
\Delta\beta = 2\left(f_k-f_i\right)^2\left(f_i-f_0\right)\frac{\pi\lambda_m^4}{c^2}\frac{dD_c}{d\lambda} \tag{A-5}
$$

It is deduced that when $f_i+f_j=2f_0$, $\Delta\beta=0$ can be obtained from Eq. (4). The condition of $f_{ijk}+f_k-f_i-f_j=0$ is known, and thereby $f_{ijk}+f_k=2f_0$. Namely, the generated FWM frequency f_{ijk} and the signal frequency f_k are symmetrical to f_0, which is plotted in Fig A.2 (a). For the degenerate case in Eq. (5), $\Delta\beta=0$ can be realized only if $f_i=f_j=f_0$. Figure A.2 (b) shows this allocation.

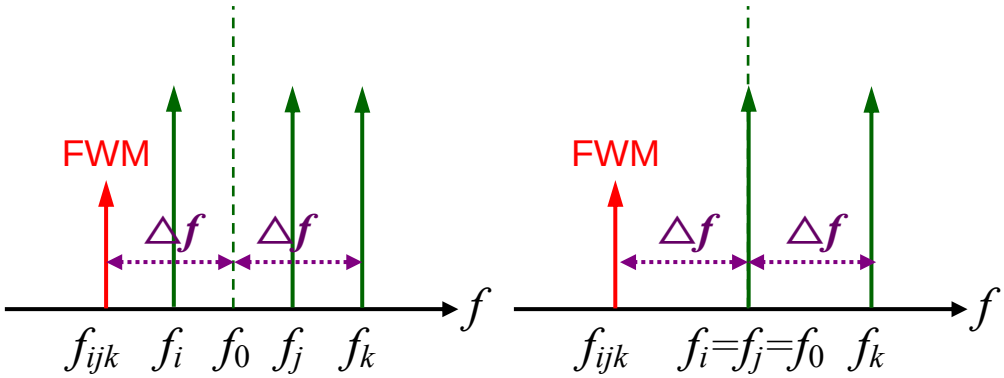

Fig A.2 Frequency allocation for $\Delta\beta = 0$

Appendix D

Measurement of zero-dispersion wavelength

Before implementing the experiment, λ_0 of the utilized DSF is measured firstly. The method for this measurement is one of the utilizations for FWM of the degenerate case. From Eq. (2.22), the phase mismatching factor becomes the following form for degenerate FWM when $f_1 = f_2$:

$$\Delta\beta = \frac{2\pi\lambda_0^4}{c^2}\left(f_1 - f_3\right)^2\left(f_1 - f_0\right)S \tag{A-6}$$

It is obvious that the phase mismatching factor $\Delta\beta$ will becomes zero when a pump frequency locates at the zero-dispersion frequency f_0, and thereby the FWM generation will become the most efficient. In other words, λ_0 dovetails with the pump wavelength, which the highest FWM power is generated at. The measurement is shown in Fig A.3.

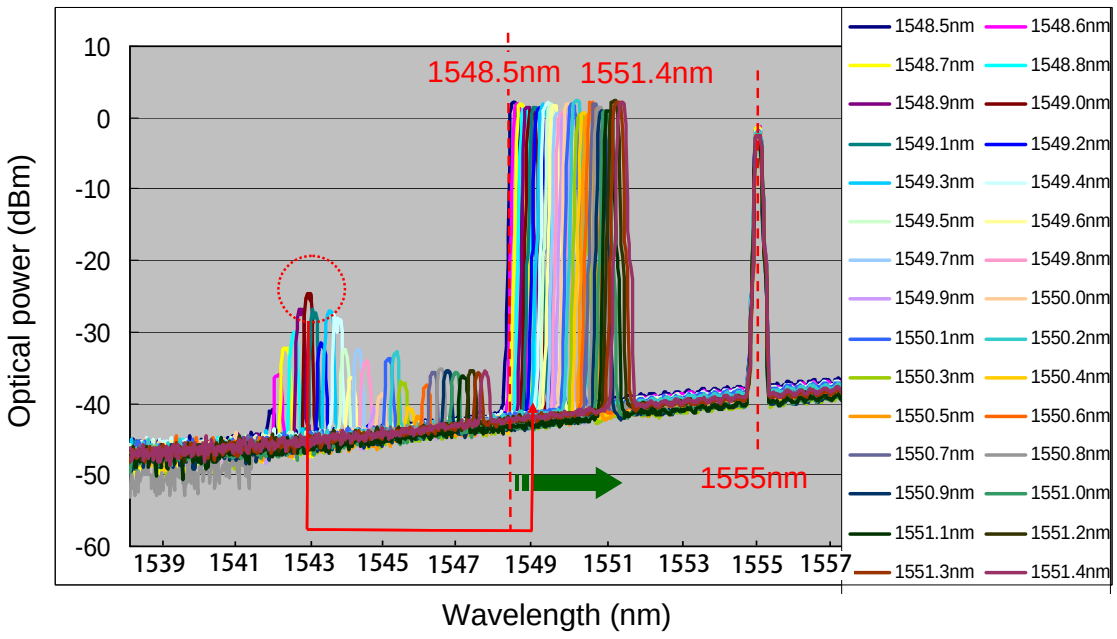

Fig A.3 Measurement of zero-dispersion wavelength

Since the ZDW of universal DSF is approximately 1550 nm, the probe wavelength is

selected to be within the range of 10nm near λ_0 and keep unchanged [1]. In our measurement, we set the fixed optical light at 1555nm. The pump light is changed slightly near 1550nm as a step of 0.1nm within a short range as shown in Fig A.3. It is clear that there is a peak FWM product at 1543nm and the corresponding pump wavelength is 1549nm, and hence, the ZDW of our utilized DSF is 1549nm.

[1] S. E. Mechels, J. B. Schlager, and D. L. Franzen, "Accurate measurements of the zero-dispersion wavelength in optical fibers," *Journal of Research of the National Institute of Standards and Technology*, Vol. 102, No. 3, pp. 333-347, May., 1997.

Appendix E

Configuration of optical demultiplexer

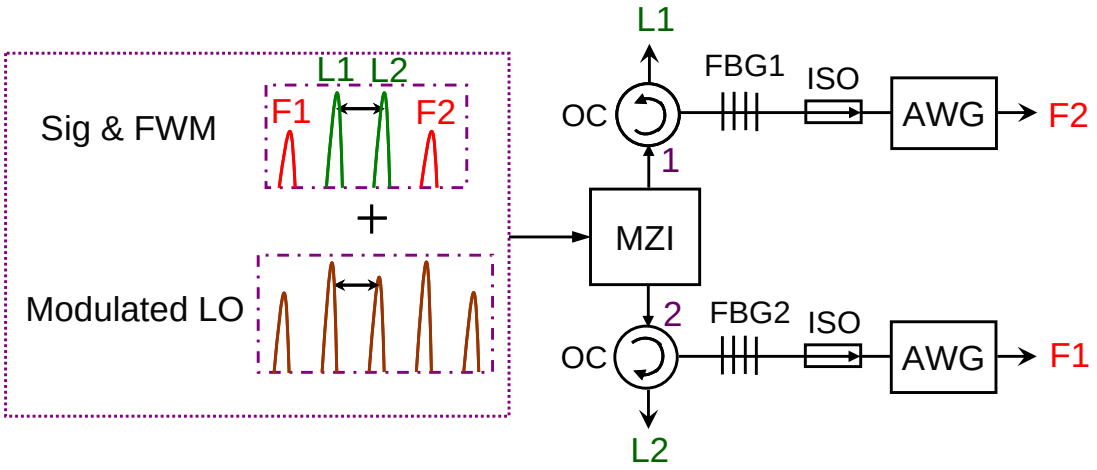

Fig A.4 Configuration of optical demultiplexer (MZI: Mach-Zehnder interferometer, OC: optical circulator, FBG: fiber Bragg grating, ISO: Isolator, AWG: Arrayed waveguide)

Appendix F

Frequency response of individual PDs

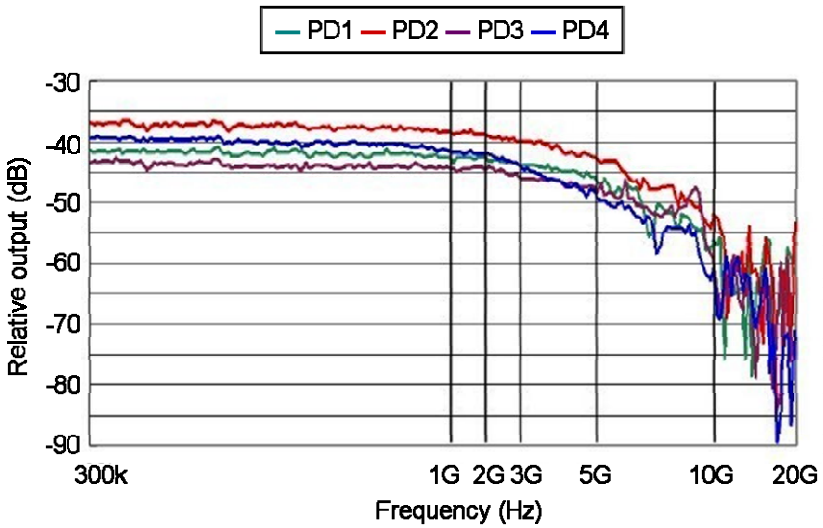

Fig A.5 Frequency response of individual PDs

Appendix G

SBS in different modulation formats

In order to observe the influence of SBS effect, firstly the measurement of CW light under our experimental situation is shown in Fig A.6. At the lower power region, both the forward power and backward power increase linearly with the increase of fiber input power. Brillouin threshold is reached at an input power of nearly 5.5dBm, since there is a substantial increase of the reflected power, shown in Fig A.6, which is dominated by the backward Stokes wave generated through SBS. The forward transmitted power reaches a saturation level of about 1.7dbm, simultaneously, for the input powers in excess of 7dbm. And the degradation of SBS can be seen clearly by optical spectrum with optical power of 2dBm and 13dBm (indicated in Fig A.6) in Fig A.7 (a) and (b), respectively. With the appearance of SBS, most of the optical power will be converted to backward Stokes wave. For this case SBS also acts as a limit factor of FWM when the optical power becomes higher.

ASK and PSK modulated optical signals are also measured in Fig A.8 (a) and (b), respectively. Brillouin threshold is 6.5dBm for ASK modulation, and for PSK modulation, both of the forward power and backward power increase linearly, so there seems no backward Stokes wave appears between the optical power of 1dBm and 10dBm. Therefore, if we consider the relatively higher input power, PSK modulation should be more adequate.

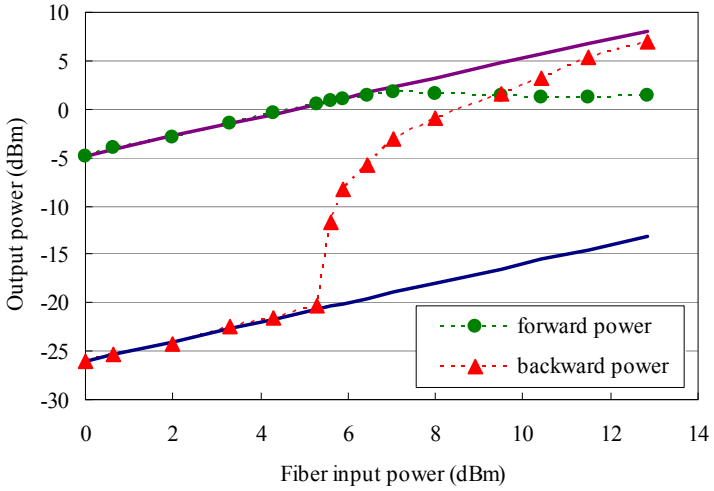

Fig A.6 SBS measurement of CW light: linear loss is 4.7dB.

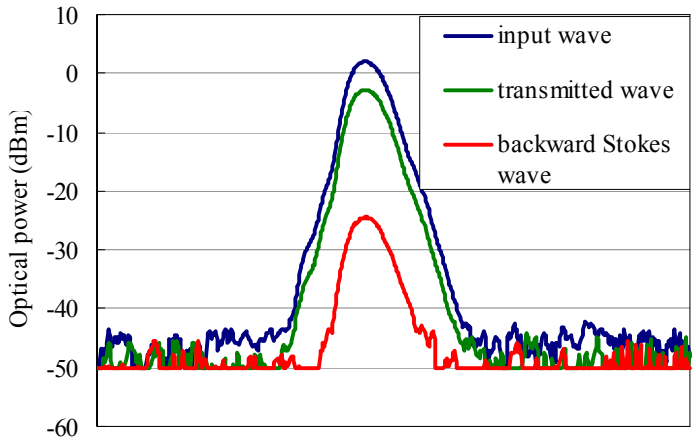

(a)

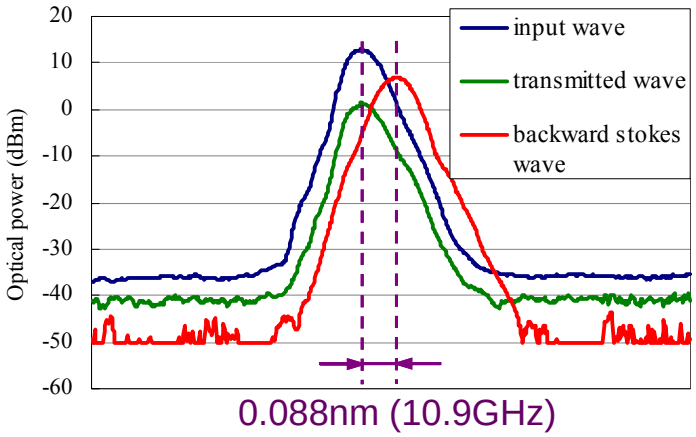

(b)

Fig A.7 Optical spectrum by SBS with optical power of (a) 2dBm, (b) 13dBm.

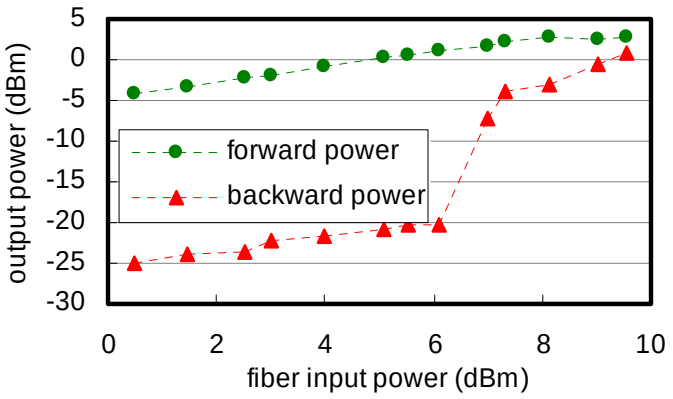

(a)

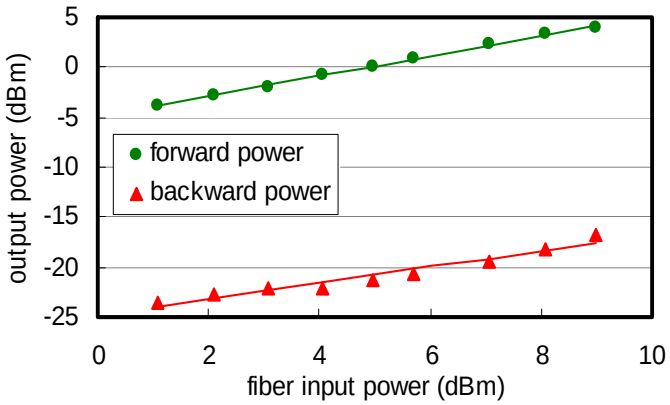

(b)

Fig A.8 SBS measurement (a) ASK modulated signal; (b) DPSK modulated signal.

Acknowledgements

First, I would like to express sincere gratitude to my supervisor Prof. Katsushi Iwashita for his invaluable guidance and encouragement throughout the three-year's research. His proper guidance, genuine encouragement and full support facilitate the completion of this dissertation. Especially, he spent considerable amount of time helping me on my research in spite of his tight schedule.

Special acknowledgement is given to my vice-advisor, Prof. Koji Nonaka, who gave me valuable suggestions on research and also provided me with kind help on experimental instruments. Oceans of thanks are also conveyed to Prof. Masayoshi Tachibana, Prof. Seiji Norimatsu and Associate Masanori Hamamura as the members of my defense committee, for their professional suggestions and supports on my research.

I am very grateful to past and present staffs of IRC, who befriended me and offered me much help on Japanese study as well as daily life. Their warm-hearted assistance will become memorable.

I address my deep gratitude to SSP Scholarship from KUT and Heiwa Nakajima Scholarship from Heiwa Nakajima Foundation for their great supports.

I would like to deliver my thanks to all the members in Iwashita Lab. They contribute to the learning climate of our lab under the direction of Iwashita sensei.

I feel indebted to my parents, for their loving care during these three years, giving me the motivation and strength and encouraging me to endeavor to achieve my goals. Words are insufficient to express the gratitude I owe to them.

Last but not least, sincere gratitude to my boyfriend who inspires me patiently and serves as spiritual support throughout the period of my study in Japan.

List of publications

Academic Journals

1. Jing Liang and Katsushi Iwashita, “Experimental Investigation of Post-Compensation for FWM Impairments Considering Inter-Channel Nonlinear Crosstalk with Digital Coherent Detection,” ***IEICE Trans. Commun.***, Vol.E94-B, No.2, pp.558-561, Feb., 2011.

2. Jing Liang and Katsushi Iwashita, “A Novel Compensation Method for FWM Impairments based on Cancellation by Estimated Components in Digital Coherent Detection,” ***IEEE Photonics Technology Letters,*** Vol.23, No.19, pp.1394-1396, Oct., 2011.

3. Jing Liang and Katsushi Iwashita, “FWM Compensation in DPSK Transmission by Reducing Detectors with Digital Coherent Detection Using Backward Propagation,” ***International Journal of Information and Electronics Engineering,*** Vol.1, No.1, pp. 99-104, Jul., 2011.

4. Jing Liang and Katsushi Iwashita, “Estimation Method for FWM Impairments Compensation with Digital Coherent Detection in WDM systems,” Under preparation.

Conference Proceedings

1. Jing Liang, Kazuhumi Nishiuchi, Katsushi Iwashita, "Inter-Channel FWM Impairments Compensation of ASK Transmission with Digital Coherent Detection," *The 36th European Conference and Exhibition on Optical Communication (**ECOC 2010)***, Turin, Italy, Paper P3.04, Sep. 2010.

2. Jing Liang and Katsushi Iwashita, "Electrical Compensation of FWM Impairment by Heterodyne Detection Using Backward Propagation," *The 14th OptoElectronics and Communications Conference (**OECC 2009)***, Hong Kong, Paper Tuk6, Jul., 2009.

3. Jing Liang and Katsushi Iwashita, "Electrical Compensation of FWM Impairment by Phase Diversity Detection via Backward Propagation," *Asia Communications and Photonics Conference and Exhibition (**ACP 2009)***, Shanghai, China, Proc. SPIE, Vol. 7632, 76321E (2009), Nov., 2009.

4. Jing Liang and Katsushi Iwashita, "Compensation for FWM in DPSK Transmission by Reducing Detectors with Coherent Detection through Digital Signal Processing," *The 3rd International Conference on Signal Acquisition and Processing (**ICSAP 2011**),* Singapore, Paper P165, Feb., 2011.

5. Jing Liang and Katsushi Iwashita, "Frequency Allocation Analysis for FWM Post-Compensation by Heterodyne Detection," *平成 21 年度電気関係学会四国支部連合大会*, Ehime, Japan, Paper 18-1，Sep., 2009.

6. Jing Liang and Katsushi Iwashita, "A Novel Compensation Method for Four-Wave

Mixing Nonlinearity Impairments with Digital Coherent Detection in Optical Communication Systems," The 3rd International Symposium on Frontier Technology (***ISFT 2011***), Kochi, Japan, Jul., 2011.

7. Kazuhumi Nishiuchi, Jing Liang, and Katsushi Iwashita, "Four-Wave Mixing Degradation Compensation with Digital Coherent Detection in Optical Amplifier Repeater System," *Asia Communications and Photonics Conference and Exhibition **(ACP 2010)***, Shanghai, China, Proc. SPIE, Vol. 7988, 798829 (2010), Dec., 2010.

8. Kazuhumi Nishiuchi, Jing Liang, and Katsushi Iwashita, "*光ヘテロダイン検波を用いた光ファイバの四光波混合補償法の検討,*" *平成 21 年度電気関係学会四国支部連合大会,* Ehime, Japan, Paper 12-14, Sep., 2009.

9. Kazuhumi Nishiuchi, Jing Liang, and Katsushi Iwashita, "Four-Wave Mixing Degradation Compensation with Digital Coherent Detection in Optical Amplifiers Repeater System," *平成 22 年度電気関係学会四国支部連合大会*, Ehime, Japan, Paper 18-23, Sep., 2010.